NOVA SCHOOL OF SCIENCE & TECHNOLOGY

DEPARTAMENTO DE QUÍMICA

LEANDRA JOSÉ SILVA RODRIGUES

Licenciada em Biologia Celular e Molecular

CHARACTERIZATION OF EXTRACELLULAR VESICLES FROM ASCITIC FLUID IN OVARIAN CANCER PATIENTS

MESTRADO EM BIOTECNOLOGIA

Universidade NOVA de Lisboa

Fevereiro, 2022

DEPARTAMENTO DE QUÍMICA

CHARACTERIZATION OF EXTRACELLULAR VESICLES FROM ASCITIC FLUID IN OVARIAN CANCER PATIENTS

LEANDRA JOSÉ SILVA RODRIGUES
Licenciado em Biologia Celular e Molecular

Orientador: Inês Azevedo Isidro, PhD, Researcher, iBET e ITQB-NOVA

Júri:

Presidente: Ana Rita Cruz Duarte

Arguentes: Maria João Carvalho Sebastião

Vogais: Inês Azevedo Isidro

MESTRADO EM BIOTECNOLOGIA

Universidade NOVA de Lisboa

Fevereiro, 2022

Characterization of extracellular vesicles from ascitic fluid in ovarian cancer patients

This thesis is dedicated to my family and friends

ACKOWLEDGEMENTS

To Rita Mendes and my supervisor Dr. Inês Isidro, who first welcomed me at iBET, I want to thank for the guidance, but also the encouragement, strength, and lots of patience given throughout this year. I took lots of learnings as a professional or person. To Dr. Catarina Brito I want to thank the guidance and feedback readily given in this project, for welcoming me and for all the lessons she taught me.

To the IPO and, more specifically, to Dr. Ana Félix and Dr. Fernanda Silva I want to thank the collaboration in this project otherwise impossible, to Dr. José Ramalho for sharing lab equipment with us and Dr. Júlia Costa for the very helpful feedback.

To other people directly involved in this project, I want to thank A.L. Sousa and E.M. Tranfield from ICG, and A.C.L. Guerreiro, C. Almeida and C. Correia from UniMS for the technical expertise and partnership.

I also want to thank Gonçalo Trindade for the great company and precious help during crazy days on lab, Catarina Gomes and Bárbara Fernandes for the help in protein quantification and Western blot, Giacomo Domenici for sharing valuable knowledge with me, Nuno Lopes and Teresa Mendes for checking me up every time since the beginning, and to my other colleagues from Advanced Cell Models Lab, Francisca Arez, Sofia Batalha, Isabella Gal and Catarina Perdigão also for the precious help and feedback. I am grateful for having this experience with you all.

I also want to thank Inova4Health – UIDB/04462/2020 and UIDP/04462/2020, a program financially supported by Fundação para a Ciência e Tecnologia/Ministério da Ciência, Tecnologia e Ensino Superior, through national funds, the fellowship PhD of Rita Mendes, UniMS, ASU and IGC for the collaboration and partnership, and iBET for providing resources and working conditions, so this project was possible.

Passando agora aos meus amigos, tenho de começar por ti, Pedro. Nestes últimos meses foste um apoio enorme para mim, como aliás sempre foste, e não existem palavras suficientes para te agradecer. Às minhas queridas Inês Góis e Patrícia Henriques, foi na faculdade também que vos conheci. Quis o destino colocar-nos parede com parede, mas a amizade foi escolha nossa e fortaleceu a cada "destropeço" que fomos encontrando e superando pelo caminho. Também às restantes "do piso de cima",

Marta Vieira, Alícia Candeias, Ana Catarina Calheta, Ana Paula Peixe, Ana Santos, Joana Galhano e Marlene Leite – foi um prazer enorme ter-vos conhecido e partilhado vivências dentro ou fora do mesmo teto. Espero que não fique por aqui e encontremos lugar para novas aventuras futuramente. Ao Pedro Gonçalves, à Joana Alves, Rita Gil, Ana Seco, Oleksandra, e Catarina Oliveira, a todos, não consigo imaginar como seria se não vos tivesse conhecido nos primeiros anos de faculdade.

Também aos meus amigos de Oeiras, Inês Romão, Tiago Fernandes, Clément, Astro (o melhor cão do mundo, sem discussão), Millia e David, obrigada por tudo. Convosco foi possível sobreviver a este ano como se estivesse em casa. Também ao João Sequeira, que é de Alvalade (de outro sítio não podia ser!), obrigada por teres estado lá, sempre que precisei ou mesmo sem aviso – estou segura de que amigos assim não existem "aos pontapés".

Finalmente, mas não menos importante, à minha família. Pai, mãe, sem vocês isto não teria sido possível. Cuidaram – e continuam a cuidar - de mim e são um exemplo que tento seguir. Sempre acreditaram em mim, quando tantas vezes fui abaixo, e por isso posso dizer que levantei. Às minhas irmãs, obrigada por tudo, convosco sou feliz e aprendo todos os dias. Ao meu padrinho José Manuel, um especial obrigado por todas as palavras de força e apoio que sempre me deu.

Aprendi um bocadinho aqui e ali com todos vocês e agradeço sempre o vosso apoio. Obrigada aos professores, aos colegas de trabalho e supervisores, às instituições por onde passei, à família, aos amigos. Obrigada a todos.

"There is nothing certain, nothing at all except the unimportance of everything I understand, and the greatness of something incomprehensible but all-important."
(Leo Tolstoy)

ABSTRACT

Ovarian cancer is the first cause of death among gynaecological malignancies in women. Most patients are diagnosed at late stages and present ascites, the accumulation of ascitic fluid in the peritoneal cavity, associated to metastasis and poor prognosis. Ascitic fluids are enriched in pro-tumorigenic components, such as extracellular vesicles (EVs) involved in the tumour microenvironment intercellular crosstalk. Despite metabolic alterations being a hallmark of cancer and highly correlated with sensitivity to treatment, the metabolite cargo is still the least explored component of EVs in ovarian cancer.

The aim of this thesis was to characterize the metabolic signature of EVs isolated from ascitic fluids in ovarian cancer patients. Methods for the characterization of EVs were first implemented using EVs isolated from an ovarian cancer cell line (ES-2), namely for the presence of EV and non-EV components by Western blot, as well as the analytical platform for metabolomics and lipidomics by LC-MS. Ultimately, EVs were isolated using differential centrifugation from ovarian cancer biofluids, including ascitic fluids and peritoneal washes as controls. Isolated and discarded fractions were characterized by Western blot; by transmission electron microscopy (TEM) for morphology, and by nanoparticle tracking analysis (NTA) for particle concentration and size, following the International Society for Extracellular Vesicles (ISEV) guidelines.

We demonstrated the recovery of EVs and increasing purity of isolates and confirmed the presence of EVs on biofluids. The metabolic characterization of ES-2 EVs suggested an enrichment in metabolic pathways involved in cancer processes. This methodology for characterization of the metabolic content of EVs can be further applied in EVs from ascitic fluids and peritoneal washes, which may elucidate the role of EVs as mediators of metabolic crosstalk in ovarian cancer tumour microenvironment and eventually uncover potential biomarkers for ovarian cancer prognosis.

Keywords: ovarian cancer, ascitic fluids, metabolic crosstalk, extracellular vesicles, differential centrifugation, metabolomics.

RESUMO

O cancro do ovário é a principal causa de morte por doenças ginecológicas em mulheres. Geralmente o diagnóstico é tardio e acompanhado por ascites, a acumulação de fluído ascítico na cavidade peritoneal associada a processos metastáticos e mau prognóstico. Os fluídos ascíticos são constituídos por componentes pró-tumorigénicos, como vesículas extracelulares (EVs) envolvidas no crosstalk intercelular estabelecido em microambientes tumorais. Alterações metabólicas são um marcador de cancro e estão relacionadas com a sensibilidade ao tratamento. Contudo, o conteúdo metabólico dos EVs é ainda o menos estudado no contexto de cancro do ovário.

O objetivo desta tese foi caraterizar o perfil metabólico de EVs isolados de fluídos ascíticos em pacientes de cancro do ovário. Métodos para caraterização de EVs foram primeiro implementados usando EVs de uma linha celular (ES-2), nomeadamente para a deteção de componentes e contaminantes de EVs por Western blot e para a análise de metabolómica/lipidómica por LC-MS. Por fim, EVs de fluídos biológicos, incluindo fluídos ascíticos e lavados peritoneais (controlos), foram isolados por centrifugação diferencial. Frações isoladas e descartadas foram caraterizadas por Western blot, por microscopia eletrónica de transmissão (TEM) para análise morfológica das partículas e por nanoparticle tracking analysis (NTA) para determinação da concentração e tamanho, seguindo as diretrizes da International Society for Extracellular Vesicles.

Foi demonstrada a recuperação de EVs no final do isolamento, o aumento de pureza das frações isoladas e a presença de EVs em fluídos biológicos. A caraterização dos EVs de ES-2 sugeriu o enriquecimento em vias metabólicas envolvidas em processos tumorais. Esta metodologia para caraterização do conteúdo metabólico pode futuramente ser aplicada em EVs de fluídos ascíticos e lavados peritoneais para elucidar o papel dos EVs como mediadores do crosstalk metabólico no microambiente tumoral e eventualmente revelar potenciais biomarcadores para o prognóstico de cancro do ovário.

Palavras-chave: cancro do ovário, fluídos ascíticos, crosstalk metabólico, vesículas extracelulares, centrifugação diferencial, metabolómica.

TABLE OF CONTENTS

LIST OF FIGURES

LIST OF TABLES

ABBREVIATIONS

ACN	Acetonitrile
AF	Ascitic fluids
AGC	Automatic gain control
CA125	Cancer antigen 125
CAFs	Cancer-associated fibroblasts
ddH_2O	Double-distilled water
DPBS	Dulbecco's phosphate-buffered saline
EOC	Epithelial ovarian cancer
ESCRT	Endosomal sorting complex required for transport
EVs	Extracellular vesicles
FWHM	Full width at half maximum
HCD	Higher-energy collisional dissociation
HDL	High density lipoproteins
HESI	Heated electrospray ionization
HGSC	High-grade serous carcinoma
HMDB	Human Metabolome Database
ILV	Intraluminal vesicles
IPA	Isopropanol
ISEV	International Society for Extracellular Vesicles
KEGG	Kyoto Encyclopedia of Genes
LC-MS	Liquid chromatography-mass spectrometry
LDL	Low density lipoproteins
LSE	Late-sorting endosome
MVB	Multivesicular body
m/z	Mass-to-charge ratio
NCE	Stepped normalized collision energies

NK cells	Natural killer cells
NTA	Nanoparticle tracking analysis
O/N	Overnight
ORA	Over Representation Analysis
PVDF	Polyvinylidene difluoride
PW	Peritoneal washes
RT	Room temperature
TBS	Tris buffered saline
TBST	Tris buffered saline Tween
TCA	mitochondrial tricarboxylic acid
TCA	Trichloroacetic acid
TEM	Transmission electron microscopy
VLDL	Very-low density lipoproteins

1. INTRODUCTION

1.1. Ovarian cancer

1.1.1. Incidence and mortality

Ovarian cancer is the eight most common cancer type in women, but the leading cause of death among gynaecological malignancies ranking fifth in cancer deaths among women worldwide[1], [2]. Only in 2020, 313 959 new cases and 207 252 deaths were reported worldwide [3]. In the United States, the risk of developing ovarian cancer during a lifetime is about 1.3%, the equivalent of 1 in 78 women [4]. Despite the incidence rate of new cases decreased on average 3.3% each year from 2009 to 2018 [5], the five-year survival rate is of 49.1%, meaning that less than half of the patients are still alive 5 years after they were diagnosed or started treatment for ovarian cancer[6].

1.1.2. Origin, progression, and diagnosis

Most ovarian cancers are sporadic and prevail in postmenopausal women. High-grade serous carcinoma (HGSC) accounts for 75% of epithelial ovarian cancers (EOC), the most frequent type of ovarian cancer[7], and 40% of EOC patients are diagnosed over the age of 65 [8]. A small percentage of EOC cases, about 10%, are hereditary and mainly attributed to mutations in the breast cancer 1 (*BRCA1*) and breast cancer 2 (*BRCA2*) genes[9]. Under abnormal physiological conditions of EOC, epithelial ovarian cancer cells invade the surrounding peritoneum and adhere to mesothelial cells, a process called transcoelomic metastasis, facilitated by CD44, β-integrins and cancer antigen 125 (CA125), expressed on the ovarian cancer cell surface, and associated with the production of ascitic fluid[10]. In late stages, most patients present the accumulation of ascitic fluid in the peritoneal cavity. The composition of ascitic fluid reflects the inflammatory environment of the underlying tumor – and high amounts of ascitic fluids (more than 500 mL) are generally associated with poor prognosis[11]. During the invasion, it has also been suggested that epithelial ovarian cancer cells acquire a mesenchy-

mal phenotype characterized by increased migratory capabilities, a process known as epithelial-to-mesenchymal transition [12]. This conversion is associated with cancer aggressiveness and reduced vulnerability to chemotherapy, which in turn may be correlated with metabolic reprogramming[13].

More than half of the EOC cases are diagnosed when cancer has already metastasized. At this stage, the five-year survival rate significantly drops by 62.3% compared to localized tumours[6]. Blood test for CA125 and transvaginal ultrasound used in combination or alone, bimanual pelvic examination and the more recent ultrasound molecular imaging techniques are some current tools to screen ovarian cancer[14]–[16]. To check for peritoneal dissemination, peritoneal washes are obtained during surgery by instilling a 50-200 mL of salt-water solution in the peritoneal cavity and recollecting the liquid again for cytology analysis [17], [18]. Positive peritoneal washing cytology is a poor prognosis indicator further correlated with tumour type and grade[19]. Symptoms of ovarian cancer (e.g. abdominal pain and bloating, early satiety, urinary urgency) are nonspecific and the disease may remain unsuspicious until late detection[20]. Ovarian cancer can only be confirmed for sure through biopsy[21]. Hence, ovarian cancer remains a challenge to diagnose early.

1.1.3. Treatment and relapse

The options to treat ovarian cancer can be summed up to three forms - surgery (for staging and tumour debulking), chemotherapy (e.g. platinum-based drugs and taxane) and radiation – which depend on histologic subtype and stage[20]. Computerised tomography scan, a preoperative imaging tool, is decisive in distinguishing patients suitable for primary debulking surgery or neoadjuvant chemotherapy prior to surgery[22]. For advanced-stage disease, the standard chemotherapeutic regimen is a combination of carboplatin and paclitaxel[23]. The combination of optimal cytoreductive surgery and chemotherapy results in more than 70% initial cure rate for EOC[24]. Yet, most women will relapse in less than 2 years and experience chemoresistant disease[25].

1.1.4. Ascites

At least one third of EOC patients are symptomatic for ascites, the accumulation of ascitic fluids in the peritoneal cavity, causing abdominal pain, early satiety, respiratory distress, fatigue and insomnia[26]. To alleviate symptoms caused by the accumulation of ascitic fluids, patients require further palliative care and repetitive paracentesis[25]. Many mechanisms are proposed to explain the unclear pathogenesis of ascitic fluids and include increased production of fluid by the peritoneum, fluid accumulation due to increased capillary permeability (facilitated by growth factors and cytokines) and fluid leakage from obstructed lymphatic vessels by tumour cells[27], [28]. Remarkably, the abnormal build-up of fluid has been linked to transcoelomic dissemination, the main route of metastasis occurring in ovarian cancer, facilitated by the enriched composition of ascitic fluids in pro-tumorigenic and anti-tumorigenic factors[29].

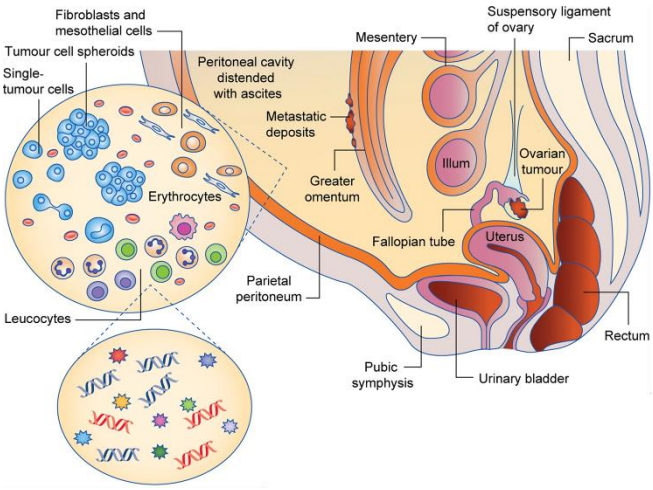

Figure 1.1 – Ascitic fluid in the peritoneal cavity of ovarian cancer patients. Source: adapted from [26]

More specifically, ascitic fluids contain a heterogeneous group of cellular (stromal cells and tumour cells as single cells or spheroids) and acellular components. The cellular fraction includes stromal cells (e.g., fibroblasts, mesothelial cells, endothelial cells, and adipocytes), innate cellular immune response factors (e.g., natural killer (NK) cells and dendritic cells), adaptative immune response factors (e.g., regulatory T cells) and cancer-associated cells (e.g., tumour-associated macrophages and cancer-associated fibroblasts (CAFs)). The acellular fraction includes angiogenesis-regulating factors (e.g., vascular endothelial growth factor and epidermal growth factor), adhesion-regulating factors (e.g., integrins), inflammatory and immune response factors (e.g., cytokines, chemokines, and bioactive lipids such as lysophosphatidic acid and sphingosine-1-phosphate[30], [31]), lysosomes, and proliferation regulating factors (e.g., lactate dehydrogenase, extracellular vesicles (EVs)). (Figure 1.1). Together with acellular components, the cellular components contribute to the tumour microenvironment and progression of ovarian cancer, presumably through soluble factors and EVs that facilitate intercommunication[32].

EVs derived from ascitic fluids have been studied, mainly regarding the transcriptome and proteome cargoes. Remarkably, microRNA content has been implicated in ovarian cancer spheroid growth[33], intact *MMP1* mRNA, whose expression is associated with poor prognosis in ovarian cancer, is selectively encapsulated in EVs that facilitate transcoelomic dissemination[34] and small EVs isolated from ascitic fluids' tumour cells are enriched in proteins associated with remodelling of the extracellular matrix, namely transforming growth factor-β-I, plasminogen activator inhibitor 1 and fibronectin, after chemotherapy[35].

1.2. Tumour microenvironment and metabolic crosstalk

1.2.1. Components of the tumour microenvironment

The tumour microenvironment, characterized by nutrient deprivation, hypoxia, immune escape and oxidative stress, is generally composed of various non-cellular components and cell types, including stroma cells and cancer cells, as described above, but also extracellular matrix and vasculature [36]. Each component can either promote tumour progression or suppress tumour formation. For example, NK cells, M1 macrophages, $CD8^+$ cytotoxic T cells, antigen-presenting cells and T-helper-1 cells act as

tumour growth suppressors, especially in the early stages of cancer. Other immune cells, such as neutrophils, regulatory T cells, tumour associated macrophages and $CD4^+$ T-helper-2 cells promote tumour immune escape by e.g., limiting the proliferation of $CD8^+$ cells (by regulatory T cells)[37]. The extracellular matrix is mainly secreted by hypoxia-stimulated CAFs and includes collagen, elastin, laminin, and fibronectin that support tumour growth and regulate intercellular and cell-matrix crosstalk[38]. EVs are a mean of molecule transfer among cells (tumorous, immune, stromal and endothelial cells) within the tumour microenvironment that, for example, deliver to tumour cells nutrients, such as amino acids, fatty acids, and TCA metabolites, to support tumour growth[36]. This mechanism of cell-to-cell communication, one of the most important within the tumour microenvironment, is associated with several cancer processes that can either promote or inhibit tumours depending on EV source cells and tumour microenvironment conditions[39]. Altogether, the tumour microenvironment constitutes a web of components with dynamic and reciprocal relationships that are important for cancer cell survival and tumour progression[37].

1.2.2. Metabolomic crosstalk in the tumour microenvironment

Metabolic alterations have long been considered a hallmark of cancer and involve catabolic and anabolic pathways of lipids, amino acids, vitamins, organic acids, carbohydrates[13]. Compared to normal cells, tumour cells have elevated energetic requirements in the evolving hostile microenvironment. In order to adapt, tumour cells increase consumption of glucose, in the presence of oxygen known as the Warburg effect or aerobic glycolysis, and glutamine[40]. Other mechanisms, such as lipogenesis and beta oxidation of fatty acids implicated in ovarian cancer' ascitic fluids, are alternatives to aerobic glycolysis as energy for tumour cells generated by reprogramming of lipid metabolism[41] and contribute to chemoresistance of cancer cells[42]. In opposition, normal cells depend mainly on mitochondrial tricarboxylic acid (TCA) and oxidative phosphorylation to accomplish their bioenergetic needs[43].

Beyond biosynthesis, metabolites can also act as signalling molecules in the tumour microenvironment. CAFs, cancer-associated adipocytes and immune cells are tumour-associated stromal cells that maintain metabolic relationships with cancer cells, resulting on tumour initiation, migration, and metastasis [36]. Radhakrishnan and colleagues demonstrated that ovarian cancer cells – and ascitic fluids –, stimulate glycolysis in normal fibroblasts and CAFs via lysophosphatidic acid, also implicated on phenotypical change of normal fibroblasts to CAFs[44]. CAFs and cancer cells can also secrete EVs that induce metabolic reprogramming by transferring bioactive molecules to recipient cells[45]. Notably, EVs derived from CAFs are internalized by cancer cells and supply them with TCA intermediates, thus altering the intracellular metabolism of cancer cells[46]. EVs derived from normal cells are also implicated in cancer processes, such as adipocyte tissue-derived EVs on evading apoptosis, sustaining proliferative signalling and promoting angiogenesis and metastasis[47].

The mechanisms of intercellular communication mediated by EVs occur both at paracrine and systemic levels. The formation of metastatic microenvironments generated by primary tumours in distant organs, or pre-metastatic niches, are influenced by EVs that deliver cargo in specific organs[48]. Fong *et al*. demonstrated that EVs reprogram metabolism non-cancer cells in the pre-metastatic niche by suppressing their glucose uptake[49].

1.3. Extracellular vesicles

The existence of EVs, suspected long before, was confirmed in the late 1960s[50]. Since then, the number of publications on the subject has increased over the years [51]. While there is no complete understanding of why they form – specific intercellular communication is now strongly supported, besides cellular waste disposal mechanism –, EVs are involved in many physiologic and pathologic processes[52]. Their composition can vary and include lipids, proteins, and nucleic acid species. In addition, as they are released to the extracellular space, EVs can be found in biofluids, such as saliva, urine, blood, plasma, and ascitic fluid[52].

Circulating cancer cells, biomolecules and EVs are emerging as biomarkers for cancer diagnosis and monitoring through liquid biopsy regarding the advantages of easier and non-invasive sample collection – this is essential in e.g., ovarian cancer as collecting tumour tissues is difficult by non-invasive means and improved diagnostic tools are necessary[53], [54]. In the case of EVs, loading cargo and cellular release can be regulated by environmental and cellular signals, including stress and inflammation [55], and cargo may correlate with clinical outcomes of cancer patients [56]. Furthermore, there is evidence that tumour cells secrete more EVs compared to non-tumour cells, which makes EVs an interesting target for anti-cancer therapy[57].

1.3.1. Nomenclature and biogenesis

The International Society for Extracellular Vesicles (ISEV) defines EVs as “the generic term for particles naturally released from cells that are delimited by a lipid bilayer and cannot replicate” [58]. EVs are released from all cell types and, despite being a highly heterogeneous group, are broadly classified in exosomes and ectosomes according to their biogenesis route, which is respectively endocytic and plasma membrane-derived[59]. Other terms, e.g. oncosomes and apoptotic bodies, can describe EV subtypes by measurable characteristics, such as size, density, morphology, function, source cell and biochemical composition [60].

Ectosomes are formed by outward budding of the plasma membrane and include microparticles and microvesicles[58]. Microvesicles are irregular in shape and can vary in a wide range of sizes, from 100 to 1000 nm[61]. Exosomes, smaller in size (typically from 30 to 150 nm)[62], have an endosomal origin and are formed by double invagination of the plasma membrane: cell membrane invagination originates early-sorting endosomes containing cell-surface proteins. Multivesicular bodies (MVBs) are

made up of intraluminal vesicles (ILVs) formed by inward budding of small late-sorting endosome (LSEs) domains. MVBs can fuse with the plasma membrane and ILVs are released through exocytosis as exosomes with an average size of 100 nm or with lysosomes to be degraded (Figure 1.2)[63], [64].

The budding process of ILVs and ectosomes is facilitated by lipids such as cholesterol, sphingomyelins and ceramides enriched in small membrane domains of LSE or ectosomes limiting membrane [65], [66]. The assembly of luminal cargo in ILVs is mediated by the four-domain endosomal sorting complex required for transport (ESCRT) and their associated protein Alix. In ectosomes there is evidence that at least ESCRT subunits I and III, together with their plasma membrane anchors, contribute to the luminal cargo [67], [68]. Therefore, some components of the assembly machinery are exclusive to ectosomes, as ILVs do not interact directly with the cell membrane. Others are common to both, such as the TSG101 (ESCRT-I protein), Alix, proteins of the tetraspanin family (e.g., CD63, CD81, CD9)[69] and integrins. These are commonly used as protein markers of EVs[58].

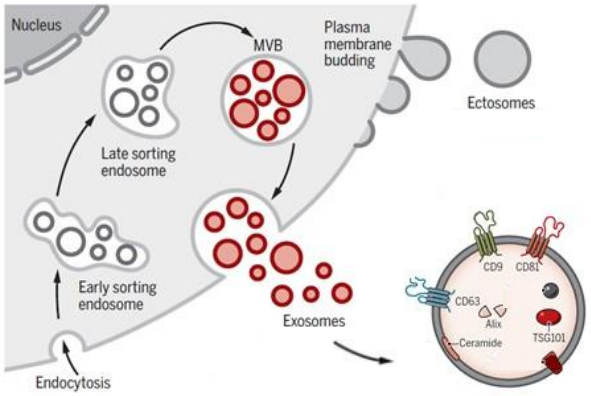

Figure 1.2 – Biogenesis pathway of ectosomes and endosomes. Source: adapted from [60].

1.3.2. Methods for EV isolation and characterization

Several methods are currently available to isolate and characterize EVs from cell culture media and biofluids. Some methods for the isolation include differential centrifugation, gradient ultracentrifugation, ultrafiltration, size-exclusion chromatography, polymer precipitation, immunoaffinity capture and microfluidics-based techniques[70]. Commercial kits to isolate EVs are also available, such as ExoQuick and EasySep[71]. Differential centrifugation is considered the "gold-standard" technique to isolate EVs and is widely used for both biofluids and cell culture media [72]. However, each method has advantages and disadvantages, namely regarding e.g., cost, efficiency, equipment required, and purity obtained, that must be evaluated before each experiment [70].

Characterization of EVs must comprise multiple techniques to support the separation of these from other particles and components. For a complete characterization of EV samples, ISEV recommends the quantification of the EV source in terms of e.g., volume of biofluid, the characterization of EV abundance by particle number and/or lipid or protein amount and the search for EV components and contaminants[58]. Many techniques are available today to provide population or single vesicle analysis. For example, the particle number of an EV population, can be assessed by nanoparticle tracking analysis (NTA). Protein composition can be characterized by Western blot, and should demonstrate the presence of EVs by detection of lipid-bilayer components (category 1) and cytosolic proteins (category 2), suggesting the isolation of lipid-bilayer particles that enclose intraluminal material as expected

for EVs, and absence of co-isolated material (category 3), such as lipoproteins, in purified samples of EVs[58]. In turn, visualization techniques, such as transmission electron microscopy (TEM), can provide information on single EVs' structure and composition (when combined with antibody detection)[73]. For the characterization of protein, metabolite, lipid content of EVs, chromatography coupled with mass spectrometry based methods are widely used for rapid screening of low concentrated molecules[74], [75].

1.4. Thesis aim

While the excessive accumulation of ascitic fluids constitutes a negative prognostic indicator in ovarian cancer, ascitic fluids are collected from patients as part of clinical procedures and are a reservoir of pro-tumorigenic components located close to the primary tumour site. EVs are among those components and their role in cancer processes, namely as mediators for the metabolic crosstalk within the tumour microenvironment, has been investigated. Ascitic fluids are associated with metastasis and chemoresistance, and metabolic alterations are considered a hallmark of cancer. In ovarian cancer, the transcriptome and proteome cargoes of EVs have been suggested in tumour progression. However, the metabolome remains poorly explored in EVs from ascitic fluids. The aim of this thesis was to characterize the metabolic signature of EVs from ascitic fluid of ovarian cancer patients. For this purpose, three main objectives were defined:

I. **Implement characterization methods with EVs derived from cell lines**. EVs from the ES-2 ovarian cancer cell line were protein characterized by Western blot, according to ISEV guidelines, and used to implement LC-MS platform for metabolomics.

II. **Characterize and validate the isolation procedure for EVs derived from biofluids according to the ISEV guidelines**. Different EV fractions were derived from ascitic fluids by differential centrifugation and characterized by Western blot, TEM and NTA. Peritoneal washes were additionally characterized as control samples.

III. **Characterize EVs derived from biofluids of ovarian cancer patients**. EVs isolated from ascitic fluids and peritoneal washes were characterized by Western blot, for the presence of CD63 and TSG101 (EV components) and apolipoprotein A-I (ApoA1-I) (non-EV component), TEM and NTA.

2. MATERIALS AND METHODS

2.1. Cell lines

EVs isolated from cell lines were used in this study for the implementation of EV characterization methods. EVs from two culture technical replicates of ES-2 ovarian cancer cell line, isolated and characterized by NTA and TEM by R. Mendes (iBET), were used for the implementation of Western blot and the analytical platform LC-MS in metabolomics and lipidomics. EVs isolated from the first culture technical replicate, ES-2 EVs I, were at 9.6×10^{10} particles/mL. EVs isolated from the second culture technical replicate, ES-2 EVs II, were at 4.5×10^{11} particles/mL (Figure S.8). In addition, the human hepatocellular carcinoma cell line Hep-G2 and cell culture media, provided by I.R. Gal (iBET), were used as controls for the lipid extraction method in lipidomics. MDA cells, provided by N. Lopes (iBET), and a concentrate of platelets collected from human blood and provided by D. Salvador (iBET) were used during the implementation of antibodies by Western blot.

2.2. Patient biofluid samples

Samples of ascitic fluids and peritoneal washes of 15 patients were collected with patient consent at Instituto Português de Oncologia de Lisboa Francisco Gentil (IPOLFG). Samples were sent immediately to the Pathological Anatomy Laboratory and centrifuged at 1200 rpm (259 × g) for 2 min in centrifuge Eppendorf 5804 R (rotor A-4-44, radius 16.1 cm). The supernatant and pellet were transferred to 15 mL or 50 mL tubes and frozen at -80 ºC, until the isolation of EVs (up to ~10 years). Supernatants of ascitic fluids were named from AF1 to AF11, and supernatants of peritoneal washes from PW1 to PW4. The volume of each sample received from IPOLFG for the isolation of EVs is listed in Table 2.1.

Samples of ascitic fluids (AF11 and AF7) and peritoneal washes (PW1) were used for step-by-step characterization of the discarded and isolated fractions collected during the isolation procedure, and for the final characterization of EVs isolated from patient samples by Western blot, NTA and TEM.

Table 2.1 – Sample identification and volume of ascitic fluids and peritoneal washes collected from 15 patients at IPOLFG for the isolation and characterization of EVs.

	ID	Volume (mL)
Ascitic fluid	AF1	25
	AF2	25
	AF3	15
	AF4	25
	AF5	25
	AF6	25
	AF7	15
	AF8	25
	AF9	25
	AF10	25
	AF11	15
Peritoneal washes	PW1	30
	PW2	15
	PW3	15
	PW4	15

2.3. Isolation of EVs from biofluids by differential centrifugation

2.3.1. Sample dilution and elimination of large components

EVs were isolated from ascitic fluids and peritoneal washes by differential ultracentrifugation, as described by Thery *et al.*[76] with minor modifications. Depending on the initial volume of ascitic fluids, 10 mL or 20 mL of sample were collected into one or two 50 mL tubes (Sarstedt, #62.547.254), respectively, and diluted in Dulbecco's phosphate-buffered saline (DPBS) (HyClone) to the final volume of 30 mL to reduce fluid viscosity. Samples of peritoneal washes were diluted when necessary up to 30 mL in a single 50 mL tube. The remaining volume of the biological samples (at least 1 mL) was stored at -80 °C for step-by-step characterization and omics. Next, samples were centrifuged at 2,000 × g (5810 R, Swing-bucket rotor A-4-81, Eppendorf), for 30 min. Pellets consisting of cells and dead cells were discarded, and the supernatants collected into new 50 mL tubes. To remove cellular debris and large particles, samples were centrifuged at 12,000 × g (Avanti J-26 XPI, JA-14 rotor, Beckman Coulter), for 45 min, and the pellets were discarded.

2.3.2. Collection of the EV fraction

Supernatants were collected into proper 31.5 mL ultracentrifuge tubes (Beckman Coulter, USA, #358126) and centrifuged at 110,282 × g (Optima LE-80K COLO2K09, SW28 rotor, Beckman Coulter), for 2 h, to precipitate EVs. Next, supernatants were discarded, and the EV pellets from the same initial sample were resuspended in 1 mL DPBS (HyClone) and pooled together. To dilute the resuspension, tubes were filled up to 30 mL using DPBS and samples were then filtered using a Filtropur S 0.45 µm filter device (Sarstedt, #83.1826), properly attached to a 30 mL syringe tip (Terumo Corporation, #A020102020102). The total filtrate was collected and filtered again using 0.22 µm filter devices (Acrodisc^{R} Syringe Filters with Supor^{R} membrane, Pall, #4612), thus removing large vesicles and membranes from the EV suspension. The final filtrate, collected into the same ultracentrifuge tube, was centrifuged at 110,282 × g (Optima LE-80K COLO2K09, SW28 rotor), for 70 min. To wash the EV pellet from proteins and other contaminants, pellets were re-suspended in 1 mL DPBS, and tubes filled again up to 30 mL. Next, samples were centrifuged at 110,282 x g (Optima LE-80K COLO2K09, SW28 rotor), for 70 min. Supernatants were discarded and the final pellet was resuspended in 100 µL of double-distilled water (ddH_2O). For Western blot (40 µL) and metabolomics (50 µL), aliquots of the resuspended pellet were snap-frozen in liquid nitrogen and stored in 1.5 mL micro tubes (Sarstedt, #72.706.200) at -80 °C. For TEM (5 µL) and NTA (5 µL), samples were stored in 1.5 mL micro tubes at -20 °C. All centrifugations were performed at 4 °C.

Extraction blanks for the EV isolation procedure were prepared by replacing biological fluid samples by ddH_2O and following the same isolation process as for ascitic fluids or peritoneal washes[77]. The total volume of discarded fractions and aliquots (1 mL) of the isolated fractions of samples AF11, AF7 and PW1 were snap frozen in liquid nitrogen and stored at -80 °C for further step-by-step characterization. Isolated fractions are collected for the subsequent isolation step and discarded fractions are discarded during the procedure of EV isolation. Samples AF5, AF6, AF8, AF10, PW2, PW3 and PW4 were processed using rotor SW-32 Ti (Beckman Coulter) assembled in Optima L100 XP (Optima Coulter) ultracentrifuge, instead of Optima LE-80K COLO2K09 (SW28 rotor), in all ultracentrifugation steps.

2.4. Characterization of EVs

2.4.1. Western blot

2.4.1.1. Determination of total protein concentration

Total protein concentration (mg/mL) of samples for Western blot characterization, including EVs and isolation fractions, was measured by Nanodrop One^{c} (Thermo Fisher Scientific) spectrophotometer. Protein A280 application and 1 Abs=1 mg/mL sample type option were set for proper measurements of

total protein concentration. For samples of EVs, ddH_2O was used as blank. Other measurements were acquired using DPBS as blank.

2.4.1.2. Protein precipitation using trichloroacetic acid

Protein precipitation by trichloroacetic acid (TCA) (Merck) was performed to isolated or discarded fractions of the isolation procedure collected for step-by-step characterization with total protein concentration below 0.3 µg/µL. First, 1 volume of 20% TCA (Merck Millipore) was added to samples (volume of sample for TCA precipitation ranged between 200 and 2800 µL, depending on initial protein concentration and volume collected), and the preparation was incubated for 10 min, at RT. Samples were centrifuged at 15,000 x g (5810 R centrifuge, fixed-angle rotor F45-30-11, Eppendorf), for 10 min (RT) and the supernatant collected and discarded carefully to not disturb the pellet. The protein pellet was washed with two volumes of EtOH 80% to remove any residual TCA. The final suspension was incubated for 10 min (AF11) at -20 °C or O/N (AF7 and PW1) at -20 °C. After centrifugation at 15,000 x g (5810 R centrifuge, fixed-angle rotor F45-30-11) for 10 min (4 °C), supernatant was discarded, and the washing step repeated for 10 min at -20 °C. Supernatant was discarded again, and the protein pellet left to air-dry. Dry pellet was then re-suspended in 5-10 µL of 2X NuPAGE™ LDS sample buffer (4X) (Invitrogen, #NP0007) and stored at -20 °C until further use.

2.4.1.3. SDS-PAGE and Western blot

Samples were prepared in 1X NuPAGE™ Lithium Dodecyl Sulfate (LDS) sample buffer (4X) (Invitrogen, #NP0007) and 1X NuPAGE™ reducing agent (10X) (Invitrogen, #NP0004) to the final volume of 20 µL and protein amount between 0.9-6.63µg, and boiled at 70 °C (ThermoMixer C), for 10 min. Next, samples were centrifuged for 5 min at 10,000 × g and loaded onto NuPAGE™ 4-12% Bis-Tris gel (Thermo Fisher Scientific, #NP0322), in a Mini Gel Tank (Thermo Fischer Scientific, #A25977) apparatus, properly filled with NuPAGE™ MOPS SDS running buffer (20X) (Invitrogen, #NP0001). Next, 500 µL of 1X NuPAGE™ antioxidant (Invitrogen, #NP0005) was added to the cathode chamber and SDS-PAGE performed at 200 V, using Electrophoresis Power Supply (EPS 600, Pharmacia Biotech).

Molecular weight-separated proteins, in the SDS-PAGE gel were transferred to polyvinylidene difluoride (PVDF) iBlot 2 Transfer Stack membranes (Invitrogen, #IB24002), using iBlot dry blotting system (Invitrogen), at 20 V, for 7 min. Blocking solution, consisting of 5% non-fat milk (PanReac AppliChem, #A0830) in 1X Tris buffered saline (TBS) (Sigma, # T6664) with 0.1% (v/v) Tween 20 (TBST) (Merck, #8.22184.0500), was prepared and incubated with membranes for 90 min, under agitation (RT), to avoid unspecific antibody binding. Polyclonal rabbit anti-CD63 (#EXOAB-CD63A-1), anti-TSG101 (#EXOAB-TSG101-1) and anti-CD81 (#EXOAB-CD81A-1) (Systems Biosciences) primary antibodies, for specific EV components, were diluted (1:1000), in blocking solution with 0.1% sodium azide, and incubated with membranes O/N (4 ºC), under agitation. Monoclonal rabbit anti-

apolipoprotein A I (Abcam, UK, #ab52945), a non-EV component, dilution (1:1000) was prepared similarly.

Next, membranes were washed in TBST, 3 times for 10 min, and incubated with diluted (1:5,000 or 1:20,000) goat anti-rabbit HRP secondary antibody (System Biosciences, SBI, # EXOAB-KIT-1) for 1 h under agitation, at RT. Membranes were washed again, with TBST as described before, and briefly with DPBS to remove Tween 20. For a chemiluminescent protein detection, membranes were incubated for 5 min in GE Healthcare Amersham™ ECL Prime Western Blotting Detection Reagent (GE Healthcare, #12316992) or Cytiva Amersham ECL Select Western Blotting Detection Reagent (GE Healthcare, #45-000-999**),** covered from light, and developed in iBright FL1500 Imaging System (Invitrogen, #A44241), using Chemi Blots mode and signal accumulation routine. A commercial Human Exosome Lysate Positive Protein Control (10 µg/µL) (SBI, # EXOAB-POS-1) was used as positive control sample for the detection of CD63, CD81 and TSG101.

2.4.2. Nanoparticle Tracking Analysis

2.4.2.1. Instrument preparation and cleaning procedure

NTA NS300 instrument (Malvern Panalytical), configured with a 405 nm laser and a Scientific CMOS camera, was properly assembled, following manufacturer's instructions. NanoSight NTA 3.3 software was initiated and flow cell, internal and external tubing connectors, washed three times, by loading 1 mL syringes (B Braun™ Injekt™, Thermo Fisher Scientific, #10303002) with filtered (0.22 µm) ddH_2O in the inlet port. Next, filtered (0.22 µm) DPBS was loaded and pumped into the flow cell, as described before. Syringe pump rate was set to 500 until flow cell was completely clean and filled, with no visible bubbles.

2.4.2.2. Sample preparation and analysis

Samples of EVs were diluted using filtrated (0.22 µm) DPBS to adjust particle concentration to 10^6-10^9 particles/mL before analysis. Samples were loaded in 1 mL syringes (B Braun™ Injekt™, Thermo Fisher Scientific**,** #10303002**)** and syringe pump rate set to 1000. Before each measurement, the flow cell was flushed with 400-500 µL of sample and camera gain adjusted, so that most particles on screen were properly focused. Camera level was set to 15, screen gain to 10.0 and detection threshold to 6. Tracks of 30 s each were recorded 3 times per sample at 20-40 frames/s with the temperature of the laser unit controlled to 22-24 °C. Particle concentration (particle/mL) and size measurements (mean, mode, standard deviation) were acquired using NanoSight NTA 3.3 software (Malvern Panalytical) and data analyzed using Microsoft Excel and GraphPad Prism 9.

2.2.1. Transmission electron microscopy

Sample processing and imaging of EVs and isolation fractions was carried out by A.L. Sousa and E.M. Tranfield from the Electron Microscopy Facility at the Instituto Gulbenkian de Ciência (IGC) as follows. First, suspended EVs were mixed (1:1) with 4% (w/v) formaldehyde in Phosphate Buffer 0.1M and fixed for 5 min. Preparations (5 µL) were then loaded on copper 100 mesh glow-discharged EM grid coated with 1% (w/v) formvar (Agar Scientific) and left to absorb for 5 min. Grids were washed in 10 drops of distilled water. Next, 1 drop of 2% (w/v) uranyl acetate was added to negative-stain grids for 5 min. Excessive liquid was removed using No. 1 Whatman filter paper. TEM was performed using an Olympus-SIS Veleta CCD camera coupled to a FEI Tecnai G2 Spirit BioTWIN microscope (FEI) at an acceleration voltage of 120 keV.

2.5. Characterization of the metabolic signature of EVs

Untargeted metabolomics and lipidomics by liquid chromatographic tandem mass spectrometry (LC-MS) platform were performed to characterize the metabolic content of EVs. In each experiment, quality controls (QCs) samples were prepared by pooling equal aliquots (30-50 µL) of samples of the same analytical run together to equilibrate the analytical platform and remove variability in retention time deviation over time[78]. The run order was as follows: blank, QC (10×), samples (3-6, randomized), QC (1×), samples (3-6, randomized), QC (1×). Blank samples were used for background subtraction[79]. In metabolomics, additional commercial samples were run after blank and before the 10 initial QCs samples to assess the system suitability using C18 column, namely Quad LC-MS QCRM, (Waters, #186007362) and amide column, namely Aminoacids mix (Thermo Scientific, #20088).

For all chromatography columns, in metabolomics and lipidomics, measurements were conducted in positive and negative modes of heated electrospray ionization (HESI) to maximize metabolite/lipid coverage. We acknowledge A. C. L. Guerreiro, C. Almeida and C. Correia and the UniMS – Mass Spectrometry Unit at ITQB/IBET (Oeiras, Portugal) for LC-MS data acquisition and data processing in Compound Discoverer software (Thermo Fischer Scientific).

2.5.1. Untargeted metabolomics

2.5.1.1. Extraction of metabolites from EVs

The extraction of metabolites was based on Altadill *et al*.[80] protocol with some modifications. Two aliquots of ES-2 EVs I and II, at 9.6×10^{10} and 4.5×10^{11} particles/mL respectively, were diluted in DPBS to obtain three different particle concentrations: 10^6, 10^8 and 10^{10} particles/m. Next, the 6 samples were split in two tubes each with 50 µL. Two volumes of ddH2O were added to each tube and 5 freeze/thaw cycles in liquid nitrogen/wet ice, of 1 min each step, were performed to disrupt EV membranes and release intravesicular content[81]. 600 µL of cold (-20 °C) methanol (Merck, #106018) were

added to samples and the mixture vortexed for 20 s and incubated at -20 °C, for 1 h, to facilitate protein precipitation. After centrifugation at 14,000 × g (5810 R centrifuge, fixed-angle rotor F45-30-11) at 4 °C, for 13 min, supernatant was collected and split into two 1.5 mL tubes, each with 250 µL of sample. In total, 24 samples were prepared.

2.5.1.2. Relative metabolite quantification by liquid chromatography-mass spectrometry (LC-MS)

Two liquid chromatography columns were used: Waters Acquity UPLC BEH Amide column (2.1x150 mm, 2.5 µm particle size, P/N 186003023) and Waters XBridge C18 column (2.1x150 mm, 3.5 µm particle size, P/N 186003023), both installed on an UltiMate 3000 UHPLC (Thermo Scientific) system coupled to a Q Exactive Focus Hybrid Quadrupole-Orbitrap Mass Spectrometer (Thermo Scientific).

For the C18 column, samples were left to dry, under vacuum conditions, in a SpeedVac (Labconco) instrument and the pellet was resuspended in 100 µL water with 0.1% formic acid (FA) (Optima LC-MS, Fisher), before injection on the column. Next, samples were injected (10 µL) onto the column at 30 °C. Flow rate was 400 µL/min. Mobile phase A consisted of water with 0.1% FA and mobile phase B of acetonitrile (ACN) with 0.1% FA, using the following program: 0-13 min, 1-99% B; 13-15 min, 99% B; 15-16 min, 99-1% B; 16-20 min, 1% B. HESI in positive mode was achieved under the following parameters: capillary voltage at 3.8 kV, capillary temperature at 320 °C, sheath gas flow of 60 a.u., auxiliary gas of 20 a.u., auxiliary gas heat temperature at 320 °C. For negative mode was as follows: capillary voltage was at 3.0 kV, capillary temperature at 320 °C, sheath gas flow of 60 a.u., auxiliary gas of 20 a.u., auxiliary gas heat temperature at 320 °C.

For the amide column, samples were directly injected (10µL) onto the column at 40 °C. Flow rate was 350 µL/min. Mobile phase A consisted of 3 mM ammonium acetate (pH 4) and mobile phase B of ACN, using the following program: 0-6 min, 90-50% B; 6-7 min, 50-40% B; 7-9 min, 40% B; 9-10 min, 40-90% B; 10-20 min, 90% B. HESI in positive and negative mode was achieved under the same parameters as for the C18 column.

Full MS scan spectra were acquired from 75 – 1125 m/z, with 70 000 in resolution (full width at half maximum, FWHM, at 200 m/z) and 1×10^6 automatic gain control (AGC). For positive mode, drift in m/z values was corrected with lock mass of m/z 144.98215 and m/z 445.12003, and for negative mode m/z 112.98550 was used. To facilitate metabolite identification, a data-dependent MS/MS acquisition method was performed using the top 3 most intense ions selected for higher-energy collisional dissociation (HCD). Stepped normalized collision energies (NCE) of 20, 40 and 60 were applied and MS/MS scan spectra were acquired at 17 500 resolution (FWHM at 200 m/z) and 1×10^5 AGC, with maximum injection time of 100 ms and dynamic exclusion of 6 s.

2.5.1.3. Data processing with XCMS

The raw spectral data recorded by the instrument as profile data was converted to centroid data using the MSConvert GUI tool of ProteoWizard software[82]. The mzML files were then pre-processed using the XCMS R language package[83], which includes algorithms to filter and identify peaks (xcmsSet()), match peaks across samples (group()), correct retention time (retcor()), fill missing peak data (fillPeaks()), but also to visualize peak intensities by retention time (getEIC()), and create report of aligned peak intensities (peakTable()) and mass-to-charge (m/z) ratios. All parameters were set to default values except the bandwidth, which was set to 10 s (bw = 10).

2.5.2. Lipidomics

2.5.2.1. Lipid extraction using isopropanol

Lipids were extracted from EVs in two different concentrations based on Sarafian et. al [84]. The first experiment was performed using 50 µL of ES-2 EVs I at 10^9 particles/mL. Three dilutions of ES-2 EVs in isopropanol (IPA) were tested, 1:1, 1:2 and 1:3. Extraction blanks (50 µL) of the EV isolation procedure were prepared similarly. All samples were prepared in replicate, called replicates of lipid extraction, and 12 samples were prepared in total.

The second experiment was performed using 50 µL of ES-2 EVs II at 4.5×10^{11} particles/mL. In, addition, 200 µL of Hep-G2 cells at 2.5×10^6 cells in ddH_2O [85] and 200 µL of Hep-G2 cell culture media were used to test the lipid extraction method efficacy. Two volumes of IPA were added to ES-2 EVs and three volumes of IPA to Hep-G2 cells and Hep-G2 cell culture media. Replicates of lipid extraction were prepared only for Hep-G2 samples. In total, 6 samples were prepared.

Samples were vortexed for 1 min and incubated at RT for 10 min. To improve protein precipitation, samples were incubated O/N at -20 °C and centrifuged at 14,000 x g (5810 R centrifuge, fixed-angle rotor F45-30-11) for 20 min at 4 °C. Supernatant was collected and stored at -20 °C.

2.5.2.2. Ultra-Performance Liquid Chromatography-Mass Spectrometry (LC-MS)

Samples of the first experiment were injected (5 µL) onto an Acquity UPLC HSS T3 column (150 mm × 2.1 mm, 1.8 µm; Waters™) at 55 °C and flow rate of 300 µL/min. Mobile phase A consisted of ACN:H2O (60:40, v:v) mixed with 10 mM ammonium formate and 0.1% formic acid and mobile phase B of IPA:ACN (90:10, v:v) mixed with 10 mM ammonium formate and 0.1% formic acid. The LC gradient was: 0-4.1 min, 40-43% B (curve 5); 4.1-4.3 min, 43-50% B (curve 6); 4.3-24.1 min, 50-54% B (curve1); 24.1-24.3 min, 54-70% B (curve 6); 24.3-36.1 min, 70-99% B (curve 1); 36.1-36.3 min, 99-40% B (curve 6); and 36.3-40 min, 40% B (curve 6). HESI in positive mode was achieved under the following parameters: capillary voltage at 3.8 kV, capillary temperature at 320 °C, sheath gas flow of 60 a.u., auxiliary gas of 20 a.u., auxiliary gas heat temperature at 320 °C. For negative mode was as follows: capillary voltage was at 3.0 kV, capillary temperature at 320 °C, sheath gas flow of 60

a.u., auxiliary gas of 20 a.u., auxiliary gas heat temperature at 320 °C. Samples (7 µL) of the second experiment were run under the same conditions, only using a different column (Acquity UPLC BEH Shield RP18 column (150 mm × 2.1 mm, 1.7 µm; Waters™).

Full MS scan spectra were acquired from 100-1500 m/z, with 70 000 in resolution (FWHM at 200 m/z) and 1×10^6 AGC. For positive mode, drift in m/z values was corrected with lock mass of m/z 144.98215 and m/z 445.12003; and for negative mode m/z 112.98550 was used. To facilitate compound identification, a data-dependent MS/MS acquisition method was performed using the top 3 most intense ions selected for HCD. NCE of 20, 40 and 60 V were applied, and MS/MS scan spectra were acquired with 17 500 resolution (FWHM at 200 m/z) and 1×10^5 AGC. The maximum injection time was set to 100 ms and the dynamic exclusion to 6 s.

2.5.3. Data processing using Compound Discoverer software

All spectra were imported to Compound Discoverer software v3.1 (Thermo Fisher Scientific). Filtering was carried to detect compounds (mass tolerance=3 ppm, min. peak intensity=1×10^7) and group compounds (mass tolerance=3 ppm, RT tolerance=0.2 min). Filtered features were then searched on the following nodes: mzCloud (precursor mass tolerance=3 ppm, FT fragment ion tolerance=5 ppm, Cosine identity search, match any activation energy, recalibrate spectra), ChemSpider (mass tolerance=3 ppm, search by formula or mass) and Predicted Compositions (mass tolerance=3 ppm, intensity threshold=0.01%, min. pattern coverage=100%). The Chemspider databases used to obtain compound IDs were the following: Kyoto Encyclopedia of Genes and Genomes (KEGG) and Human Metabolome Database (HMDB) for metabolomics; LipidMAPS for lipidomics. mzLogic data analysis node was applied to combine information of mzCloud with Chemspider. For metabolomics and lipidomics (experiment 1), compounds with any type of annotation from mzCloud, ChemSpider or Predicted compositions were exported. For experiment 2 (lipidomics), compounds were only considered if they were identified as full match in the ChemSpider search or mzCloud search.

2.5.4. Metabolite pathway analysis using MetaboAnalyst

Compounds from metabolomics, identified by Compound Discoverer, were further analysed using MetaboAnalyst v.5.0 online platform[86]. The list of compound names was entered as a one column data for enrichment analysis by Over Representation Analysis (ORA) approach. The database used was Small Molecule Pathway Database (SMPDB). From lipidomics, only features detected in the ES-2 EVs samples with peak intensity above 1×10^6 were considered.

3.
RESULTS AND DISCUSSION

3.1. Implementation of characterization methods for EVs

3.1.1. Western blot for the detection of EV and non-EV protein components

Western blot remains the most used technique to evaluate EV isolates for the presence of EV and non-EV protein components. Several EV proteins, both membrane proteins (category 1) and cytosolic proteins (category 2), are suggested by the ISEV for a complete characterization[58]. Proteins with transmembrane domains and glycosylphosphatidylinositol (GPI)-anchored proteins, such as tetraspanins (e.g., CD63) and integrins, confirm the presence of lipid-bilayer structures. Cytosolic proteins, such as TSG101 and heat shock protein HSP70, suggest enclosure of luminal material as expected for EVs. Further characterization of non-EV proteins (category 3) disclose the purity degree of isolates. Apolipoproteins, such as apolipoprotein A-I (ApoA-I), suggest the co-isolation of lipoproteins. ISEV also suggests that at least one protein of the three mentioned categories must be analysed, thus confirming the nature and purity of EV isolates [58]. In this study, two membrane proteins, CD63 and CD81, one cytosolic, TSG101, and one non-EV component, ApoA-I, were tested by Western blot.

3.1.1.1. Antibody implementation using positive control sample

Detection of EV components

Antibodies for EV components were implemented using a commercial positive control sample consisting of a lysate of exosomes isolated from human serum. The secondary antibody dilution was at 1:5,000. Membranes were exposed to LED light for different times, 13 s (CD63), 14 s (TSG101), and 1 min 45 s (CD81), in iBright FL1500 Imaging System. CD63 was detected using ECL Select Western Blotting Detection Reagent, instead of ECL Prime Western Blotting Detection Reagent, since otherwise no signal was detected. Both detection reagents are suitable for low protein levels but the former is the most sensitive[87]. Contrary to the specific bands expected[88], multiple bands were observed in each membrane at various molecular weights (Figure 3.1), most of them at >50 kDa. In each membrane,

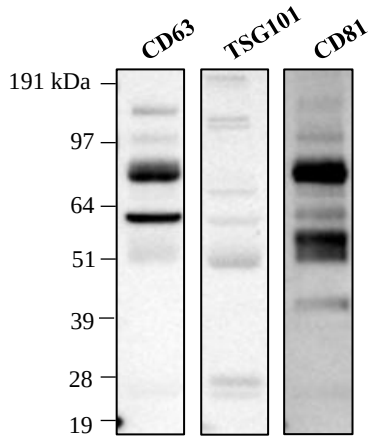

Figure 3.1 – **Western blot analysis of Human Exosome Lysate Positive Protein Control with anti-CD63, anti-TSG101 and anti-CD81**. CD63, TSG101 and CD81 were detected in positive control used for antibody implementation. Each lane was loaded with 15 µg of protein. Uncropped blots are available as supplementary material (Figure S.1)

bands had different signal intensities, such as 62 kDa and ~52-58 kDa (less intense) bands in CD63 membrane. Sharp and smeared bands were also observed, such as 62 kDa and ~52-58 kDa (smeared) bands in CD63 membrane, and ~51-60 kDa and 64 kDa bands in TSG101 membrane.

Western blot results (e.g., band intensity, range of molecular weights, single/multiple bands) for CD63, CD81 and TSG101 proteins may vary depending on the EV source sample and EV isolation method used. Exosomes isolated from feline plasma and urine by the same differential centrifugation method originated single or multiple bands at the expected molecular weights in Western blot analysis of CD63, CD81 and TSG101 [89]. Therefore, we may observe different Western blot results for EVs isolated from ascitic fluids, peritoneal washes, or serum. EVs are categorized according to their characteristics into heterogenous groups: exosomes, for example, differ in size, content, and cellular origin [90] and biological samples contain different categories of EVs originated from different cell types[91]. Exosomes of the positive control sample were isolated from human serum using the commercial ExoQuick™ kit, but it is possible that a population, rather than a single group of EVs, was isolated.

Moreover, based on Deun *et al*. [92] exosomes isolated by four different methods (ultracentrifugation, OptiPrep density gradient centrifugation, ExoQuick and Total Exosome Isolation) displayed different CD63 and TSG101 protein levels. In specific, the ExoQuick preparations harvested more contaminating non-vesicle proteins and were less enriched in exosome markers when compared to the ultracentrifugation preparations[92]. Thus, we can hypothesize that the positive control sample did not consist of a pure EV isolate, and that the multiple bands observed were non-specific. In this case, CD63, CD81 and TSG101 blocking peptides could have been used to help differentiate specific bands from non-specific bands [93].

On the other hand, multiple bands at various molecular weights can be originated if proteins have isoforms or post-translational modifications[93]. In fact, both glycosylated and deglycosylated CD63 (~25 kDa) have been found enriched in exosomes isolated from human immunodeficiency virus type-

1 infected cell culture supernatants[94]. TSG101 isoforms have been found and implicated in several cancer types, such as in nasopharyngeal carcinoma[95] and Burkitt lymphoma [96]. CD81 encoding transcript variants were also found in humans[97]. Moreover, tumour-cell derived EVs are highly glycosylated[98], therefore we may observe higher molecular weight forms of surface glycosylated proteins in tumour EVs[99]. If multiple bands in the positive control sample were non-specific due to the isolation method, we may expect better results for EVs isolated by differential centrifugation. If the problem was caused by multiple isoforms or post-translational modifications, we may expect different results for EVs isolated from different sample sources. Therefore, samples of EVs or EV components from different sources, as well as some protocol variations, were tested prior to EVs from patient samples.

ApoA-I as non-EV component

Co-isolation of lipoproteins, such as very-low density lipoproteins (VLDL), low density lipoproteins (LDL), high density lipoproteins (HDL), and chylomicrons, is a common setback in many EV purification techniques. Chylomicrons are formed in enterocytes and contain ApoA-I transiently before transferring it to HDL when reaching the bloodstream[100]. ApoA-I is present in ascitic fluids and has been suggested as biomarker to differentiate late-stage variants of ovarian cancer [101]. The lipidic nature of lipoproteins may interfere with downstream characterization of EVs by metabolomics/lipidomics. Therefore, ApoA-I antibody was implemented as purity control for EVs, using ascitic fluids and a concentrate of platelets as positive control sample in different total protein amounts (2, 5, 10 and 20 µg).

As expected for the predicted molecular weight of ApoA-I (31 kDa) [102], a sharp band was detected at ~26 kDa in both ascitic fluids and platelets (Figure 3.2), and signals were more intense with the increase in total protein. An additional band at ~51-57 kDa was observed, but not for ascitic fluids (Figure S.2). Although a loading control sample would be needed to confirm the following claiming, the ApoA-I protein detection appears to have originated more intense bands in platelets, suggesting that ApoA-I is more abundant in platelets than in the sample of ascitic fluid tested. In such case, it is possible that the conditions used to reduce ApoA-I in increased amounts may have been insufficient and caused protein aggregation in multimers due to the formation of disulfide bonds [93]. This is suggested as the extra band is approximately twice the molecular weight of the expected band. If a single band is detected in ascitic fluids, later in this study we may characterize EVs isolated from biological samples for the presence of different molecular weight proteins by incubating simultaneously membranes with more than one primary antibody. This way we can save as much sample as possible for other characterization methods, namely metabolomics.

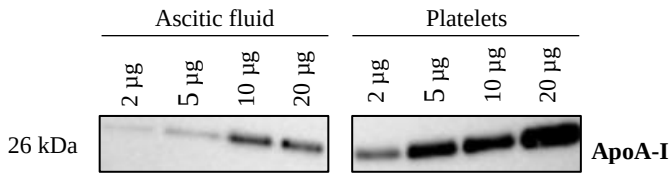

Figure 3.2 – **Western blot analysis of ascitic fluids and platelets at different total protein amounts with anti-ApoA-I.** ApoA-1 was detected in ascitic fluids and platelets (control) at 2, 5, 10 and 20 µg amounts of total protein. Uncropped blots are available as supplementary material (Figure S.2).

3.1.1.2. Troubleshooting and protocol optimization

After preliminary results using the positive control sample, some protocol variations regarding sample preparation and electrophoresis conditions were tested. During the implementation of antibodies, samples were boiled at 70 °C, for 10 min, to denature proteins in NuPAGE™ LDS Sample Buffer and NuPAGE™ Sample Reducing Agent, thus following the instructions of the Western blot reagent's manufacturer. Proteins with transmembrane domains, such as CD63 and CD81, may aggregate when boiled at higher temperatures [103]. This time, two conditions of sample preparation were tested side-by-side using the SBI positive control sample. One sample was denatured at 70 °C for 10 min, as before, and the other was denatured at 95 °C for 5 min. A similar pattern of bands was observed in both conditions (Figure 3.3.A). Therefore, the initial conditions of protein denaturation, 70 °C for 10 min, were maintained for the next experiments.

Jong *et al*. run tetraspanins under non-reducing conditions and observe disparate results, e.g. smeared CD63 for non-reducing SDS-PAGE and multiple band CD63 for reducing SDS PAGE [104]. Hence, non-reducing conditions were tested for CD63 and CD81 in ES-2 EVs. A similar pattern of

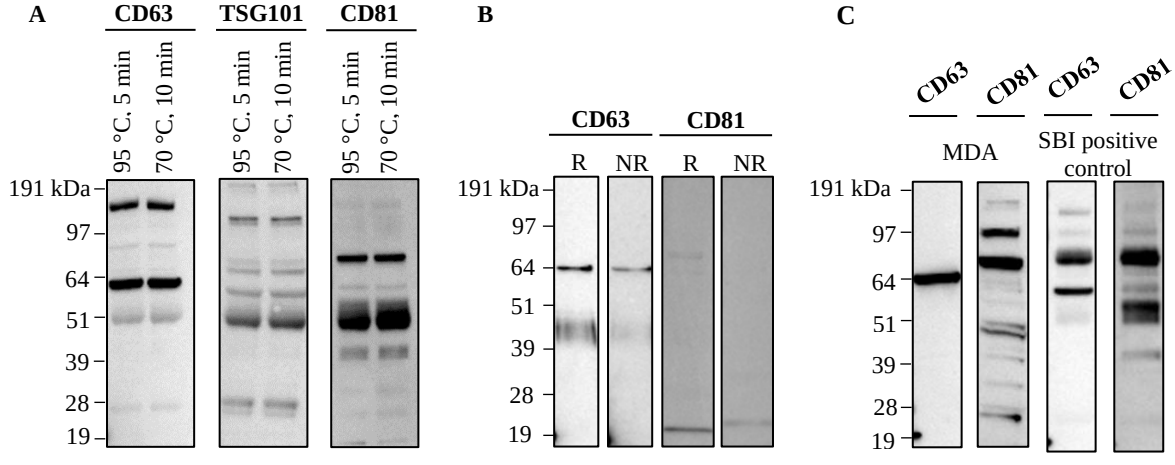

Figure 3.3 – **Western blot analysis of cells and EVs prepared in different conditions with anti-CD63, anti-TSG101 and anti-CD81.** A) CD63, TSG101 and CD81 were detected in Human Exosome Lysate Positive Protein Control prepared at different conditions of time and temperature for protein denaturation. Each lane was loaded with 10 µg of protein. B) CD63 and CD81 were detected in ES-2 EVs run under reducing (R) and non-reducing (NR) SDS-PAGE conditions. Each lane was loaded with 4.31 µg of protein. C) CD63 and CD81 were detected in MDA cells and Human Exosome Lysate Protein Positive Control with different patterns. Each lane was loaded with 15 µg of protein. Uncropped blots are available as supplementary material (Figure S.3, Figure S.4, Figure S.5, respectively).

bands was observed in both conditions (Figure 3.3.B) and the initial reducing conditions were maintained for next experiments. Interestingly, no multiple bands were observed in this experiment. For reducing conditions, one sharp band at ~64 kDa and one smeared band at ~40-50 kDa were detected in CD63 membranes. In CD81 membrane, one sharp band was detected at ~21 kDa. Compared to previous experiments, different protein amounts (15 µg vs. 4.31 µg) and secondary antibody dilutions (1:5,000 vs. 1:20,000) were used in different samples (positive control vs. ES-2 EVs).

To understand whether results in Figure 3.3.B were sample-related, anti-CD63 and anti-CD81 antibodies were tested in MDA cells using 15 µg of protein (Figure 3.3.C). Multiple bands were detected in CD81 membranes, but with different intensities compared to the SBI positive control. Also, a single band was detected in CD63 membrane of MDA cells. Depending on sample, CD63 can be detected at a very wide range of molecular weights and the most intense bands observed in MDA cells or SBI positive control were within reported ranges (from ~35 to >110 kDa) [105], [106]. In fact, tumour cell derived EVs are highly glycosylated and compared to cell membranes, several glycosylations are more enriched in EVs than in the source cell[98]. This can explain the observations in ES-2 EVs, as several forms of glycosylated CD63 were observed. In MDA cells, a single glygosylated form was observed.

Altogether, it was possible to conclude that the temperature of protein denaturation and electrophoresis conditions did not significantly impact the outcome. Different samples, however, led to different results, and may be associated with EV isolation protocols and EV source samples. Moreover, a secondary antibody dilution of 1:20,000 was tested with improving results for TSG101 (Figure S.6), encouraging further tests using ES-2 cells and EVs.

3.1.1.3. Characterization of EVs from cells by Western blot

According to the ISEV guidelines, for a complete assessment of EV proteins collected from cell culture conditioned media by Western blot, EVs and the source cells should be loaded side-by-side in specified protein amounts [58]. Western blot for EVs collected from the conditioned medium of ES-2 cell culture and ES-2 cells was performed accordingly using 4 µg of protein. In CD63 membranes, a band at ~64 kDa was detected in ES-2 cells and EVs (Figure 3.4). Another band (smeared) at ~40-50 kDa, was also detected but only in EVs. In TSG101 membranes, between 39 and 66 kDa, one sharp band at ~60 kDa and other less intense bands, at ~39, 49, 50 and 66 kDa, were detected for ES-2 cells. Another band at ~63 kDa was detected, but only for EVs. Interestingly, bands at ~50 kDa in cells and EVs seem to not be the same, despite having the same molecular weight. In EVs membrane, this band was more intense than the other of higher molecular weight. In CD81 membranes, between 14 and 28 kDa, one band at ~26 kDa was detected in ES-2 cells. Two other bands at ~21 kDa ~28 kDa, the second being the most intense, were also detected but only for EVs.

Compared to their source cells, EVs must be enriched in reported EV components [58]. In exosomes and microvesicles, the glycosylated CD63 and the non-glycosylated CD81 (expected molecular weight: ~26 kDa) are the most common markers among the tetraspanin family [107]. Compared to ES-2 cells, the glycosylated CD63, as suggested by the smeared band and high molecular weight band at ~64 kDa, was enriched in EVs [107], [108], as well as the non-glycosylated CD81 protein (band at ~21 kDa) [107]. The enrichment in TSG101, with expected molecular weight of 50-52 kDa[106], was not as clear. EVs may have not been fully lysed, as TSG101 can not be detected in intact ES-2 EVs [109]. Another possibility is that ES-2 EVs have low TSG101 levels as observed in Neuro2a cell line compared to neuro2a EVs [110]. Ultimately, ES-2 EVs have been previously characterizaed by TEM and NTA by R. Mendes (Figure S.8) and altogether results support the isolation of EVs.

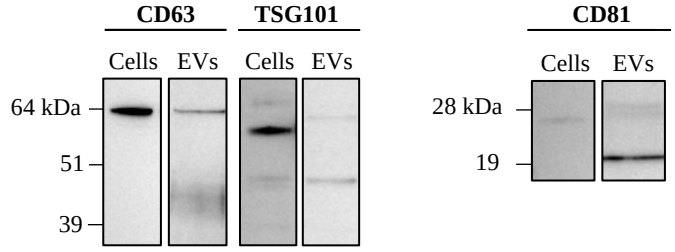

Figure 3.4 – **Western blot analysis of ES-2 cells and EVs with anti-CD63, anti-TSG101 and anti-CD81.** Each lane was loaded with 4 µg of protein. Uncropped blots are available as supplementary material (Figure S.7).

3.1.2. Characterization of ES-2 EVs metabolic signature

Mass spectrometry techniques are the method of choice for the characterization of many molecules, including proteins, metabolites, and lipids. LC-MS uses a liquid mobile phase composed of two-liquid gradient and a stationary phase from which analytes are slowly released as a result of changes in the gradient. Despite lipids may be considered a subset of metabolites, they require different solvents for mass spectrometry[111]. In this study, ES-2 cell-derived EVs were used to implement the metabolomic workflow that can be further applied to characterize the lipid content of EVs from different biofluids by LC-MS.

3.1.2.1. Untargeted metabolomics

ES-2 EVs I and II were prepared for metabolite extraction in three different concentrations to test the minimum amount of EVs necessary to generate good peak signals on LC-MS: 10^6, 10^8 and 10^{10} particles/mL, considering the initial particle concentration of the ES-2 EVs samples (9.6×10^{10} and 4.5×10^{11} particles/mL, for ES-2 EVs I and ES-2 EVs II respectively) and reported EV concentration ($10^{11\text{-}12}$ particles/mL)[80] used in metabolomics. Replicates of metabolite extraction were also prepared along with EVs to evaluate the reproducibility of the metabolite extraction method. In total, 24 samples were analysed in C18 column and amide column, each in positive and negative modes of ionization to maximize metabolome coverage.

QCs were prepared for different uses by pooling equal amounts of the biological test samples together into a single representative sample. In this study, 10 initial QCs (conditioning QCs) were used to equilibrate the analytical platform prior to sample analysis by coating sites in the analytical system that absorb metabolites to remove variability in compound retention times, calculated as the time spent by compounds on the column from injection to detection, and stabilize the detector response[78]. Data obtained during this phase is variable and must be removed prior to any following data processing[78]. In addition, QCs at the middle and at the end of the run were used to check for systematic errors, such as changes in retention time and peak shape, that can later be mathematically corrected[78].

Variations in retention time deviation were observed in conditioning QCs (Figure S.9), emphasizing the importance of incorporating them prior to analysis. To achieve higher reproducibility data, the first 7 conditioning QCs were removed from subsequent processing of data (Figure 3.5). The same procedure was applied for the other columns and modes of ionization.

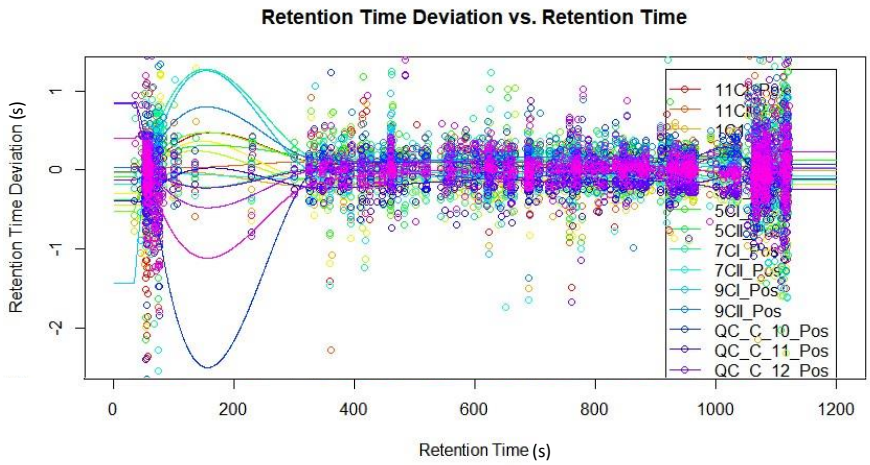

Figure 3.5 – **Retention time deviation vs. retention time of extracted metabolites from ES-2 EVs.** Data obtained by LC-MS using C18 column and positive ionization mode was processed with XCMS package. First conditioning QCs used to equilibrate column and improve reproducibility of data originated high variability in retention time deviation (Figure S.9). For this reason, only last 3 QCs (in the figure) were considered for subsequent data processing.

Once corrected the retention time deviation, the extracted ion chromatograms (EIC) containing the intensity of signals at 80-1100 m/z by retention time, for both columns in positive and negative modes of ionization, were extracted using XCMS R package (Figure 3.6). For the C18 column and positive mode, 1130 features (i.e., peak groups representing the same analyte) were identified. For the C18 column and negative mode, 1075 features were identified. For the amide column and positive mode, 930 features were identified. For the amide column and negative mode, 973 features were identified. High intensity peaks at the beginning and end of the separation zone may indicate contaminants. We hypothesized whether centrifuge tubes and filters used during the EV isolation procedure were releasing plastic polymers onto samples due to mechanical forces[112], [113]. Bearing that in mind, we implemented extraction blanks, prepared by replacing the biological samples with water and applying the same EV isolation procedure, to check for contaminants [114]. Features identified in biological

samples and blanks can be considered contaminants and used for baseline subtraction. Moreover, EICs revealed humps throughput the separation zone. These humps may suggest poor sample preparation and purification or that samples are too complex to be chromatographically resolved. In this case, ultra-high resolution mass spectrometry techniques are recommended [115].

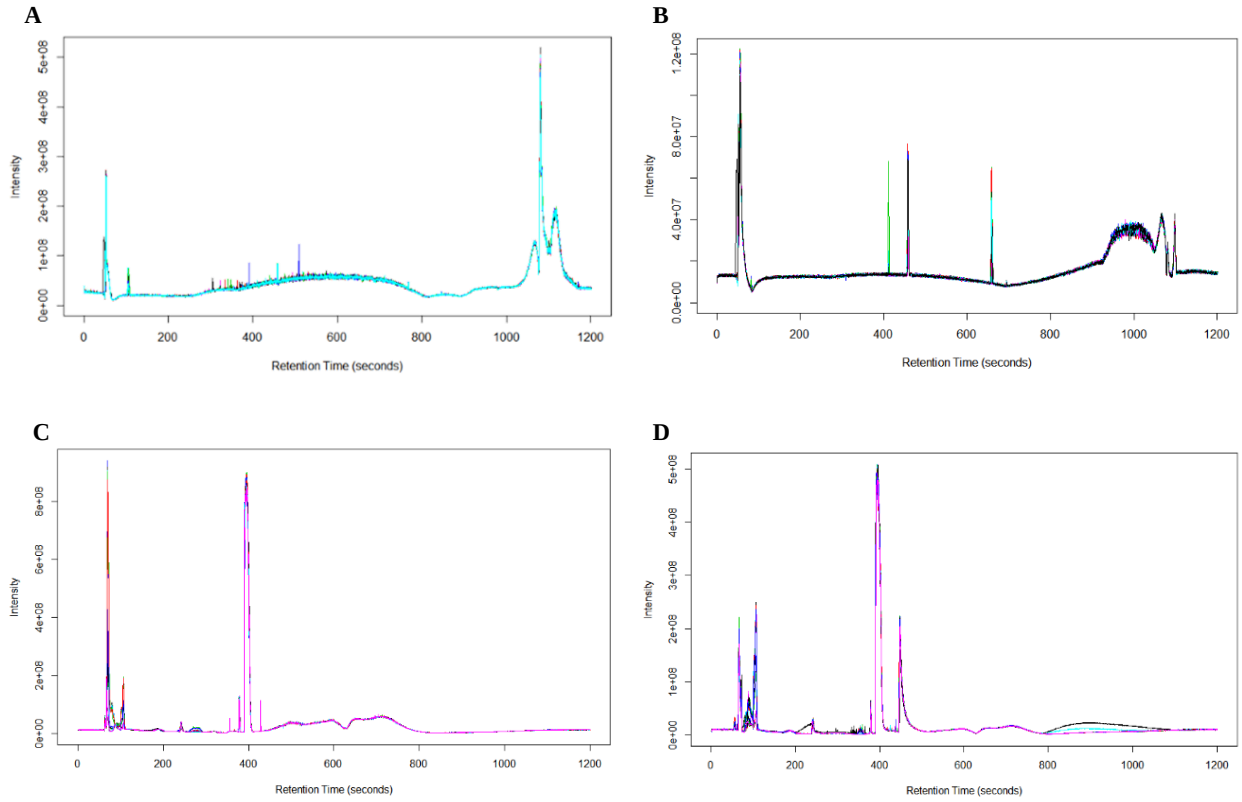

Figure 3.6 – **Extraction ion chromatograms (EIC) using C18 and amide columns in positive and negative ionization modes by XCMS**. A – C18 (positive mode); B – C18 (negative mode); C – amide (positive mode); D – amide (negative mode).

The optimal range of peak intensity considered for this MS equipment was 10^6-10^9[116]. Detailed analysis (Table 3.1) indicates that for C18 column most peaks were within the optimal range and a smaller proportion was at suboptimal intensity (less frequent) or above 10^9. More specifically, in negative mode of ionization, the percentage of optimal peaks to total peaks were 90.9%, 91.0% and 91.4% on average for the two metabolite extraction replicates using ES-2 EVs I and II samples at 10^6, 10^8 and 10^{10}, respectively. In positive mode of ionization, were 98.1%, 98.2% and 98.5%, respectively. For the amide column, most peaks have suboptimal intensity. Less than 40% of peaks were within the optimal range, thus, compound identifications may be more reliable for C18 column. More specifically, in negative mode of ionization, the percentage of optimal peaks to total peaks were 33.0%, 32.1% and 32.9% on average for the two metabolite extraction replicates using ES-2 EVs I and II samples at 10^6, 10^8 and 10^{10}, respectively. In positive mode of ionization, were 35.6%, 34.6% and 36.2%, respectively. The three EV concentrations tested, 10^6, 10^8 and 10^{10} particles/mL, did not lead to much different ratios.

This may have been caused by insufficient membrane lysis to extract the EV metabolome. In fact, intact particles on precipitate after metabolite extraction were observed by TEM (Figure S.11). Variations on the protocol can be tested such e.g. freeze/thaw cycles with higher thawing temperature coupled to a sonication step[117]. Moreover, more peaks with optimal intensity were identified using C18 column. This may be correlated with the sample concentration step performed after metabolite extraction and before LC-MS analysis only performed using samples for C18 column.

Table 3.1 – **Total features identified in ES-2 EVs by peak intensity using XCMS R package**. ES-2 EVs I and II were prepared in three concentrations, 10^6, 10^8 and 10^{10} particles/mL (P/mL), for metabolite extraction in replicates of extraction. Optimal peak intensities are between 10^6-10^9.

		C18 (positive)			C18 (negative)			Amide (positive)			Amide (negative)		
	P/mL	$<10^6$	10^6-10^9	$>10^9$	$<10^6$	10^6-10^9	$>10^9$	$<10^6$	10^6-10^9	$>10^9$	$<10^6$	10^6-10^9	$>10^9$
ES-2 EVs I	10^{10}	5	1113	12	95	979	1	620	373	0	649	324	0
		6	1112	12	94	980	1	628	365	0	653	320	0
	10^8	4	1114	12	97	977	1	652	341	0	662	311	0
		13	1105	12	89	985	1	645	348	0	656	317	0
	10^6	9	1109	12	96	978	1	637	356	0	648	325	0
		7	1111	12	93	981	1	635	358	0	650	323	0
ES-2 EVs II	10^{10}	4	1114	12	89	985	1	644	349	0	654	319	0
		5	1113	12	88	986	1	644	349	0	657	316	0
	10^8	8	1110	12	95	979	1	650	343	0	666	307	0
		10	1108	12	104	970	1	649	344	0	659	314	0
	10^6	9	1109	12	108	966	1	641	352	0	655	318	0
		13	1105	12	92	982	1	645	348	0	655	318	0

To evaluate the reproducibility of the metabolite extraction method, each replicate of extraction was plotted for the three particle concentrations tested of the two ES-2 EV samples. A linear relationship was found in all conditions: peaks of extraction replicates were very similar to each other ($r^2 > 0.9$) suggesting reproducibility of the method (Figure 3.7). Additionally, the coefficient of variation (CV) of extraction replicates was calculated and considered acceptable up to 20%. Results confirmed the reproducibility of the method. For the C18 column positive mode, 88% or more features had CV<20% in replicates of extraction prepared from ES-2 EVs samples at 10^6, 10^8 and 10^{10} particles/mL. For the other columns or ionization modes were as follows: for the C18 column negative, 91%; for the amide column positive mode, 82%; amide column (negative mode), 87%.

Further analysis was carried using the Compound Discoverer software. For the C18 column and positive mode, 46 compounds were identified (Table S.1). For the C18 column and negative mode, 20 compounds were identified (Table S.2). For the amide column and positive mode, 102 compounds were identified (Table S.3). For amide column and negative mode, 87 compounds were identified (Table S.4). Out of 66 metabolites, 11 lipids or lipid-like molecules, 12 amino acids, peptides, or analogues, and 4 benzenoids were identified in C18 column. Out of 189 metabolites, 46 lipids or lipid-like molecules, 11 amino acids, peptides or analogues, and 19 benzenoids were identified in amide column.

For pathway analysis, compounds were imported to MetaboAnalyst and analysed by column, both ionization modes together. For the input data of C18 column (Table S.5), the top three pathways identified in both positive and negative modes of ionization were glutathione metabolism (p-value = 0.0905, enrichment ratio = 3.899), ammonia recycling (p-value = 0.182, enrichment ratio = 2.561) and

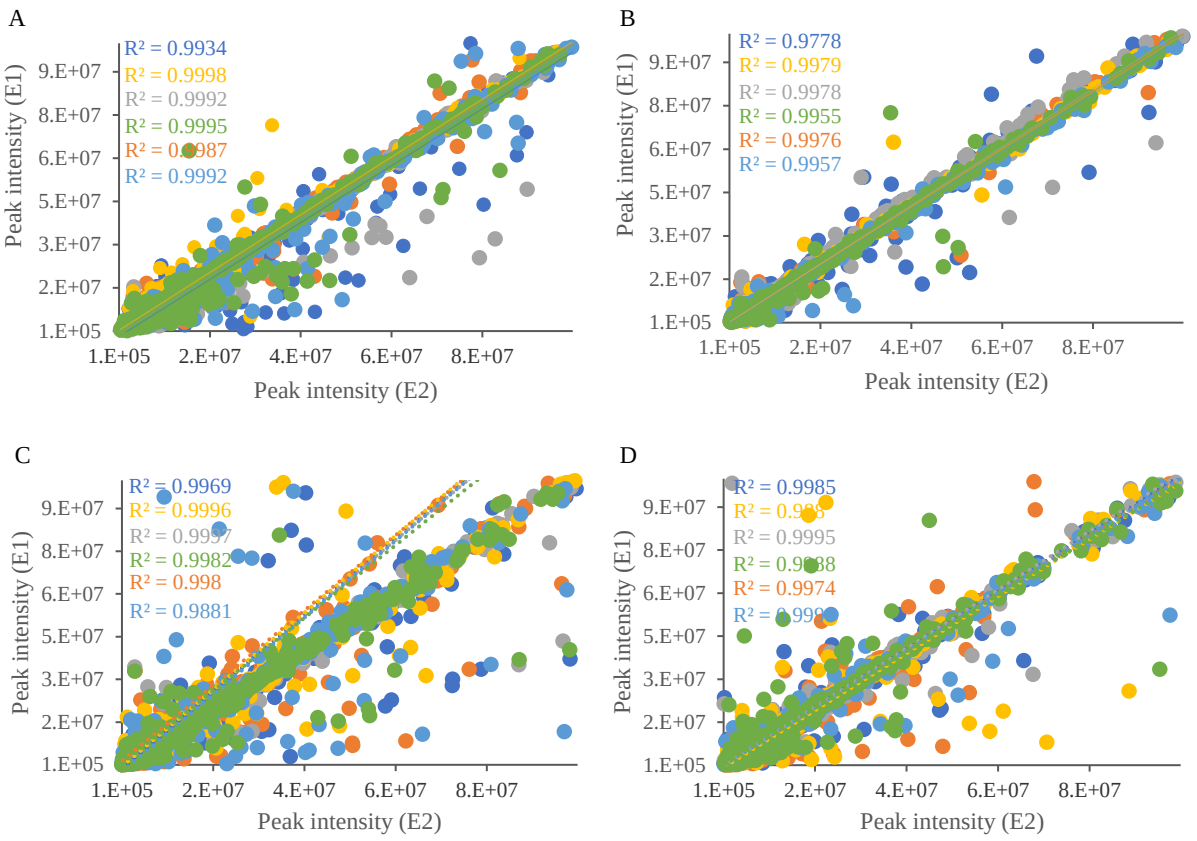

Figure 3.7 – **Peak intensity of features identified in metabolite extraction replicates from ES-2 EVs.** A – C18 column and positive mode; B – C18 column and negative mode; C – Amide column and positive mode; D – Amide column and negative mode. Dark blue – ES-2 EVs I at 10^6 particles/mL; Yellow – ES-2 EVs II at 10^6 particles/mL; Grey – ES-2 EVs I at 10^8 particles/mL; Green – ES-2 EVs II at 10^8 particles/mL; Orange – ES-2 EVs I at 10^{10} particles/mL; Light blue – ES-2 EVs II at 10^{10} particles/mL. E1 – replicate 1 of metabolite extraction; E2 – replicate 2 of metabolite extraction).

glycerol phosphate shuttle (p-value = 0.239, enrichment ratio = 3.717) (Figure 3.8.A) (Table S.6). For the amide column (Table S.7), the three top pathways identified in both positive and negative modes of ionization were riboflavin metabolism (p-value = 0.0912, enrichment ratio = 1.835), fatty acid biosynthesis (p-value = 0.237, enrichment ratio = 1.075) and beta oxidation of very long chain fatty acids (p-value = 0.0912, enrichment ratio = 1.835) (Figure 3.8.B)(Table S.8).

It has been reported that in ovarian cancer, adipocytes of the omentum provide neoplastic cells fatty acids, and induce beta oxidation to support tumour growth [118]. The fatty acid oxidation acts as an efficient and selective source of energy for nutrient deprived cancer cells by generating large amounts of ATP [119]. Moreover, ovarian CAFs supply neoplastic cells cysteine and glutathione to protect cells from chemotherapy. Cysteine helps maintain balance in cells exposed to redox stress caused by chemotherapy as a component of glutathione[36]. Similarly, an enrichment in riboflavin, involved in lipid metabolism[120], has been associated with chemoresistance in ovarian cancer [121]. Another source of nutrients for tumours are amino acids, namely glutamine. The enzymatic conversion of glutamine into glutamate, with pro-tumorigenic signalling activity, originates the by-product ammo-

nia which is enriched in the tumour microenvironment and further recycled into glutamate and downstream amino acids as a nitrogen source to support tumour biomass [122]. Also, the metabolism of glycerol-3-phosphate, a component of the glycerol phosphate shuttle, associated with glycolysis, de novo synthesis of triglycerides and oxidative phosphorylation [123], is in ovarian cancer associated with tumour migration and poor prognosis by the activity of glycerol-3-phosphate acyltransferase [124].

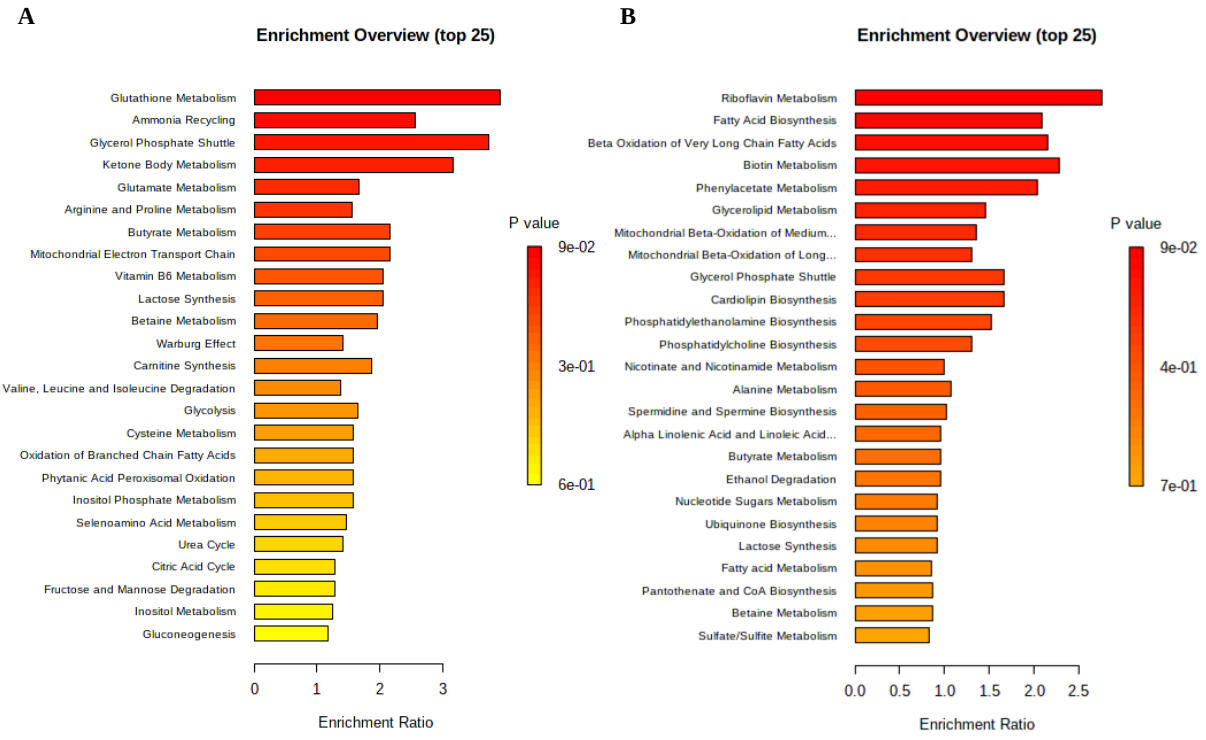

Figure 3.8 – **Top 25 of enriched metabolite sets on ES-2 EVs by LC-MS untargeted metabolomics using C18 and amide columns**. Compounds identified using Compound Discoverer were imported to MetaboAnalyst for pathway analysis of C18 (A) and amide (B) column metabolites.

Altogether, these results sustain the hypothesis that ES-2 EVs contain pro-tumorigenic metabolites, such as amino acids and lipids, and stimulated a change of approach from untargeted metabolomics to lipidomics for a more targeted characterization of the EV content.

3.1.2.2. Lipidomics

For the lipidomic approach, two experiments were conducted. The first experiment was performed using a less concentrated sample (1×10^9 particles/mL), prepared from ES-2 EVs at 9.6×10^{10} particles/mL for three IPA dilutions (1:1, 1:2 and 1:3), and generated few intense peaks in all conditions tested (Figure 3.9.C) and Compound Discoverer identified only 4 compounds with full match from mzCloud, ChemSpider or Predicted compositions nodes (Table S.9). From the total ion chromatograms (TIC), some of the peaks found in extraction blanks (Figure 3.9.A) matched with peaks found in EV samples Figure 3.9.B). Therefore, the extraction blank sample must be used for contaminant subtraction

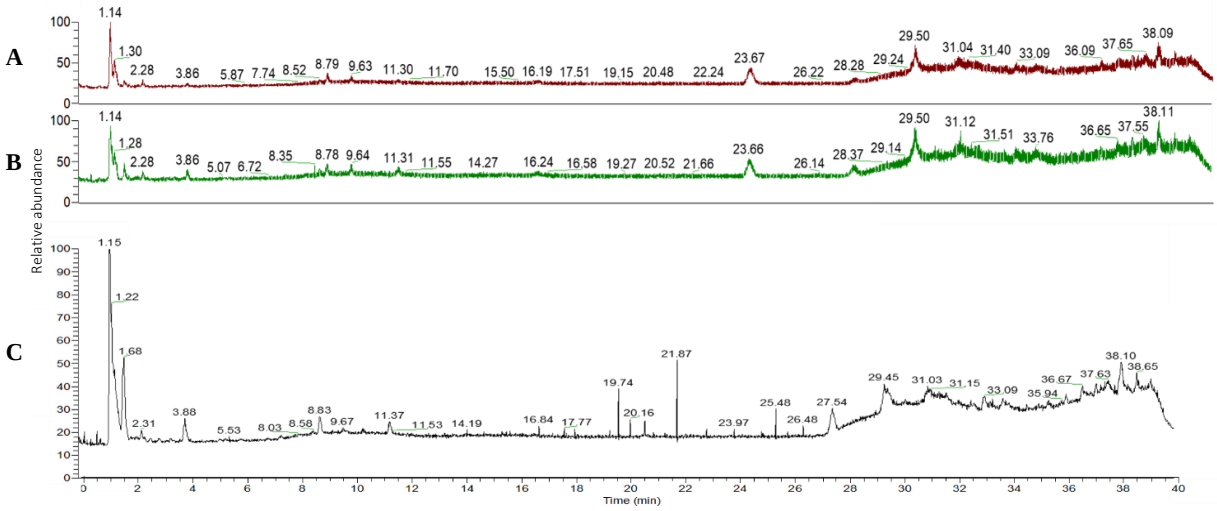

Figure 3.9 – **Total ion chromatograms of extraction blank, ES-2 EVs and QC**. A – Extraction blank of the isolation procedure; B – ES-2 EVs; C – QC generated by pooling all samples (extraction blanks and ES-2 EVs) together. Three lipid extraction conditions were tested, 1:1, 1:2 and 1:3 dilution of EVs (at 10^9 particles/mL) in IPA.

to allow more reliable compound identifications and we may need to increase the concentration of particles. Because few peaks were detected, a further analysis using MetaboAnalyst was not conceivable.

The second experiment was performed using the more concentrated ES-2 EVs sample (4.5×10^{11} particles/mL) of the two ES-2 EVs samples. Another sample of Hep-G2 cells and Hep-G2 cell culture media were implemented to assess the efficacy of the lipid extraction method. If lipids were identified in Hep-G2 samples, then we could hypothesize that in the first experiment lipids were extracted but were at very low levels to be detected by the implemented analytical platform.

For the positive mode of ionization, 68 compounds were identified in all samples, including EVs (Table S.10). For the negative mode of ionization, 18 compounds were identified in all samples (Table S.11). For both modes of ionization (Table S.12), the top three pathways identified using MetaboAnalyst platform were betaine metabolism (p-value =0.0723, enrichment ratio =4.435), methylhistidine metabolism (p-value =0.0833, enrichment ratio = 11.641) and urea cycle (p-value = 0.126, enrichment ratio = 3.210) (Figure 3.10) (Table S.13).

Betaine is a specific ovarian cancer metabolite, derived from the choline metabolism and involved in the methylation cycle, with increased levels on EOC and metastatic ovarian cancer tissue compared to normal [125]. Methylation in several cell types is associated with malignant phenotypes of cancer [126]. Methylhistidine, resulting from elevated protein degradation, is a proposed marker of colorectal cancer [127] further associated with tissue repair and remodelling, alterations in the inflammatory response and redox imbalance [128]. Moreover, the dysregulation of the urea cycle has been considered a metabolic hallmark in cancer, with implications on the anabolism of molecules, such as pyrimidines, implicated in tumour proliferation and aggressiveness [129].

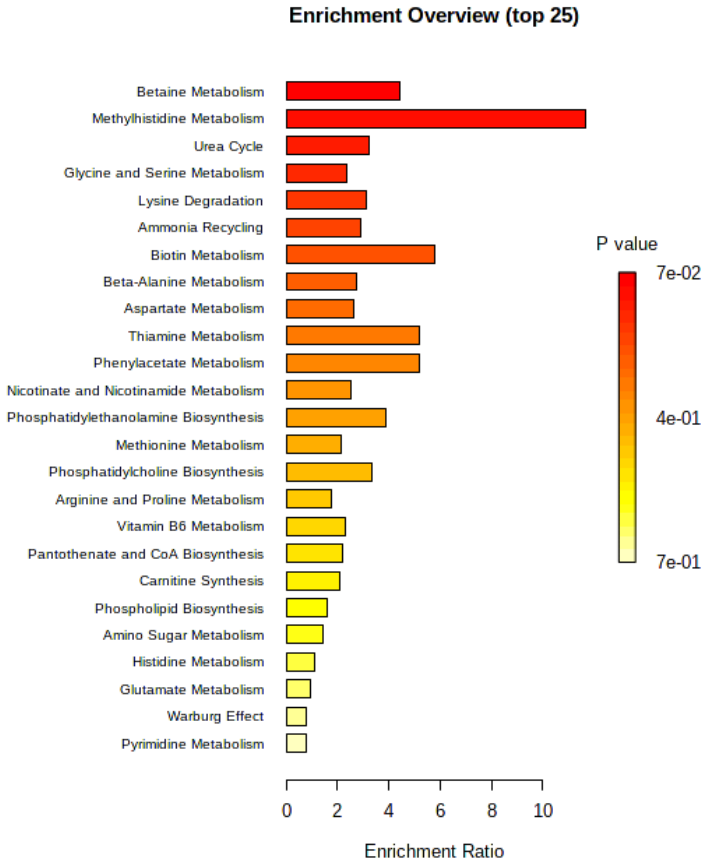

Figure 3.10 – **Top 25 of enriched metabolite sets on ES-2 EVs by LC-MS lipidomics**. Compounds identified using Compound Discoverer were imported to MetaboAnalyst for pathway analysis.

From Hep-G2 results, peaks were more intense for cells than cell culture media, and further analysis of identified compounds was not investigated for it was not the scope of the experiment. However, results from cells suggested that the method for lipid extraction led to the recovery of lipids – if the first experiment led to little intense peaks, then it most likely was not method-related but due to the concentration of EVs (too low) as proposed before. Therefore, better outcomes for EVs might be achieved if the concentration of particles was increased.

3.2. Validation of EV isolation protocol in patient biofluids

3.2.1. Characterization of patient cohort

Ascitic fluids and peritoneal washes were obtained during surgical resection of ovarian tumours from 15 patients with different subtypes: 11 high-grade serous adenocarcinoma (HGSC), 1 low-grade serous carcinoma (LGSC), 1 endometrioid carcinoma (EC) and 1 non-gynaecologic adenocarcinoma (NGC) (Table 3.2). Since the accumulation of ascitic fluids represents a poor disease prognosis, peritoneal washes were collected from patients without ascitic fluids and used as control group of a less aggressive disease.

Table 3.2 - **Ascitic fluids and peritoneal washes used for EV isolation and patient characterization**. Diagnostic: HGSC – High-grade serous adenocarcinoma; LGSC – Low-grade serous adenocarcinoma; EC – endometrioid carcinoma; NGD – non-gynaecologic adenocarcinoma. Status: NPC – positive for neoplastic cells; DD – deceased from the disease; DF – disease free; DC – disease carrier. C125 – C125 levels in ascitic fluids or peritoneal washes. N.A. – not available.

	ID	Harvest date	Patient age	Liquid cytology	Diagnostic	Stage	Status	CA125 (U/mL)
Ascitic fluid	AF1	31.01.2012	73	NPC	HGSC	IVB	DD	6872.9
	AF2	07.05.2013	56	NPC	HGSC	IIIC	DD	31423.0
	AF3	17.05.2013	62	NPC	HGSC	IIIC	DD	83582.3
	AF4	06.05.2013	60	N.A.	N.A.	IC	DF	724.3
	AF5	16.09.2015	60	NPC	HGSC	IVA	DF	561.4
	AF6	31.10.2013	65	NPC	HGSC	IIIC	DF	98836.0
	AF7	05.10.2013	73	NPC	HGSC	IIIB	DC	88858.8
	AF8	21.11.2011	64	NPC	HGSC	IIIC	DD	3776.4
	AF9	N.A.	N.A.	N.A.	N.A.	N.A.	N.A.	877.0
	AF10	13.05.2015	69	NPC	HGSC	IIIC	DC	22755.2
	AF11	31.05.2013	57	NPC	HGSC	IIIA	DD	1751.7
Peritoneal washes	PW1	18.12.2020	72	NPC	HGSC	IIIC	DC	3707.5
	PW2	06.01.2021	84	NPC	EC	IA	DD	7778.6
	PW3	23.02.2021	43	NPC	HGSC	IVA	DF	9299.1
	PW4	23.04.2021	62	NPC	NGD	IVB	DD	928.1

3.2.2. Step-by-step characterization of the isolation fractions

Differential centrifugation for the isolation of EVs is suitable for large volume preparation and provides low contamination risk with additional isolation reagents [70]. The low cost technique is also the most used for metabolomic studies of the EV content[130]. For these reasons, a differential centrifugation-based method was implemented in this study for the isolation of EVs from patient samples. A step-by-step characterization of the isolation procedure provides information on the efficiency of the isolation method and/or the purity of the isolates[131]. During the isolation procedure (Figure 3.11) fractions to be isolated ("isolated fractions") or discarded ("discarded fractions") were collected and characterized by the three characterization methods, Western blot, TEM and NTA. Two samples of ascitic fluid, AF7 and AF11, and another sample of peritoneal washes, PW1, were used for this purpose. Isolated fractions include the source biological sample (AF/PW), supernatants collected during differential centrifugation (S2 and S3), resuspended pellets and filtrate during washing steps (RP4, FP4, RP5) and the final pellet (EVs). Discarded fractions include pellets collected during the differential centrifugation (P2 and P3) and supernatants collected after ultracentrifugation steps (S4, S5 and S6).

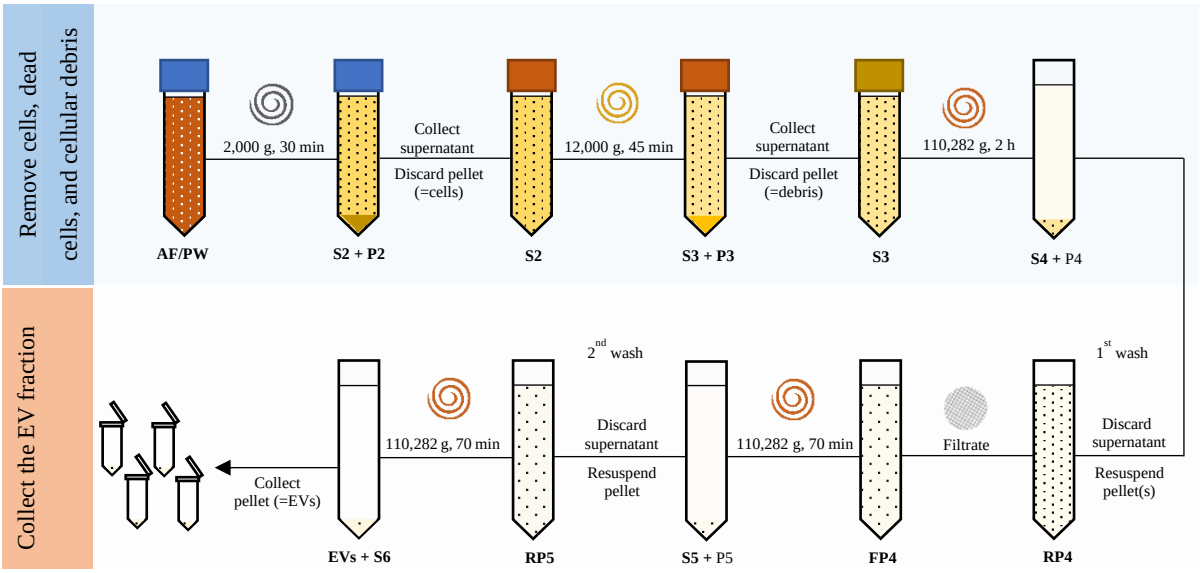

Figure 3.11 – **Fractions of all steps in the isolation process.** In bold are fractions characterized by NTA, TEM and WB for step-by-step characterization of the isolation process. **AF/PW** – ascitic fluid or peritoneal washes; **S2** – supernatant after low-speed centrifugation; **P2** – pellet after low-speed centrifugation; **S3** – supernatant after high-speed centrifugation; **P3** – pellet after high-speed centrifugation; **S4** – supernatant after 1st ultracentrifugation; P4 – pellet after 1st ultracentrifugation (EV fraction); **RP4** – re-suspended pellet after 1st ultracentrifugation; **FP4** – filtrate of re-suspended pellet after 1st ultracentrifugation; **S5-** supernatant after 2nd ultracentrifugation; P5 – pellet after 2nd ultracentrifugation (EV fraction); **RP5** – P5 fraction re-suspended in 30 mL; **S6** – supernatant after 3rd ultracentrifugation; **EVs-** fraction of purified exosomes.

3.2.2.1. Protein detection by Western blot

Samples of isolated and discarded fractions were tested for the presence of EV components, CD63 and TSG101, and non-EV component, ApoA-I, by Western blot. Samples with low protein concentration (less than 0.3 µg/µL) were protein concentrated using TCA prior to the characterization. Except for AF11 RP5, all other concentrated fractions were loaded in equal protein amounts onto gels along with non-concentrated fractions by biological sample. CD81 and CD63 are in the same ISEV category and biological samples were limited as indicated by the protein quantification assays. For this reason, CD81 was not analysed in ascitic fluids and peritoneal washes.

No signal was detected for CD63, TSG101 and ApoA-I in AF11 RP5 (0.9 µg) lane (Figure 3.12). RP5 is an isolated fraction, therefore the volume collected for step-by-step characterization by Western blot, TEM and NTA was as small as possible to not interfere with the EV recovery by the last isolated fraction. The theoretical protein concentration after precipitation was insufficient so that RP5 could be loaded in equal protein amounts as the other AF11 fractions, thus only 0.9 µg of protein were used instead of 6.63 µg. Besides the small volume used for TCA precipitation, RP5 is also a more diluted fraction when compared with e.g., FP4. Furthermore, we characterized AF11 RP4 and FP4 fractions with and without TCA precipitation, and it suggested that protein is lost during TCA precipitation (Figure S.10)[132]. All these factors may have contributed to the lack of signals for CD63, TSG101 and ApoA-I, which in turn may not be correlated with the presence or absence of EV and non-EV components in AF11 RP5 fraction.

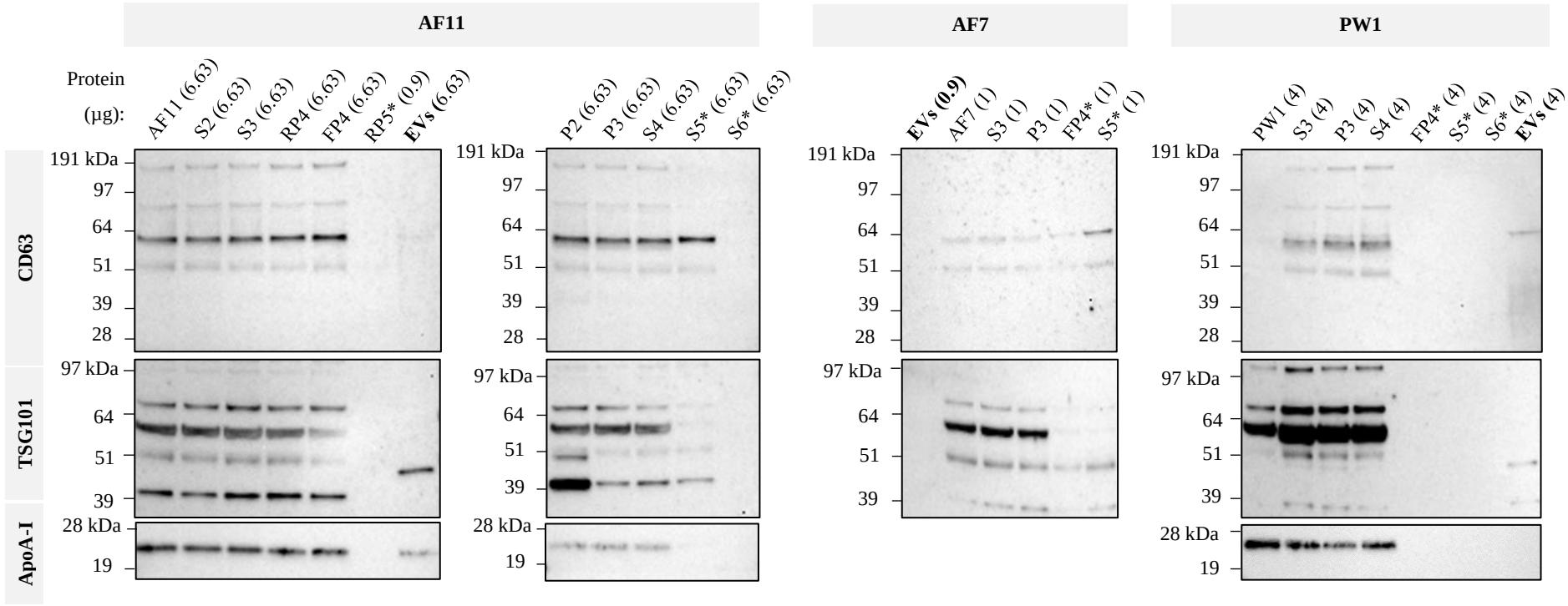

Figure 3.12 – **Western blot analysis of AF11, AF7 and PW1 isolated and discarded fractions with anti-CD63, anti-TSG101 and anti-ApoA-I.** Fractions marked with "*" were protein precipitated using TCA before Western blot. Total protein (µg) was loaded as indicated in each lane. Uncropped blots are available as supplementary material (Figure S.10).

Bands were detected in CD63 and TSG101 EVs lanes of AF11, thus suggesting recovery of EVs by the end of the isolation procedure. Although very faint, the band observed in CD63 membrane is at ~64 kDa and a faint smear further suggests the enrichment in several forms of glycosylated CD63 not observed in other fractions, as seen in ES-2 EVs. Also, in TSG101 membrane a single band at ~50 kDa was observed only in EVs. A band with the same molecular weight was observed in ES-2 EVs but was not enriched when compared to the ES-2 cells, nor was the most intense band. In AF11, the ~50 kDa band is unique among other bands in isolated fractions, suggesting that it may be specific to the antibody. Other bands observed in isolated fractions except EVs, both in TSG101 and CD63 membranes, may be non-specific and possibly caused by the high complexity of samples, as observed in the positive control sample used to implement antibodies (Figure 3.1). In purification protocols, we can expect the last fraction to be less heterogenous than all other fractions, and that was observed in this step-by-step-characterization of AF11, AFF7 and PW1 samples. In PW1, similar results as for AF11 were observed in EVs lane, with the enrichment in glycosylated CD63 and ~50 kDa TSG10, using 4 μg of protein. In AF7, no bands were detected in EVs lanes, possibly because the total protein (0.9 μg) was too low so CD63 and TSG101 could be detected. For this reason, the characterization of EVs isolated from other ascitic fluids and peritoneal washes in subsequent experiments was performed using 4 μg of total protein, whenever possible.

A single band in ApoA-I AF11 EVs lane was also observed. Despite that, compared to other isolated fractions the signal intensity of ApoA-I in EVs was weaker suggesting that there was sample purification in some degree from this contaminant. In PW1, ApoA-I was detected in the biological fluid, but not in EVs. Lipoproteins can be very abundant in biofluids when compared to EVs. For example, lipoprotein are estimated to be 20 to 100 fold more abundant than EVs in serum [133], [134]. It is reported that ultracentrifugation-based methods cannot separate completely small EVs from lipoproteins[135]. Therefore, we can hypothesize that lipoproteins containing ApoA-I, such as HDL and chylomicrons, were co-isolated with AF11 EVs. Unless the two groups of particles are characterized separately, this can be problematic for metabolomic applications using EVs from biofluids, as the source of molecules such as lipids could either be EVs or lipoproteins[136]. As observed before in ascitic fluids (Figure 3.2), a single ApoA-I band at ~26 kDa (Figure S.10) was observed in PWs fractions. For this reason, ApoA-I and CD63 antibodies were incubated simultaneously in all next experiments for ascitic fluids and peritoneal washes with the purpose of sample rationing.

Overall, we observed that more heterogenous or complex fractions originated multiple bands in Western blots. Also, the isolation procedure led to the removal of contaminants, specifically ApoA-I, in some degree until the final step. Positive results for CD63 and TSG101 suggested the recovery of EVs by the end of the isolation. However, to be sure NTA and TEM were further carried out.

3.2.2.2. Determination of size and particle concentration by NTA

All isolation fractions of AF11 were further analysed by NTA to determine particle concentration and size among isolated and discarded fractions. The NTA method is used for the analysis of particles in liquid suspensions[137]. The particle size and concentration, with direct and real-time visualization supported by the specially developed software, is based on the Brownian motion and laser light scattering properties of the particles, captured by a scientific digital camera[137].

Differential centrifugation is used to separate EVs based on their sedimentation efficiency, which is proportional to their sizes[138]. Small EVs (50-150 nm), such as exosomes, sediment at centrifugation forces in the range of 100,000 to 200,000 × g, and large EVs (150-1000 nm), such as microvesicles, large oncosomes and ectosomes[58], in the range of 10,000 to 20,000 × g[139]. In this study, a clearing step was performed at 2,000 × g to remove cells and dead cells from biological fluids, followed by another centrifugation at 12,000 × g to sediment cell debris and large EVs. Subsequent centrifugations were all performed at 110,282 × g to recover small, purified EVs.

The particle size distribution, normalized to the total particle count (Figure 3.13.A and B), revealed five or more peaks in most fractions, indicating polydispersity. Some peaks of the isolated fractions matched with others in the corresponding discarded fraction, including peaks at the size range of 50-150 nm until the S3/P3 step, performed at 12,000 × g. This may indicate that small EVs were lost at first steps of the protocol. Adding to this, size distribution of fractions towards the final steps of the isolation procedure seemed to be widening and peaks shifting towards larger sizes. Compared to the first isolated fraction, consisting of ascitic fluids, in which the most intense peak was at 113.5 nm, in EVs the most intense peak was at 178.5 nm. Similarly, the most intense peak in P2 was at 121.5 nm and in S6 at 140.1 nm. In addition to small EVs loss in isolated fractions, it is possible that particle agglomeration was contributing to the detection of large-sized particle populations, compared to small-sized populations which in parallel were decreasing. Particle agglomeration is a phenomenon described in high-speed centrifugation methods to isolate EVs[140]. The agglomeration of EVs has implications on their concentration and size determination, and complete resuspension of agglomerates either by e.g., shear force or trypsin may damage EVs[141].

Moreover, the particle size distribution of the EVs fraction demonstrated three peaks, specifically at 134.5 nm, 178.5 nm (the most intense) and 234.5 nm, and the mean size was 195.1 nm. Compared to the P3 fraction, we expected smaller size distribution and the most intense peak to be at smaller size ranges[139]. However, the most intense peak in P3 was at 86.5 nm and particles ranged from 13.5 nm to 421.5 nm. In EVs, particle size ranged from 59.5 to 517.5 nm. Despite this observation, small vesicles

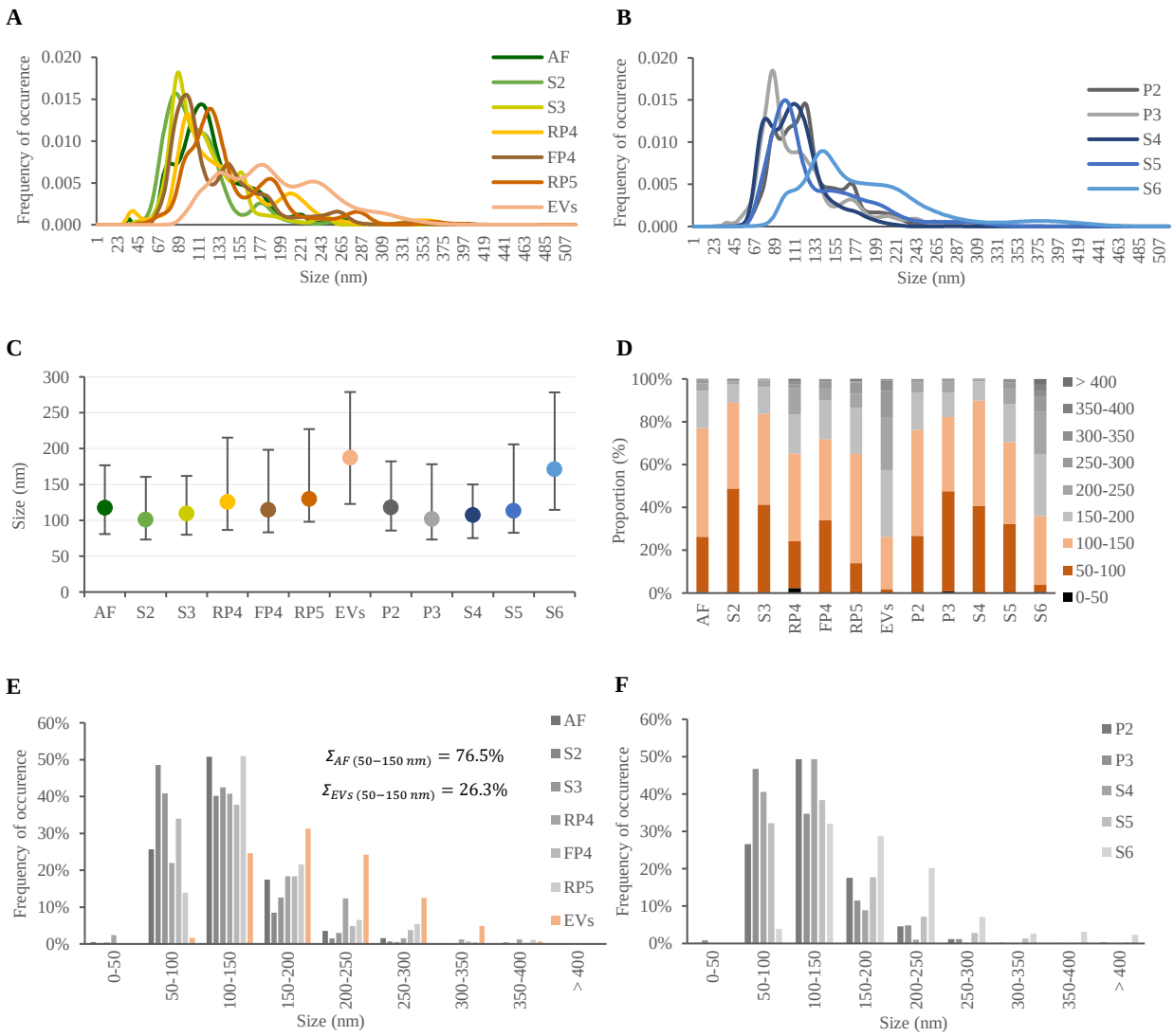

Figure 3.13 – **Particle size distribution in isolated and discarded fractions of AF11 by NTA**. A, B – Particle size distribution normalized to total particle count. C – Size median (markers), lower decile, D10, (bottom whisker) and upper decile, D90, (top whisker) of all fractions; D – Proportion (%) of particles per size range; E, F – Particle size distribution normalized to total particle count per size range.

were still detected in the latter fraction, as expected. However, it is important to note that other small sized structures, such as protein aggregates and lipoproteins[133] may have been co-isolated with EVs. There are two classes of lipoproteins containing ApoA-I, the non-EV protein component used in this project to evaluate the purity degree of EV isolates and detected in EVs during step-by-step characterization by Western blot (Figure 3.12), which are HDL and chylomicrons[100]. HDLs are sized from 7 to 13 nm, thus can be separated from EVs based on differences in size by ultracentrifugation techniques[71]. HDLs were not expected in isolated EVs, but chylomicrons can be expected as they range from 75 to 1200 nm and are separated from EVs using methods based on density differences, such as sucrose gradient density separation [71] that are combined with ultracentrifugation for improved purity, but lower EV yields compared to differential centrifugation[130], and are also reported in metabolomic

studies[142]. If chylomicrons were in fact co-isolated with EVs, it is possible that the second washing step had little impact on the purity degree of EVs from ApoA-I [143].

The median diameter, lower (D10) and upper deciles (D90) of isolated and discarded fractions were represented in Figure 3.13.C. All fractions had median sizes ranging from 100 to 200 nm. Among the isolated fractions, S2 had the lowest and EVs the highest median, specifically 101 nm and 187.1 nm, respectively. Among the discarded fractions, P3 had the lowest and S6 the highest median, 102 nm and 171 nm, respectively. From fractions S2 and P3, the median diameter, lower and upper deciles showed an overall tendency to increase until the last fraction of isolated and discarded fractions, confirming what we had observed in Figure 3.13.A and B, and once again suggesting the decrease in small particles from the second centrifugation of the isolation procedure (Figure 3.13.D). The frequency of particles within 50-150 nm decreased throughout the isolation procedure in isolated fractions. Inversely, in discarded fractions there was an enrichment in those particles until the first ultracentrifugation step, suggesting small particle loss. Compared to other fractions, in which most particles are within 50-100 m or 100-150 nm, EVs is the only fraction in which most particles (31.8%) are within 150-200 nm (Figure 3.13. E and F). The percentage of particles within 50-150 nm was the following for isolated fractions: 76.5%, 88.7%, 83.3%, 62.7%, 71.9%, 64.8% and 26.3%, in ascitic fluid, S2, S3, RP4, FP4, RP5 and EVs, respectively. The percentage of particles within 50-150 nm was the following for discarded fractions: 75.9%, 81.4%, 89.9%, 70.5% and 35.7%, in P2, P3, S4, S5 and S6, respectively.

Ultimately, 1.6×10^6 particles were isolated in EVs fraction from unprocessed ascitic fluid containing 2.0×10^9 particles. Recovery of small EVs is calculated as the recovered to total EVs ratio and for ultracentrifugation based methods is reported to range between 5-25% [144]. In this study, the recovery of small vesicles (50-150 nm) was 27.9%. However, NTA does not allow to discriminate EV populations from other particles of similar size and ApoA-I was detected by Western blot, which suggests indeed the presence of non-EV particles that may impact the recovery calculations.

Although small particles are expected to be enriched during centrifugation cycles of 100,000 × g for biofluids [145], we observed loss of these particles throughout the procedure and an increase in median size by the last isolated fraction. In fact, ultracentrifugation based-methods are reportedly less efficient at pelleting smaller particles and are associated with co-isolation of lipoproteins[71]. Protocols for centrifugation-based methods may require adaptations, as the choice of rotor, length of centrifugations, and washing steps may impact the EV yield and purity of isolates [146] and optimized protocols have been proposed[147]. In differential centrifugation, a compromise has to be found as repeated ultracentrifugation steps can damage EVs, and promote aggregation and co-isolation of contaminants, and inefficient washing can increase protein contamination[148]. Bearing this in mind, Chang *et al.* proposed a protocol to isolate EVs based on immunoaffinity that is further compatible with metabolomics[149]. The authors claimed that more and high pure exosomes could be collected from cell culture media compared to traditional ultracentrifugation methods and generate a higher number of features

in metabolomics using aptamer-based immunoaffinitive magnetic composites (MagG@PEI@DSP@aptamer).

3.2.2.3. Analysis of EV morphology by TEM

To complete the step-by-step characterization, isolated and discarded fractions of AF11 were further analysed by TEM for morphology assessment. Under the drying conditions used on TEM, EVs display a cup-shape like morphology [150]. A decrease in sample complexity from the first to the last step of the isolation procedure was observed, with less components in number and heterogeneity being observed (Figure 3.14). From images of S5 and S6 fractions, some EV-like particles seemed to have been lost, as suspected previously with NTA results (Figure 3.13). These supernatants were collected before and after the second washing step and were discarded. The presence of non-EV material in EVs fractions, as suggested by Western blot (Figure 3.12), and loss of EVs during the second washing step should be analysed in more detail, because the second washing step may have little impact on the purity degree of isolated EVs and additionally cause loss of important material[143]. Because the AF11 RP5 was low in protein, we could not further investigate this issue based on Western blot results. Nevertheless, and as expected, round cup-shaped particles sized ~100 nm were observed suggesting the recovery of small vesicles, such as exosomes, from ascitic fluids. These particles were very close to each other, thus suggesting agglomeration as suspected from NTA results. In ultracentrifugation-based protocols this issue may result in lower EV yields[151] and can affect NTA results[139] which are used in metabolomics and EV recovery calculations. Large-sized populations of particles were detected by NTA, but as the representative image suggests, it is possible that those were caused by particle agglomeration. Chylomicrons were not observed in the analysed images of AF11 EVs, and if present, HDLs would hardly be noticed considering their small size (7-13 nm)[71]. Therefore, we could not confirm the presence of ApoA-I containing lipoproteins in AF11.

In PW1 and AF7, round cup-shaped vesicles were also observed, suggesting the presence of EVs (Figure 3.15). Additionally, in AF7 sample, round vesicles were also observed but without the characteristic cup-shape morphology, indicating that those vesicles may not be EVs and, based on morphology and size (~100 nm), possibly are chylomicrons[152]. However, it is important to note that not all EVs display the cup-shape morphology in TEM (negative stain) and, for this reason, can be mistaken by lipoproteins[153]. In PW1 sample, more heterogeneous components were observed, specifically light and shapeless structures, also without the cup-shape morphology, not expected for EVs. These structures may have been co-isolated because of their similar size to EVs. In AF7, the EV-like particles also formed agglomerates. In AF11, AF7 and PW1 were observed EV-like particles with variable size, small (50-150 nm) and large (>150 nm) vesicles, indicating the isolation of a population of EVs, as expected for biofluids[91].

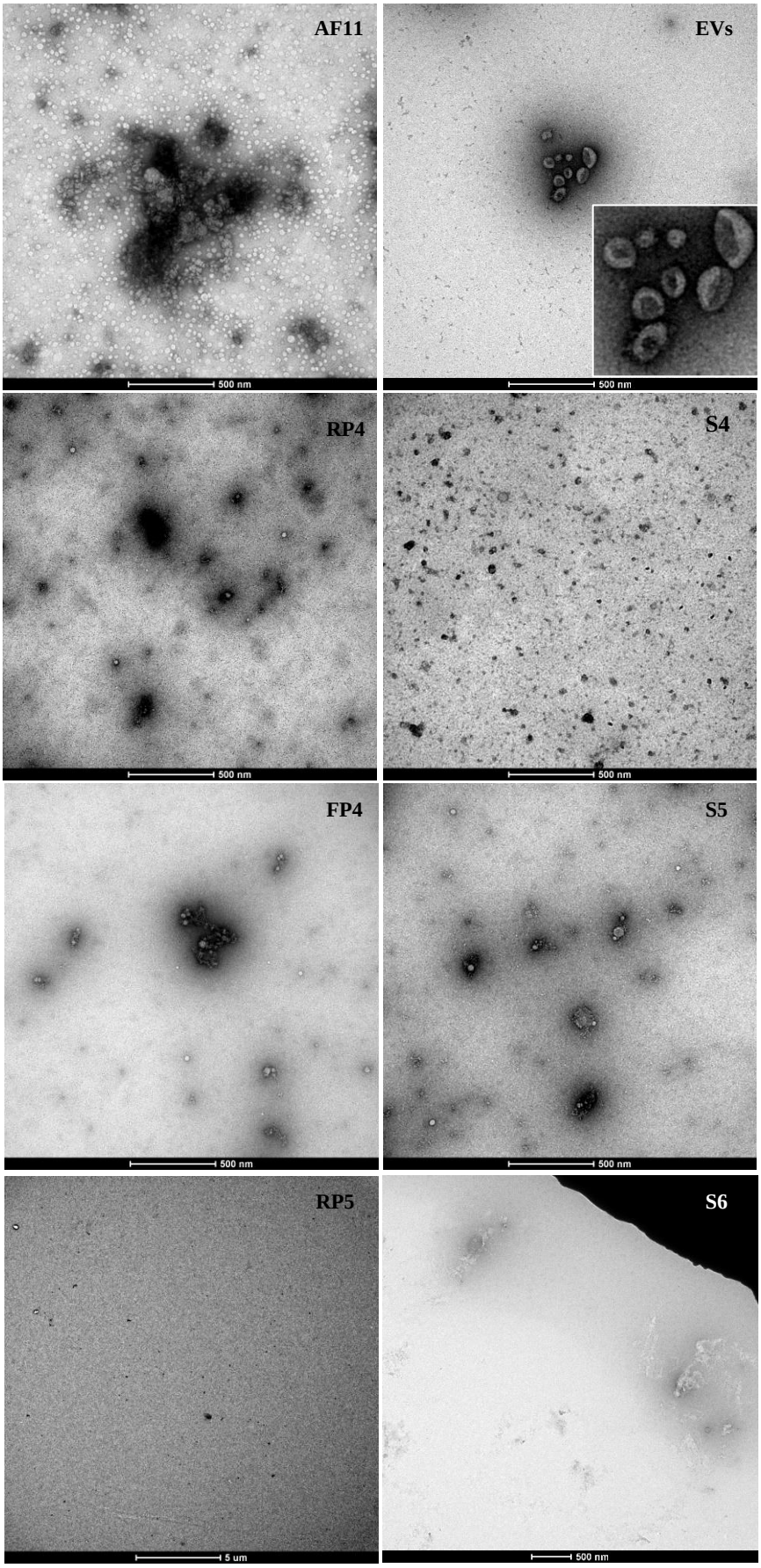

Figure 3.14 – **TEM analysis of AF11 isolated and discarded fractions**. EVs were negatively stained and analysed by TEM. Scale bars are indicated at the bottom of each image.

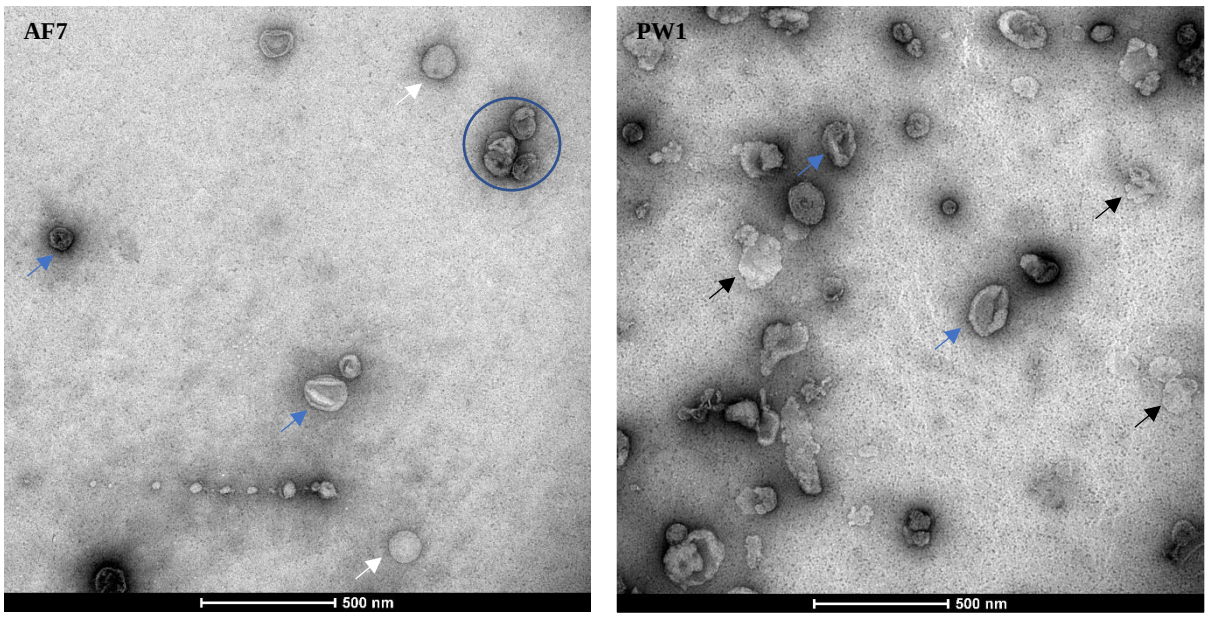

Figure 3.15 – **TEM analysis of EVs isolated from AF7 and PW1**. Preparations were negatively stained and analysed by TEM. Representative images are shown for AF7 (left) and PW1 (right) EVs. Scale bars are indicated at the bottom of each image. EVs with cup-shape morphology are indicated with blue arrows. Lipoproteins are indicated with white arrows. Co - isolated particles without cup-shape morphology are indicated with black arrows. EV agglomerates are indicated with blue circle.

Altogether, results from the three characterization techniques suggested the isolation of small EVs from biofluids. From Western blot results, EV components were detected in AF11 and PW1. From NTA results, small (50-150 nm) and large particles (150-1000 nm) were detected in AF11 EVs. From TEM results, cup-shaped vesicles were observed in AF11, AF7 and PW1 EVs. Despite there was evidence of EV loss, lipoprotein contamination and EV agglomeration, there was confidence in claiming that EVs were isolated from ascitic fluids and peritoneal washes. Therefore, the isolation and characterization of EVs from other patient samples was carried out afterwards.

3.3. Characterization of EVs isolated from patient samples

3.3.1. Protein detection by Western blot

EVs isolated from all samples of ascitic fluids and peritoneal washes were characterized by Western blot for the presence of EV and non-EV components, in parallel with the source biological fluid. A different pattern of bands in CD63 membrane was observed in EVs when compared to the source ascitic fluid or peritoneal washes sample (Figure 3.16). In most biofluids, a sharp band at ~64 kDa was observed with little smearing. In contrast, a smearing pattern was observed in most EVs, particularly in EVs from ascitic fluids. This smearing covered a wide range of molecular weights, from ~30 kDa to >191 kDa, as expected for CD63 [154]. Among ascitic fluids, only AF4 EVs had a single band at ~60

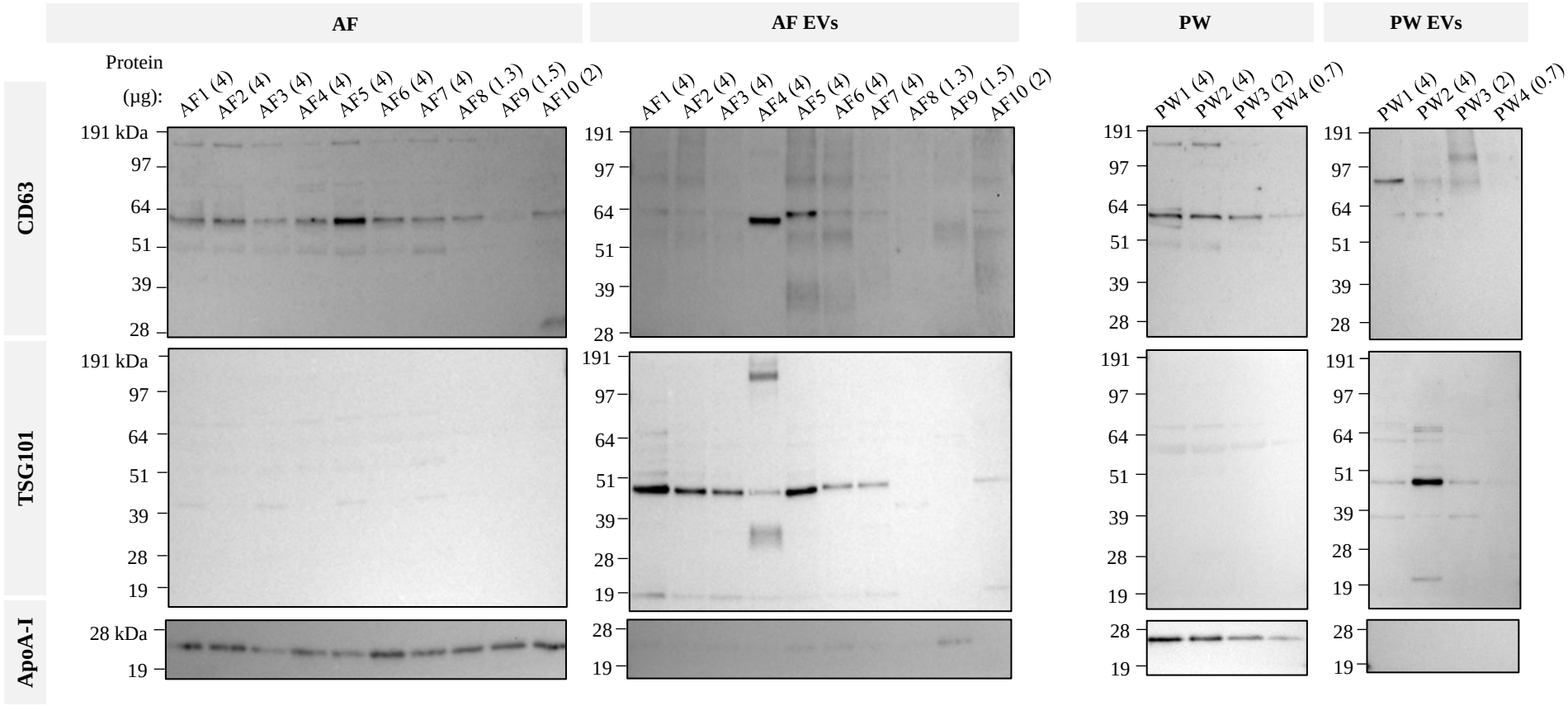

Figure 3.16 – **Western blot analysis of EVs and biofluids with anti-CD63, anti-TSG101 and anti-ApoA-I**. AF – ascitic fluids. PW – peritoneal washes. Total protein (µg) was loaded as indicated in each lane. Uncropped blots are available as supplementary material (Figure S.12).

kDa, suggesting that AF4 EVs may be enriched in a specific glycosylated from of CD63. Also, ~50 kDa TSG101 band was fainter in comparison to other AF EVs loaded in equal protein amounts, as well as two extra bands not observed in other samples. Among peritoneal washes, the smearing was more evident in PW3 but still less than the majority of ascitic fluids. More states of glycosylation were observed for EVs, and the degree of glycosylation may be an indicator of EV enrichment compared to other components[98], as previously observed for ES-2, AF11 and PW1 EVs. Compared to the source ascitic fluid or peritoneal washes, the ~50 kDa TSG101 band was much more intense in EVs than in biofluids, as previously observed for AF11 and PW1 EVs in step-by-step characterization, suggesting the enrichment in TSG101 EVs by the last isolation fraction. Moreover, AF7 EVs were once again analysed and this time we could confirm the presence of CD63, TSG101, and the contaminant ApoA-I, suggesting that in step-by-step characterization the total protein levels were indeed too low so that proteins could be detected. Based on results obtained for all patient samples, Western blot results were better when using EV total protein of at least 2 µg. PW1 EVs were also analysed for the second time, and, compared to the first experiment (Figure 3.12), the smeared CD63 was not observed but a high molecular weight band (~85 kDa) appeared, suggesting that within the same sample more than one type of EVs were isolated and for the amount of protein tested we may not be able to see that variability. Lastly, compared to biofluids, a single band of ApoA-I (~26 kDa) much less intense was observed for EVs, indicating that the contaminant was removed in some degree from initial sample to the last fraction collected.

3.3.2. Determination of particle size and concentration by NTA

All EV fractions from ascitic fluids and peritoneal washes were further analysed by NTA. Most particles were distributed over a wide range of sizes, more specifically from 20.5 nm (PW1) to 748.5 nm (AF10), and the most intense peaks in each sample were between 107.5 nm (AF9) and 255.5 nm (AF4) (Figure 3.17. A and B). Most samples have four or more peaks, some with double or triple the size of others suggesting particle agglomeration. Only AF9 was more abundant in particles sized from 50 to 150 nm, as 59.70% of the particles were within that range (Figure 3.17. C). Other samples were as follows: 4.54%, 7.07%, 4.96%, 1.66%, 22.26%, 21.57%, 15.76%, 28.99%, 8.37%, 26.25%, 34.91%, 11.83%, 20.60% and 18.34%, in AF1, AF2, AF3, AF4, AF5, AF6, AF7, AF8, AF10, AF11, PW1, PW2, PW3 and PW4 samples, respectively. However, 7 out of 15 samples were more abundant in particles sized up to 200 nm than sized over 200 nm. AF4 had the lowest percentage of particles sized up to 200 nm and AF9 the highest percentage, in specific 19.27% and 85.89%, respectively. In addition, median size ranged from 136.5 nm in AF9 to 244.1 nm in AF4 (Figure 3.17. D). AF4 had the highest protein concentration (3.177 µg/µL) and AF9 one of the lowest (0.116 µg/µL), but no linear relationship was found between the protein concentration and median size in EVs from patient samples (Figure S.13).

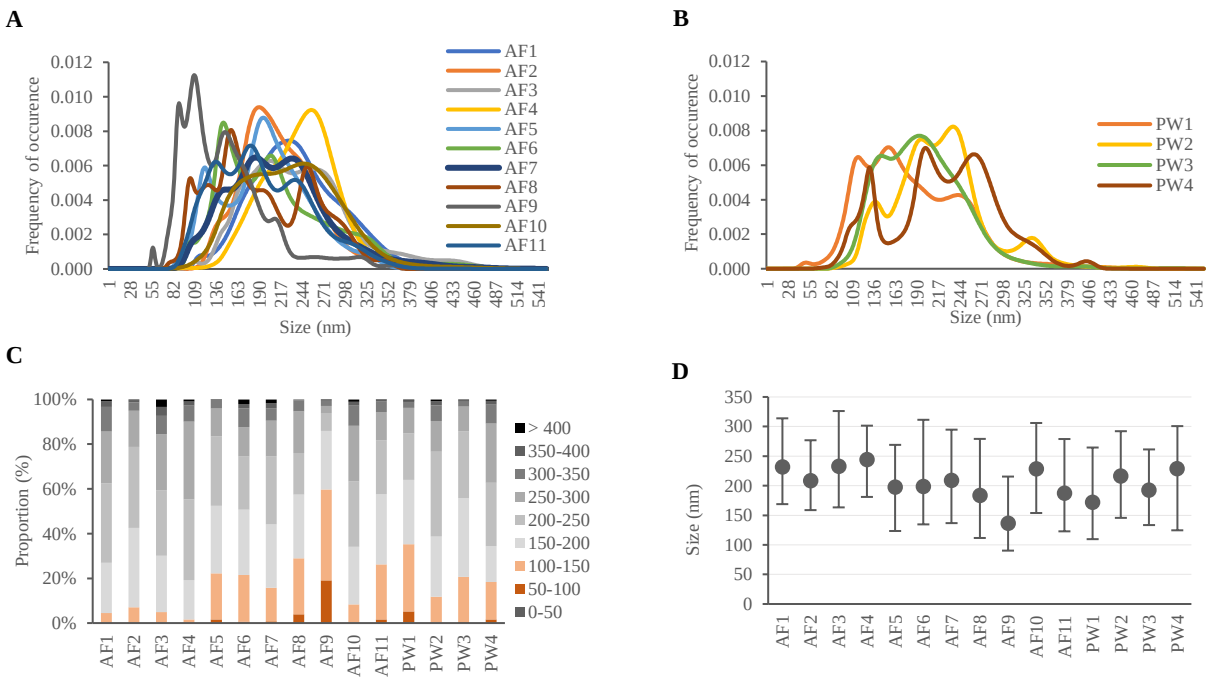

Figure 3.17 – **Particle size distribution of EVs from patient samples by NTA**. A, B – Particle size distribution normalized to total particle count. D – Size median (markers), lower decile, D10, (bottom whisker) and upper decile, D90, (top whisker) of all fractions; C – Proportion (%) of particles per size range.

Median sizes higher than expected for small EVs may suggest protein agglomerates, as indeed observed during step-by-step characterization, but also large sized EVs, such as microvesicles (100-1000 nm)[155]. Li *et al*. isolated EVs from peritoneal washes of benign ovarian cyst patients and ascitic fluids of ovarian cancer patients by differential centrifugation and observed that the mean sizes were of 86.4 nm and 138.9 nm, respectively[156]. However, their observations were based on TEM images, that additionally revealed the occurrence of particle agglomerates, and the peritoneal washes analysed were benign. In this study, the average particle mean in ascitic fluids was 211.5 ± 28.1 nm and in malign peritoneal washes was 205.5 ± 19.3 nm, based on NTA method.

The particle concentrations were also obtained for patient samples by NTA, and results were very heterogenous among samples. Particle count ranged from 1.52×10^6 (AF7 EVs) to 1.45×10^9 (AF4 EVs) particles (Figure 3.19). Ultimately, the least concentrated sample was AF7 with 1.52×10^{10} particles/mL and the most concentrated sample was AF4 with 1.45×10^{13} particles/mL. Only the first five samples would be suitable for lipidomics if the same conditions used on ES-2 EVs II (4.5×10^{11} particles/mL) were to be applied.

Total protein can correlate with EVs, but also with protein contamination and may vary if a lysis step is performed. Particle number and total protein were further analysed, and there was observed a linear relationship between the two parameters (Figure 3.18). AF4 EVs had the higher protein concentration (3.117 µg/µL) and particle number, therefore was removed from linear regression. The purity of EV samples can be determined by the ratio of particle number to total protein. Webber *et al*. suggested

that samples isolated from biofluids by centrifugation and washing protocols having $<2\times10^9$ particles/µg ratios were considered unpure [143]. In this study, all samples had ratios below 4.25×10^6 particles/µg. Although particle number may increase with total protein, higher levels of total protein may indicate contamination. Despite that, as the authors stated, disease may alter the protein content of EVs, and biofluids used for the study were only collected from healthy donors[143]. Therefore, although interesting to investigate, caution is necessary when analysing purity ratios.

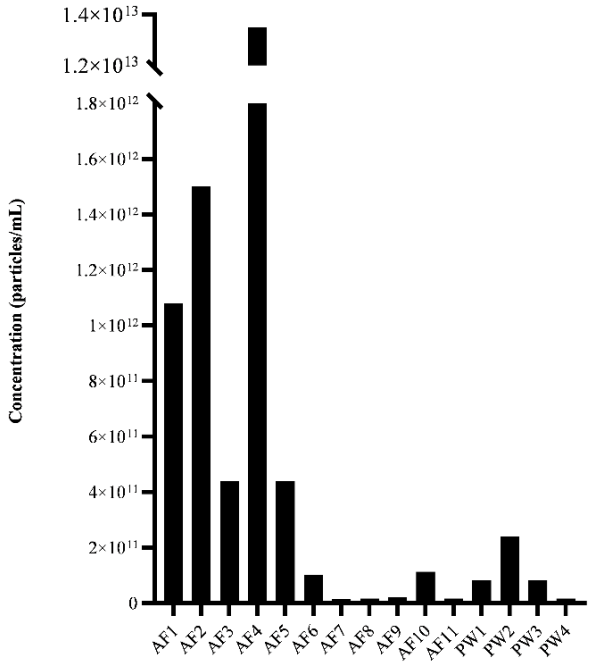

Figure 3.19 – **Particle concentration of EVs samples from ascitic fluids and peritoneal washes**.

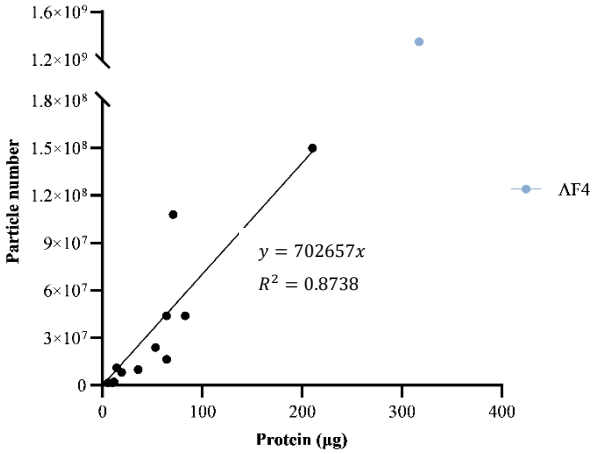

Figure 3.18 – **Linear relationship between total protein (µg) and particle number in EVs from patient samples.** AF4, indicated in blue, was removed from the linear regression, $y = 702657x, R^2 = 0.8738$, as it was very different from all other samples in particle number and total protein.

3.3.3. Analysis of EV morphology by TEM

During step-by-step characterization we confirmed the isolation of EVs in AF11, AF7 and PW1. From subsequent Western blot and NTA experiments using all the other patient samples, different results were obtained in Western blot, particle concentration and protein concentration for AF4 EVs. As AF9 EVs was among the top three of samples in lower protein concentration (0.116 μg/μL) and particle concentration (2.12×10^{10} particles/mL), this sample was analysed for comparison.

More particles were observed in AF4 EVs than in AF9 EVs, as expected from NTA results (Figure 3.20). However, other structures without the characteristic cup-shape of EVs were also observed in AF4 EVs. These may be protein aggregates and, in such case, may contribute to the elevated protein concentration of this sample. Moreover, observed EV-like particles in AF4 EVs seemed to be smaller than those of AF9 EVs. This goes against the observations from NTA (Figure 3.17), as AF9 EVs were the most enriched sample in particles within the range of small EVs. The median size of particles was 136.5 nm in AF9 EVs and 244.1 nm in AF4 EVs. In fact, very small particles were observed in AF9 EVs by TEM, but they do not seem to have the morphology of EVs.

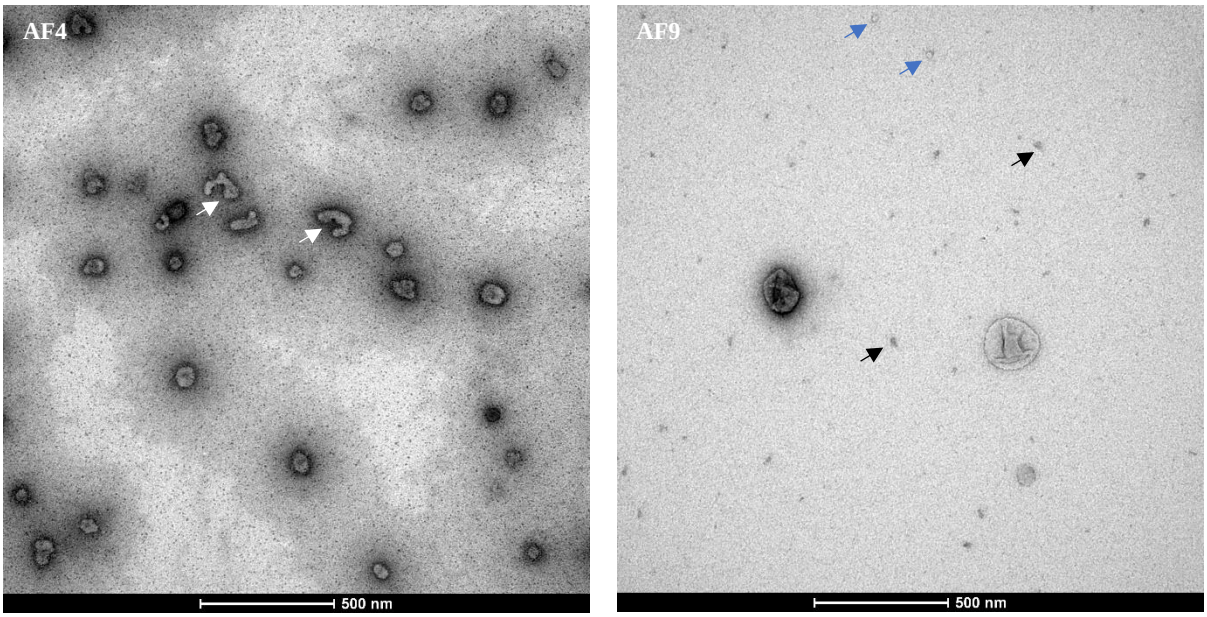

Figure 3.20 – **Morphology and size of AF4 and AF9 EVs by TEM**. AF4 (left), high in total protein and particle concentration, compared to AF9 (right), low in total protein and particle concentration. Samples were negatively stained and analysed by TEM. Scale bars are indicated at the bottom of each image. White arrows indicate suspected protein aggregates. Black arrows indicate small particles. Blue arrows indicate small lipoproteins.

In addition, small vesicles that may be lipoproteins were also observed, and based on size (up to 70 nm) possible are VLDLs[152]. The fact that NTA results may be impacted by the co-isolation of other particles without discriminating them and by particle agglomeration, reinforces the need of several methods for a complete characterization of isolated EVs and recalls caution regarding size and concentration determination by NTA. Lastly, samples were collected from different patients. This may suggest that the variability observed in the analysed parameters, namely size, particle concentration, protein concentration and CD63/TSG101 assessment, were correlated with some clinical parameter, such as

diagnostic or disease stage. In fact, PW1 EVs TEM images (Figure 3.15) also revealed the isolation of EV-like particles larger than those of AF4 EVs. However, further studies with larger cohorts and complete patient characterization should be performed to determine the relevance of this hypothesis.

Altogether, results from Western blot, NTA and TEM suggested the recovery of EVs by the end of the isolation procedure, but also variability among ascitic fluids that may be interesting to further investigate. Ascitic fluids occur in late-stage disease and may provide information on the clinical state of a patient. Further analysis of the EVs content would certainly help to uncover more differences observed among samples of ascitic fluids, and possibly between the two groups analysed in this study, ascitic fluids and peritoneal washes used as control.

4. CONCLUSION

The accumulation of ascitic fluids in the peritoneal cavity of ovarian cancer patients is associated with poor prognosis[29]. These fluids constitute a tumour microenvironment essential for metastatic cancer and are enriched in EVs[11]. Several studies have been conducted with EVs to better understand their role in ovarian cancer and suggested their implication in tumour progression, as indicated by studies based on transcriptome and proteome cargos of EVs from ascitic fluids[33]–[35]. The role of EVs in the metabolic crosstalk occurring within the tumour microenvironment is also being investigated[36]. However, the study of the metabolome cargoes of EVs from ascitic fluids remains to be explored.

The aim of this study was to characterize the metabolic signature of EVs isolated from ascitic fluids of ovarian cancer patients. Bearing that in mind, methods for the characterization of EVs from cell lines and isolation of EVs from ascitic fluids were implemented and validated, following the ISEV recommendations for the evaluation of nature and purity of the EVs. Furthermore, analytical platforms for the characterization of the metabolic signature of EVs from cell lines were implemented.

For the implementation of antibody-based Western blot, a commercial exosome lysate and platelets were used as positive control for the detection of EV components (CD63, CD81 and TSG101) and non-EV components (ApoA-I), respectively. We observed that CD63, TSG101 and CD81 could display bands at different molecular weights, depending on the isolation method and source of EVs, and that ApoA-I displayed a single band for ascitic fluids at protein amounts up to 20 µg.

The Western blot conditions were then further applied to EVs from ES-2 cell line, already characterized by NTA and TEM. CD63, CD81 and TSG101 were detected, thus confirming the isolation of EVs. Based on this, ES-2 EVs could then be used to implement metabolomics, using two chromatography columns (C18 and amide columns) and two modes of sample ionization (positive and negative), and lipidomics, using one column and both ionization modes, by LC-MS. The pathway analysis of ES-2 EVs revealed the enrichment in metabolites mainly involved in the glutathione metabolism, ammonia recycling and glycerol phosphate shuttle, when using the C18 column, and in the riboflavin metabolism, fatty acid biosynthesis and beta oxidation of very long chain fatty acids, when using the amide column. These pathways are associated with several tumoral processes, such as tumour growth, tumour migration and chemoresistance[36], [119], [121].

The enrichment of EVs in lipids and amino acids stimulated a change of approach from metabolite to lipid characterization. A targeted characterization of amino acids was attempted but the EVs concentrations required by the analytical platform used were unfeasible to conduct further experiments. From lipidomic analysis, using a C18 column, lipids and amino acids associated with tumoral processes,

such as tissue repair and redox imbalance[128], mainly involved in betaine metabolism, methylhistidine metabolism and urea cycle, were detected. Future work either targeting amino acids or lipids would be interesting to investigate using EVs isolated from ascitic fluids, as initially proposed in this study, as well as the original patient sample as control for the evaluation of EV biomarker potential. Furthermore, internal standards can be used for more accurate compound identification and quantification[157].

Regarding patient samples, including ascitic fluids and peritoneal washes (as control), a differential centrifugation-based method for the isolation of EVs was implemented and validated by the characterization of isolated and discarded fractions collected throughout the procedure by Western blot, TEM and NTA. The Western blot characterization suggested the recovery of CD63 and TSG101 enriched particles from samples AF11 and PW1 and the increasing purity of isolated fractions throughout the isolation procedure, further confirmed by TEM. The recovery of particles within the size range of small and large EVs and further detection of cup-shape particles, by NTA and TEM respectively, confirmed the isolation of EVs in AF11.

Lastly, EVs isolated from ascitic fluids and peritoneal washes were also characterized by Western Blot, NTA and TEM. We confirmed the isolation of EVs and observed variability among samples of ascitic fluids by all methods, as suggested by the enrichment of particles in different size ranges, concentration, and protein amount. Based on these methods, major differences between ascitic fluids and the control group were not identified.

Although the isolation of EVs from ascitic fluids was confirmed, the characterization of the isolation procedure also suggested particle agglomeration, confirmed by NTA and TEM, and co-isolation of other non-EV components, namely ApoA-I containing-lipoproteins, confirmed by Western blot and TEM. The co-isolation of lipoproteins, namely chylomicrons, is common in differential centrifugation-based methods due to their similar size to EVs. Bearing this in mind, we can explore immunoaffinity or density gradient-based methods to increase yield and purity of isolates, further compatible with metabolomics studies, in future experiments[149], [158].

In summary, we could isolate and characterize EVs, based on protein markers of EVs and co-elution contaminants, size, and morphology of particles, from ascitic fluids by the implementation of different methods. We also implemented methods for the study of EV metabolome/lipidome by LC-MS using EVs from cell lines. These methods can further be used to explore the metabolite content of EVs from patient samples and investigate their potential role as biomarkers or therapeutic target in ovarian cancer.

BIBLIOGRAPHY

[1] "Worldwide cancer data | World Cancer Research Fund International." [Online]. Available: https://www.wcrf.org/dietandcancer/worldwide-cancer-data/. [Accessed: 13-May-2021].

[2] The American Cancer Society medical and editorial content team, "Key Statistics for Ovarian Cancer," *American Cancer Society*, 2019. [Online]. Available: https://www.cancer.org/cancer/ovarian-cancer/about/key-statistics.html. [Accessed: 06-Oct-2021].

[3] H. Sung *et al.*, "Global Cancer Statistics 2020: GLOBOCAN Estimates of Incidence and Mortality Worldwide for 36 Cancers in 185 Countries," *CA. Cancer J. Clin.*, vol. 71, no. 3, pp. 209–249, 2021.

[4] L. A. Torre *et al.*, "Ovarian cancer statistics, 2018," *CA. Cancer J. Clin.*, vol. 68, no. 4, pp. 284–296, 2018.

[5] "Surveillance, Epidemiology, and End Results Program." [Online]. Available: https://seer.cancer.gov/. [Accessed: 02-Apr-2021].

[6] "Ovarian Cancer — Cancer Stat Facts." [Online]. Available: https://seer.cancer.gov/statfacts/html/ovary.html. [Accessed: 02-Apr-2021].

[7] "Ovarian Cancer Statistics | Ovarian Cancer Research Alliance." [Online]. Available: https://ocrahope.org/patients/about-ovarian-cancer/statistics/. [Accessed: 06-Nov-2021].

[8] F. Deng *et al.*, "Age is associated with prognosis in serous ovarian carcinoma," *J. Ovarian Res.*, vol. 10, no. 1, p. 36, Dec. 2017.

[9] J. Prat, A. Ribé, and A. Gallardo, "Hereditary ovarian cancer," *Hum. Pathol.*, vol. 36, no. 8, pp. 861–870, Aug. 2005.

[10] E. Kipps, D. S. P. Tan, and S. B. Kaye, "Meeting the challenge of ascites in ovarian cancer : new avenues for therapy and research Europe PMC Funders Author Manuscripts," *Nat Rev Cancer*, vol. 13, no. 4, pp. 273–282, 2013.

[11] C. Steidel, F. Ender, A. Rody, N. von Bubnoff, and F. Gieseler, "Biologically active tissue factor-bearing larger ectosome-like extracellular vesicles in malignant effusions from ovarian cancer patients: Correlation with incidence of thrombosis," *Int. J. Mol. Sci.*, vol. 22, no. 2, pp. 1–10, Jan. 2021.

[12] J. Roche, "The epithelial-to-mesenchymal transition in cancer," *Cancers*, vol. 10, no. 2. MDPI AG, 16-Feb-2018.

[13] A. Morandi, M. L. Taddei, P. Chiarugi, and E. Giannoni, "Targeting the metabolic reprogramming that controls epithelial-to-mesenchymal transition in aggressive tumors," *Front. Oncol.*, vol. 7, no. MAR, pp. 1–19, 2017.

[14] A. Chandra *et al.*, "Ovarian cancer: Current status and strategies for improving therapeutic outcomes," *Cancer Med.*, vol. 8, no. 16, pp. 7018–7031, Nov. 2019.

[15] K. K. Gupta, V. K. Gupta, and R. W. Naumann, "Ovarian cancer: Screening and future directions," *International Journal of Gynecological Cancer*, vol. 29, no. 1. BMJ Publishing Group, pp. 195–200, 01-Jan-2019.

[16] R. Patni, "Screening for ovarian cancer: An update," *J. Midlife. Health*, vol. 10, no. 1, p. 3, 2019.

[17] A. Goyal and T. M. Elsheikh, "Nongynecologic Fluid and Brushing Cytology," in *Pathobiology*

of Human Disease: A Dynamic Encyclopedia of Disease Mechanisms, Elsevier Inc., 2014, pp. 3359–3378.
[18] "Definition of peritoneal washing - NCI Dictionary of Cancer Terms - National Cancer Institute." [Online]. Available: https://www.cancer.gov/publications/dictionaries/cancer-terms/def/peritoneal-washing. [Accessed: 08-Dec-2021].
[19] S. Naz *et al.*, "Role of peritoneal washing cytology in ovarian malignancies: Correlation with histopathological parameters," *World J. Surg. Oncol.*, vol. 13, no. 1, pp. 1–5, 2015.
[20] C. Stewart, C. Ralyea, and S. Lockwood, "Ovarian Cancer: An Integrated Review," *Semin. Oncol. Nurs.*, vol. 35, no. 2, pp. 151–156, 2019.
[21] "Tests for Ovarian Cancer." [Online]. Available: https://www.cancer.org/cancer/ovarian-cancer/detection-diagnosis-staging/how-diagnosed.html. [Accessed: 05-Nov-2021].
[22] A. Sahdev, "CT in ovarian cancer staging: How to review and report with emphasis on abdominal and pelvic disease for surgical planning," *Cancer Imaging*, vol. 16, no. 1. BioMed Central Ltd., p. 19, 02-Aug-2016.
[23] A. Desai, "Epithelial ovarian cancer: An overview," *World J. Transl. Med.*, vol. 3, no. 1, p. 1, 2014.
[24] N. Ahmed and K. L. Stenvers, "Getting to know ovarian cancer ascites: Opportunities for targeted therapy-based translational research," *Front. Oncol.*, vol. 3 SEP, no. September, pp. 1–12, 2013.
[25] M. Cohen and P. Petignat, "The bright side of ascites in ovarian cancer," *Cell Cycle*, vol. 13, no. 15, p. 2319, 2014.
[26] M. L. Puiffe *et al.*, "Characterization of ovarian cancer ascites on cell invasion, proliferation, spheroid formation, and gene expression in an in vitro model of epithelial ovarian cancer," *Neoplasia*, vol. 9, no. 10, pp. 820–829, 2007.
[27] C. E. Ford, B. Werner, N. F. Hacker, and K. Warton, "The untapped potential of ascites in ovarian cancer research and treatment," *Br. J. Cancer*, vol. 123, no. 1, pp. 9–16, 2020.
[28] B. P. Rickard *et al.*, "Malignant ascites in ovarian cancer: Cellular, acellular, and biophysical determinants of molecular characteristics and therapy response," *Cancers (Basel).*, vol. 13, no. 17, 2021.
[29] D. S. Tan, R. Agarwal, and S. B. Kaye, "Mechanisms of transcoelomic metastasis in ovarian cancer," *Lancet Oncology*, vol. 7, no. 11. Elsevier, pp. 925–934, 01-Nov-2006.
[30] M. Murph and G. B. Mills, "Targeting the lipids LPA and S1P and their signalling pathways to inhibit tumour progression," *Expert Rev. Mol. Med.*, vol. 9, no. 28, pp. 1–18, Oct. 2007.
[31] G. Hong, L. M. Baudhuin, and Y. Xu, "Sphingosine-1-phosphate modulates growth and adhesion of ovarian cancer cells," *FEBS Lett.*, vol. 460, no. 3, pp. 513–518, Nov. 1999.
[32] S. Kim, B. Kim, and Y. S. Song, "Ascites modulates cancer cell behavior, contributing to tumor heterogeneity in ovarian cancer," *Cancer Sci.*, vol. 107, no. 9, pp. 1173–1178, 2016.
[33] A. Mitra *et al.*, "Extracellular vesicles derived from ascitic fluid enhance growth and migration of ovarian cancer cells," *Sci. Rep.*, vol. 11, no. 1, pp. 1–11, 2021.
[34] A. Yokoi *et al.*, "Malignant extracellular vesicles carrying MMP1 mRNA facilitate peritoneal dissemination in ovarian cancer," *Nat. Commun.*, vol. 8, no. 1, pp. 1–15, Mar. 2017.
[35] B. Bortot *et al.*, "Small extracellular vesicles from malignant ascites of patients with advanced ovarian cancer provide insights into the dynamics of the extracellular matrix," *Mol. Oncol.*, vol. 15, no. 12, pp. 3596–3614, Dec. 2021.
[36] C. A. Lyssiotis and A. C. Kimmelman, "Metabolic Interactions in the Tumor Microenvironment," *Trends Cell Biol.*, vol. 27, no. 11, pp. 863–875, 2017.
[37] N. M. Anderson and M. C. Simon, "The tumor microenvironment," *Curr. Biol.*, vol. 30, no. 16, pp. R921–R925, Aug. 2020.
[38] S. Brassart-Pasco, S. Brézillon, B. Brassart, L. Ramont, J. B. Oudart, and J. C. Monboisse, "Tumor Microenvironment: Extracellular Matrix Alterations Influence Tumor Progression," *Frontiers in Oncology*, vol. 10. Frontiers Media S.A., p. 397, 15-Apr-2020.
[39] C. Cavallari, G. Camussi, and M. F. Brizzi, "Extracellular vesicles in the tumour microenvironment: Eclectic supervisors," *International Journal of Molecular Sciences*, vol. 21, no. 18. MDPI AG, pp. 1–21, 02-Sep-2020.
[40] A. N. Lau and M. G. Vander Heiden, "Metabolism in the Tumor Microenvironment," *Adv. Exp.*

Med. Biol., vol. 1263, pp. 1–11, 2020.
[41] R. R. Chen *et al.*, "Targeting of lipid metabolism with a metabolic inhibitor cocktail eradicates peritoneal metastases in ovarian cancer cells," *Commun. Biol.*, vol. 2, no. 1, 2019.
[42] X. Chen, S. Chen, and D. Yu, "Metabolic reprogramming of chemoresistant cancer cells and the potential significance of metabolic regulation in the reversal of cancer chemoresistance," *Metabolites*, vol. 10, no. 7. MDPI AG, pp. 1–15, 01-Jul-2020.
[43] N. Ahmed, R. Escalona, D. Leung, E. Chan, and G. Kannourakis, "Tumour microenvironment and metabolic plasticity in cancer and cancer stem cells: Perspectives on metabolic and immune regulatory signatures in chemoresistant ovarian cancer stem cells," *Semin. Cancer Biol.*, vol. 53, no. August, pp. 265–281, 2018.
[44] R. Radhakrishnan *et al.*, "Ovarian cancer cell-derived lysophosphatidic acid induces glycolytic shift and cancer-associated fibroblast-phenotype in normal and peritumoral fibroblasts," *Cancer Lett.*, vol. 442, pp. 464–474, Feb. 2019.
[45] D. Lucchetti, C. R. Tenore, F. Colella, and A. Sgambato, "Extracellular Vesicles and Cancer : A Focus on," pp. 1–19, 2020.
[46] A. Achreja, H. Zhao, L. Yang, T. H. Yun, J. Marini, and D. Nagrath, "Exo-MFA – A 13C metabolic flux analysis framework to dissect tumor microenvironment-secreted exosome contributions towards cancer cell metabolism," *Metab. Eng.*, vol. 43, no. Pt B, pp. 156–172, Sep. 2017.
[47] J. A. Moraes *et al.*, "Adipose tissue-derived extracellular vesicles and the tumor microenvironment: Revisiting the hallmarks of cancer," *Cancers (Basel).*, vol. 13, no. 13, pp. 1–23, 2021.
[48] Q. Dong, X. Liu, K. Cheng, J. Sheng, J. Kong, and T. Liu, "Pre-metastatic Niche Formation in Different Organs Induced by Tumor Extracellular Vesicles," *Frontiers in Cell and Developmental Biology*, vol. 9. Frontiers Media S.A., 20-Sep-2021.
[49] M. Y. Fong *et al.*, "Breast-cancer-secreted miR-122 reprograms glucose metabolism in premetastatic niche to promote metastasis," *Nat. Cell Biol.*, vol. 17, no. 2, pp. 183–194, Feb. 2015.
[50] E. Bazzan *et al.*, "Critical review of the evolution of extracellular vesicles' knowledge: From 1946 to today," *International Journal of Molecular Sciences*, vol. 22, no. 12. MDPI, 02-Jun-2021.
[51] E. M. Veziroglu and G. I. Mias, "Characterizing Extracellular Vesicles and Their Diverse RNA Contents," *Front. Genet.*, vol. 11, no. July, pp. 1–30, 2020.
[52] Y. Yuana, A. Sturk, and R. Nieuwland, "Extracellular vesicles in physiological and pathological conditions," *Blood Rev.*, vol. 27, no. 1, pp. 31–39, Jan. 2013.
[53] H. S. Ahn *et al.*, "Plasma protein biomarkers associated with higher ovarian cancer risk in brca1/2 carriers," *Cancers (Basel).*, vol. 13, no. 10, pp. 1–18, 2021.
[54] R. Wei, S. Liu, S. Zhang, L. Min, and S. Zhu, "Cellular and Extracellular Components in Tumor Microenvironment and Their Application in Early Diagnosis of Cancers," *Analytical Cellular Pathology*, vol. 2020. Hindawi Limited, 2020.
[55] S. Gurunathan, M. H. Kang, and J. H. Kim, "A comprehensive review on factors influences biogenesis, functions, therapeutic and clinical implications of Exosomes," *International Journal of Nanomedicine*, vol. 16. Dove Medical Press Ltd, pp. 1281–1312, 17-Feb-2021.
[56] M. Mostafazadeh, N. Samadi, H. Kahroba, B. Baradaran, S. Haiaty, and M. Nouri, "Potential roles and prognostic significance of exosomes in cancer drug resistance," *Cell and Bioscience*, vol. 11, no. 1. BioMed Central Ltd, p. 1, 01-Dec-2021.
[57] M. P. Bebelman, M. J. Smit, D. M. Pegtel, and S. R. Baglio, "Biogenesis and function of extracellular vesicles in cancer," *Pharmacology and Therapeutics*, vol. 188. Elsevier Inc., pp. 1–11, 01-Aug-2018.
[58] C. Théry *et al.*, "Minimal information for studies of extracellular vesicles 2018 (MISEV2018): a position statement of the International Society for Extracellular Vesicles and update of the MISEV2014 guidelines," *J. Extracell. Vesicles*, vol. 7, no. 1, 2018.
[59] C. Théry, A. Clayton, S. Amigorena, and and G. Raposo, "Isolation and Characterization of Exosomes from Cell Culture Supernatants," *Curr. Protoc. Cell Biol.*, pp. 30:3.22:3.22.1–3.22.29, 2006.

[60] K. W. Witwer and C. Théry, “Extracellular vesicles or exosomes? On primacy, precision, and popularity influencing a choice of nomenclature,” *J. Extracell. Vesicles*, vol. 8, no. 1, 2019.
[61] S. Gurung, D. Perocheau, L. Touramanidou, and J. Baruteau, “The exosome journey: from biogenesis to uptake and intracellular signalling,” *Cell Communication and Signaling*, vol. 19, no. 1. BioMed Central Ltd, p. 47, 01-Dec-2021.
[62] L. Doyle and M. Wang, “Overview of Extracellular Vesicles, Their Origin, Composition, Purpose, and Methods for Exosome Isolation and Analysis,” *Cells*, vol. 8, no. 7, p. 727, Jul. 2019.
[63] R. Kalluri and V. S. LeBleu, “The biology, function, and biomedical applications of exosomes,” *Science (80-.).*, vol. 367, no. 6478, 2020.
[64] Y. Zhang, Y. Liu, H. Liu, and W. H. Tang, “Exosomes : biogenesis , biologic function and clinical potential,” *Cell Biosci.*, pp. 1–18, 2019.
[65] K. Trajkovic *et al.*, “Ceramide triggers budding of exosome vesicles into multivesicular endosomes,” *Science (80-.).*, vol. 319, no. 5867, pp. 1244–1247, Feb. 2008.
[66] E. Cocucci and J. Meldolesi, “Ectosomes and exosomes : shedding the confusion between extracellular vesicles,” *Trends Cell Biol.*, vol. 25, no. 6, pp. 364–372, 2015.
[67] T. Juan and M. Fürthauer, “Biogenesis and function of ESCRT-dependent extracellular vesicles,” *Seminars in Cell and Developmental Biology*, vol. 74. Elsevier Ltd, pp. 66–77, 01-Feb-2018.
[68] B. Shen, N. Wu, M. Yang, and S. J. Gould, “Protein targeting to exosomes/microvesicles by plasma membrane anchors,” *J. Biol. Chem.*, vol. 286, no. 16, pp. 14383–14395, Apr. 2011.
[69] Z. Andreu and M. Yáñez-Mó, “Tetraspanins in extracellular vesicle formation and function,” *Front. Immunol.*, vol. 5, no. SEP, p. 442, 2014.
[70] D. Yang *et al.*, “Progress, opportunity, and perspective on exosome isolation - Efforts for efficient exosome-based theranostics,” *Theranostics*, vol. 10, no. 8. Ivyspring International Publisher, pp. 3684–3707, 2020.
[71] K. Brennan *et al.*, “A comparison of methods for the isolation and separation of extracellular vesicles from protein and lipid particles in human serum,” *Sci. Rep.*, vol. 10, no. 1, pp. 1–13, 2020.
[72] S. Subcommittee, F. Royo, C. Th, J. M. Falc, and R. Nieuwland, “Methods for Separation and Characterization of Extracellular Vesicles : Results of a Worldwide Survey Performed by the ISEV Rigor and,” 2020.
[73] S. Tiwari, V. Kumar, S. Randhawa, and S. K. Verma, “Preparation and characterization of extracellular vesicles,” *Am. J. Reprod. Immunol.*, vol. 85, no. 2, p. e13367, Feb. 2021.
[74] A. Zebrowska, A. Skowronek, A. Wojakowska, P. Widlak, and M. Pietrowska, “Metabolome of exosomes: Focus on vesicles released by cancer cells and present in human body fluids,” *Int. J. Mol. Sci.*, vol. 20, no. 14, 2019.
[75] K. L. Schey, J. M. Luther, and K. L. Rose, “Proteomics characterization of exosome cargo,” *Methods*, vol. 87. Academic Press Inc., pp. 75–82, 01-Oct-2015.
[76] C. Théry, S. Amigorena, G. Raposo, and A. Clayton, “Isolation and Characterization of Exosomes from Cell Culture Supernatants and Biological Fluids,” *Curr. Protoc. Cell Biol.*, vol. 30, no. 1, Mar. 2006.
[77] J. Ivanisevic and E. J. Want, “From samples to insights into metabolism: Uncovering biologically relevant information in LC- HRMS metabolomics data,” *Metabolites*, vol. 9, no. 12, pp. 1–30, 2019.
[78] D. Broadhurst *et al.*, “Guidelines and considerations for the use of system suitability and quality control samples in mass spectrometry assays applied in untargeted clinical metabolomic studies,” *Metabolomics*, vol. 14, no. 6, pp. 1–17, 2018.
[79] E. Zelena *et al.*, “Development of a robust and repeatable UPLC - MS method for the long-term metabolomic study of human serum,” *Anal. Chem.*, vol. 81, no. 4, pp. 1357–1364, Feb. 2009.
[80] T. Altadill *et al.*, “Enabling metabolomics based biomarker discovery studies using molecular phenotyping of exosome-like vesicles,” *PLoS One*, vol. 11, no. 3, pp. 1–17, 2016.
[81] X. Luo, M. An, K. C. Cuneo, D. M. Lubman, and L. Li, “High-Performance Chemical Isotope Labeling Liquid Chromatography Mass Spectrometry for Exosome Metabolomics,” *Anal. Chem.*, vol. 90, no. 14, pp. 8314–8319, Jul. 2018.

[82] M. C. Chambers *et al.*, "A cross-platform toolkit for mass spectrometry and proteomics," *Nature Biotechnology*, vol. 30, no. 10. Nature Publishing Group, pp. 918–920, 10-Oct-2012.
[83] H. P. Benton, D. M. Wong, S. A. Trauger, and G. Siuzdak, "XCMS2: Processing tandem mass spectrometry data for metabolite identification and structural characterization," *Anal. Chem.*, vol. 80, no. 16, pp. 6382–6389, Aug. 2008.
[84] M. H. Sarafian *et al.*, "Objective set of criteria for optimization of sample preparation procedures for ultra-high throughput untargeted blood plasma lipid profiling by ultra performance liquid chromatography-mass spectrometry," *Anal. Chem.*, vol. 86, no. 12, pp. 5766–5774, 2014.
[85] J. Vasconcelos e Sá *et al.*, "Unveiling dynamic metabolic signatures in human induced pluripotent and neural stem cells," *PLoS Comput. Biol.*, vol. 16, no. 4, pp. 1–20, 2020.
[86] Z. Pang *et al.*, "MetaboAnalyst 5.0: Narrowing the gap between raw spectra and functional insights," *Nucleic Acids Res.*, vol. 49, no. W1, pp. W388–W396, Jul. 2021.
[87] GE Healthcare, "Amersham ECL Western blotting detection reagents and analysis system," pp. 1–44, 2006.
[88] "Human Exosome Lysate Positive Protein Control," vol. 5066, p. 5066.
[89] D. Li *et al.*, "Isolation and identification of exosomes from feline plasma, urine and adipose-derived mesenchymal stem cells," *BMC Vet. Res.*, vol. 17, no. 1, pp. 1–8, 2021.
[90] L. Zhu *et al.*, "Isolation and characterization of exosomes for cancer research," *J. Hematol. Oncol.*, vol. 13, no. 1, pp. 1–24, 2020.
[91] F. Yuan, Y.-M. Li, and Z. Wang, "Preserving extracellular vesicles for biomedical applications: consideration of storage stability before and after isolation," *Drug Deliv.*, vol. 28, no. 1, pp. 1501–1509, Jan. 2021.
[92] J. Van Deun *et al.*, "The impact of disparate isolation methods for extracellular vesicles on downstream RNA profiling," *J. Extracell. Vesicles*, vol. 3, no. 1, pp. 1–14, 2014.
[93] "Western blot troubleshooting tips | Abcam." [Online]. Available: https://www.abcam.com/help/western-blot-troubleshooting-tips. [Accessed: 12-Nov-2021].
[94] G. C. Sampey *et al.*, "Exosomes from HIV-1-infected cells stimulate production of pro-inflammatory cytokines through trans-activating response (TAR) RNA," *J. Biol. Chem.*, vol. 291, no. 3, pp. 1251–1266, 2016.
[95] H. H. Chua, T. Kameyama, A. Mayeda, and T. H. Yeh, "Cancer-specifically re-spliced TSG101 mRNA promotes invasion and metastasis of nasopharyngeal carcinoma," *Int. J. Mol. Sci.*, vol. 20, no. 3, 2019.
[96] M. Ferrer, S. López-Borges, and P. A. Lazo, "Expression of a new isoform of the tumor susceptibility TSG101 protein lacking a leucine zipper domain in Burkitt lymphoma cell lines," *Oncogene*, vol. 18, no. 13, pp. 2253–2259, Apr. 1999.
[97] "CD81 molecule [Homo sapiens (human)]." [Online]. Available: https://www.ncbi.nlm.nih.gov/gene/975. [Accessed: 08-Nov-2021].
[98] N. Nishida-Aoki, N. Tominaga, N. Kosaka, and T. Ochiya, "Altered biodistribution of deglycosylated extracellular vesicles through enhanced cellular uptake," *J. Extracell. Vesicles*, vol. 9, no. 1, p. 1713527, Jan. 2020.
[99] N. Tominaga, K. Hagiwara, N. Kosaka, K. Honma, H. Nakagama, and T. Ochiya, "RPN2-mediated glycosylation of tetraspanin CD63 regulates breast cancer cell malignancy," *Mol. Cancer*, vol. 13, no. 1, pp. 1–11, May 2014.
[100] K. M. Wasan, D. R. Brocks, S. D. Lee, K. Sachs-Barrable, and S. J. Thornton, "Impact of lipoproteins on the biological activity and disposition of hydrophobic drugs: Implications for drug discovery," *Nature Reviews Drug Discovery*, vol. 7, no. 1. pp. 84–99, Jan-2008.
[101] G. Hariprasad, R. Hariprasad, L. Kumar, A. Srinivasan, S. Kola, and A. Kaushik, "Apolipoprotein A1 as a potential biomarker in the ascitic fluid for the differentiation of advanced ovarian cancers," *Biomarkers*, vol. 18, no. 6, pp. 532–541, Sep. 2013.
[102] "Recombinant Anti-Apolipoprotein A I antibody [EP1368Y] (ab52945) | Abcam." [Online]. Available: https://www.abcam.com/apolipoprotein-a-i-antibody-ep1368y-ab52945.html. [Accessed: 16-Nov-2021].
[103] "Western blot sample preparation | Abcam." [Online]. Available: https://www.abcam.com/protocols/sample-preparation-for-western-blot. [Accessed: 12-Nov-2021].

[104] A. Y. Jong *et al.*, "Large-scale isolation and cytotoxicity of extracellular vesicles derived from activated human natural killer cells," *J. Extracell. Vesicles*, vol. 6, no. 1, 2017.
[105] M. P. Oksvold *et al.*, "Expression of B-Cell surface antigens in subpopulations of exosomes released from B-cell lymphoma cells," *Clin. Ther.*, vol. 36, no. 6, 2014.
[106] J. Gomes *et al.*, "Extracellular Vesicles from Ovarian Carcinoma Cells Display Specific Glycosignatures," *Biomolecules*, vol. 5, no. 3, pp. 1741–1761, Aug. 2015.
[107] Y. Liang, W. S. Eng, D. R. Colquhoun, R. R. Dinglasan, D. R. Graham, and L. K. Mahal, "Complex N-linked glycans serve as a determinant for exosome/microvesicle cargo recruitment," *J. Biol. Chem.*, vol. 289, no. 47, pp. 32526–32537, 2014.
[108] N. Tominaga, K. Hagiwara, N. Kosaka, K. Honma, H. Nakagama, and T. Ochiya, "RPN2-mediated glycosylation of tetraspanin CD63 regulates breast cancer cell malignancy," *Mol. Cancer*, vol. 13, no. 1, pp. 1–11, 2014.
[109] S. Y. Ko *et al.*, "Cancer-derived small extracellular vesicles promote angiogenesis by heparin-bound, bevacizumab-insensitive VEGF, independent of vesicle uptake," *Commun. Biol.*, vol. 2, no. 1, pp. 1–17, 2019.
[110] H. Sork *et al.*, "Heterogeneity and interplay of the extracellular vesicle small RNA transcriptome and proteome," *Sci. Rep.*, vol. 8, no. 1, pp. 1–12, Dec. 2018.
[111] R. Smith, A. D. Mathis, D. Ventura, and J. T. Prince, "Proteomics, lipidomics, metabolomics: A mass spectrometry tutorial from a computer scientist's point of view," *BMC Bioinformatics*, vol. 15, no. Suppl 7, p. S9, 2014.
[112] M. Cuhra, T. Bø'hn, and P. Cuhra, "In plastico: Laboratory material newness affects growth and reproduction of Daphnia magna reared in 50-ml polypropylene tubes," *Sci. Rep.*, vol. 7, no. 1, pp. 1–10, Apr. 2017.
[113] M. Huang, T. S. Horwitz, C. Zweiben, and S. K. Singh, "Impact of extractables/leachables from filters on stability of protein formulations," *J. Pharm. Sci.*, vol. 100, no. 11, pp. 4617–4630, Nov. 2011.
[114] T. Martínez-Sena *et al.*, "Monitoring of system conditioning after blank injections in untargeted UPLC-MS metabolomic analysis," *Sci. Rep.*, vol. 9, no. 1, pp. 1–9, 2019.
[115] N. Kuhnert, F. Dairpoosh, G. Yassin, A. Golon, and R. Jaiswal, "What is under the hump? Mass spectrometry based analysis of complex mixtures in processed food-lessons from the characterisation of black tea thearubigins, coffee melanoidines and caramel," *Food Funct.*, vol. 4, no. 8, pp. 1130–1147, 2013.
[116] W. Zhang and P. X. Zhao, "Quality evaluation of extracted ion chromatograms and chromatographic peaks in liquid chromatography/mass spectrometry-based metabolomics data," *BMC Bioinformatics*, vol. 15, no. 11, p. S5, Oct. 2014.
[117] L. Tao *et al.*, "Metabolomics identifies serum and exosomes metabolite markers of pancreatic cancer," *Metabolomics*, vol. 15, no. 6, pp. 1–11, 2019.
[118] K. M. Nieman *et al.*, "Adipocytes promote ovarian cancer metastasis and provide energy for rapid tumor growth," *Nat. Med.*, vol. 17, no. 11, pp. 1498–1503, Nov. 2011.
[119] M. E. Monaco, "Fatty acid metabolism in breast cancer subtypes," *Oncotarget*, vol. 8, no. 17. Impact Journals LLC, pp. 29487–29500, 2017.
[120] X. Bian *et al.*, "Riboflavin deficiency affects lipid metabolism partly by reducing apolipoprotein B100 synthesis in rats," *J. Nutr. Biochem.*, vol. 70, pp. 75–81, Aug. 2019.
[121] R. Yang, Z. Wei, and S. Wu, "Lumiflavin increases the sensitivity of ovarian cancer stem-like cells to cisplatin by interfering with riboflavin," *J. Cell. Mol. Med.*, vol. 23, no. 8, pp. 5329–5339, Aug. 2019.
[122] I. Elia and M. C. Haigis, "Metabolites and the tumour microenvironment: from cellular mechanisms to systemic metabolism," *Nature Metabolism*, vol. 3, no. 1. Nature Research, pp. 21–32, 01-Jan-2021.
[123] V. Raimondi, F. Ciccarese, and V. Ciminale, "Oncogenic pathways and the electron transport chain: a dangeROS liaison," *British Journal of Cancer*, vol. 122, no. 2. Springer Nature, pp. 168–181, 21-Jan-2020.
[124] R. Marchan *et al.*, "Glycerol-3-phosphate acyltransferase 1 promotes tumor cell migration and poor survival in ovarian carcinoma," *Cancer Res.*, vol. 77, no. 17, pp. 4589–4601, Sep. 2017.
[125] M. Y. Fong, J. McDunn, and S. S. Kakar, "Identification of metabolites in the normal ovary and

their transformation in primary and metastatic ovarian cancer," *PLoS One*, vol. 6, no. 5, pp. 1–12, 2011.
[126] S. Tatekawa *et al.*, "Methylosystem for cancer sieging strategy," *Cancers*, vol. 13, no. 20. MDPI, 02-Oct-2021.
[127] Y. Deng *et al.*, "Profiling of polar urine metabolite extracts from Chinese colorectal cancer patients to screen for potential diagnostic and adverse-effect biomarkers," *J. Cancer*, vol. 11, no. 23, pp. 6925–6938, Oct. 2020.
[128] J. Huang, A. M. Mondul, S. J. Weinstein, E. D. Karoly, J. N. Sampson, and D. Albanes, "Prospective serum metabolomic profile of prostate cancer by size and extent of primary tumor," *Oncotarget*, vol. 8, no. 28, pp. 45190–45199, Apr. 2017.
[129] R. Keshet, P. Szlosarek, A. Carracedo, and A. Erez, "Rewiring urea cycle metabolism in cancer to support anabolism," *Nature Reviews Cancer*, vol. 18, no. 10. Nature Publishing Group, pp. 634–645, 01-Oct-2018.
[130] D. Dudzik *et al.*, "Perspectives and challenges in extracellular vesicles untargeted metabolomics analysis," *TrAC - Trends in Analytical Chemistry*, vol. 143. Elsevier B.V., p. 116382, 01-Oct-2021.
[131] T. Baranyai *et al.*, "Isolation of exosomes from blood plasma: Qualitative and quantitative comparison of ultracentrifugation and size exclusion chromatography methods," *PLoS One*, vol. 10, no. 12, pp. 1–13, 2015.
[132] E. Fic, S. Kedracka-Krok, U. Jankowska, A. Pirog, and M. Dziedzicka-Wasylewska, "Comparison of protein precipitation methods for various rat brain structures prior to proteomic analysis," *Electrophoresis*, vol. 31, no. 21, pp. 3573–3579, Oct. 2010.
[133] J. B. Simonsen, "What Are We Looking At? Extracellular Vesicles, Lipoproteins, or Both?," pp. 920–922.
[134] N. Karimi *et al.*, "Detailed analysis of the plasma extracellular vesicle proteome after separation from lipoproteins," *Cell. Mol. Life Sci.*, vol. 75, no. 15, pp. 2873–2886, 2018.
[135] B. W. Sódar *et al.*, "Low-density lipoprotein mimics blood plasma-derived exosomes and microvesicles during isolation and detection," *Sci. Rep.*, vol. 6, no. 1, pp. 1–12, Apr. 2016.
[136] Y. Sun, K. Saito, and Y. Saito, "Lipid profile characterization and lipoprotein comparison of extracellular vesicles from human plasma and serum," *Metabolites*, vol. 9, no. 11, pp. 10–14, 2019.
[137] J. Gross, S. Sayle, A. R. Karow, U. Bakowsky, and P. Garidel, "Nanoparticle tracking analysis of particle size and concentration detection in suspensions of polymer and protein samples: Influence of experimental and data evaluation parameters," *Eur. J. Pharm. Biopharm.*, vol. 104, pp. 30–41, Jul. 2016.
[138] A. Yekula *et al.*, "Large and small extracellular vesicles released by glioma cells in vitro and in vivo," *J. Extracell. Vesicles*, vol. 9, no. 1, p. 1689784, Jan. 2020.
[139] H. T. Hu, T. Nishimura, and S. Suetsugu, "Ultracentrifugal separation, characterization, and functional study of extracellular vesicles derived from serum-free cell culture," *STAR Protoc.*, vol. 2, no. 3, Sep. 2021.
[140] R. Linares, S. Tan, C. Gounou, N. Arraud, and A. R. Brisson, "High-speed centrifugation induces aggregation of extracellular vesicles," *J. Extracell. Vesicles*, vol. 4, no. 1, 2015.
[141] K. Abhange *et al.*, "Small extracellular vesicles in cancer," *Bioactive Materials*, vol. 6, no. 11. KeAi Communications Co., pp. 3705–3743, 01-Nov-2021.
[142] F. Royo *et al.*, "Hepatocyte-secreted extracellular vesicles modify blood metabolome and endothelial function by an arginase-dependent mechanism," *Sci. Rep.*, vol. 7, no. January, pp. 1–15, 2017.
[143] J. Webber and A. Clayton, "How pure are your vesicles?," *J. Extracell. Vesicles*, vol. 2, no. 1, p. 19861, Jan. 2013.
[144] B. Talebjedi, N. Tasnim, M. Hoorfar, G. F. Mastromonaco, and M. De Almeida Monteiro Melo Ferraz, "Exploiting Microfluidics for Extracellular Vesicle Isolation and Characterization: Potential Use for Standardized Embryo Quality Assessment," *Front. Vet. Sci.*, vol. 7, no. January, pp. 1–18, 2021.
[145] W. Oosthuyzen *et al.*, "Quantification of human urinary exosomes by nanoparticle tracking analysis," *J. Physiol.*, vol. 591, no. 23, pp. 5833–5842, 2013.

[146] A. Cvjetkovic, J. Lötvall, and C. Lässer, “The influence of rotor type and centrifugation time on the yield and purity of extracellular vesicles,” *J. Extracell. Vesicles*, vol. 3, no. 1, pp. 1–11, 2014.
[147] S. M. Langevin *et al.*, “Balancing yield, purity and practicality: a modified differential ultracentrifugation protocol for efficient isolation of small extracellular vesicles from human serum,” *RNA Biol.*, vol. 16, no. 1, pp. 5–12, 2019.
[148] D. K. Jeppesen *et al.*, “Comparative analysis of discrete exosome fractions obtained by differential centrifugation,” *J. Extracell. Vesicles*, vol. 3, no. 1, pp. 0–16, 2014.
[149] M. Chang, Q. Wang, W. Qin, X. Shi, and G. Xu, “Rational Synthesis of Aptamer-Functionalized Polyethylenimine-Modified Magnetic Graphene Oxide Composites for Highly Efficient Enrichment and Comprehensive Metabolomics Analysis of Exosomes,” *Anal. Chem.*, vol. 92, no. 23, pp. 15497–15505, Dec. 2020.
[150] M. K. Jung and J. Y. Mun, “Sample preparation and imaging of exosomes by transmission electron microscopy,” *J. Vis. Exp.*, vol. 2018, no. 131, 2018.
[151] L. Wang, T. F. Bruce, S. Huang, and R. K. Marcus, “Isolation and quantitation of exosomes isolated from human plasma via hydrophobic interaction chromatography using a polyester, capillary-channeled polymer fiber phase,” *Anal. Chim. Acta*, vol. 1082, pp. 186–193, 2019.
[152] M. Yao, J. Chen, J. Zheng, M. Song, D. J. McClements, and H. Xiao, “Enhanced lymphatic transport of bioactive lipids: Cell culture study of polymethoxyflavone incorporation into chylomicrons,” *Food Funct.*, vol. 4, no. 11, pp. 1662–1667, Nov. 2013.
[153] R. E. Veerman *et al.*, “Molecular evaluation of five different isolation methods for extracellular vesicles reveals different clinical applicability and subcellular origin,” *J. Extracell. Vesicles*, vol. 10, no. 9, p. e12128, Jul. 2021.
[154] G. van Niel *et al.*, “The Tetraspanin CD63 Regulates ESCRT-Independent and -Dependent Endosomal Sorting during Melanogenesis,” *Dev. Cell*, vol. 21, no. 4, pp. 708–721, 2011.
[155] A. lie Ståhl, K. Johansson, M. Mossberg, R. Kahn, and D. Karpman, “Exosomes and microvesicles in normal physiology, pathophysiology, and renal diseases,” *Pediatric Nephrology*, vol. 34, no. 1. Springer Verlag, pp. 11–30, 01-Jan-2019.
[156] Y. Li *et al.*, “Malignant ascite-derived extracellular vesicles inhibit T cell activity by upregulating Siglec-10 expression,” *Cancer Manag. Res.*, vol. 11, pp. 7123–7134, 2019.
[157] J. F. Xiao, B. Zhou, and H. W. Ressom, “Metabolite identification and quantitation in LC-MS/MS-based metabolomics,” *TrAC - Trends Anal. Chem.*, vol. 32, pp. 1–14, 2012.
[158] F. Royo *et al.*, “Hepatocyte-secreted extracellular vesicles modify blood metabolome and endothelial function by an arginase-dependent mechanism,” *Sci. Rep.*, vol. 7, no. 1, pp. 1–15, Feb. 2017.

A. SUPPLEMENTARY MATERIAL

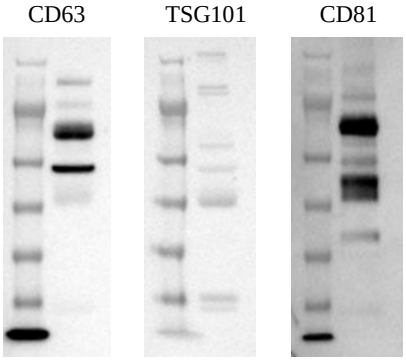

Figure S.1 - **Uncropped scan of Human Exosome Lysate Positive Protein Control with anti-CD63, anti-TSG101 and anti-CD81.** From left to right: CD63, TSG101 and CD81 membranes exposed to LED light for 13 s, 14 s and 1 min 45 s, respectively. Polyclonal rabbit anti-CD63 (#EXOAB-CD63A-1), anti-TSG101 (#EXOAB-TSG101-1) and anti-CD81 (#EXOAB-CD81A-1) (SBI) primary antibodies were used at 1:1,000 dilution. Goat anti-rabbit HRP secondary antibody (SBI, # EXOAB-KIT-1) was used at 1: 5,000 dilution. CD63 membrane was incubated with Cytiva Amersham ECL Select Western Blotting Detection Reagent (GE Healthcare, 45-000-999), and the others with GE Healthcare Amersham™ ECL Prime Western Blotting Detection Reagent (GE Healthcare, # 12316992). Detection was performed in iBright FL1500 Imaging System (Invitrogen, #A44241), using Chemi Blots protocol.

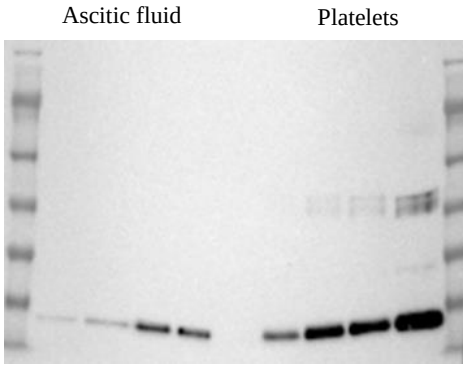

Figure S.2 – **Uncropped scan of ascitic fluids and platelets at different total protein amounts (2, 5, 10 and 20 µg) with anti-ApoA-I.** Monoclonal rabbit anti-ApoA-I (Abcam, UK, #ab52945) primary antibody was used at 1:1,000 dilution. Goat anti-rabbit HRP secondary antibody (SBI, # EXOAB-KIT-1) was used at 1: 20,000 dilution. Membrane was incubated with GE Healthcare Amersham™ ECL Prime Western Blotting Detection Reagent (GE Healthcare, # 12316992). Detection was performed in iBright FL1500 Imaging System (Invitrogen, #A44241), using Chemi Blots protocol, for 1 min.

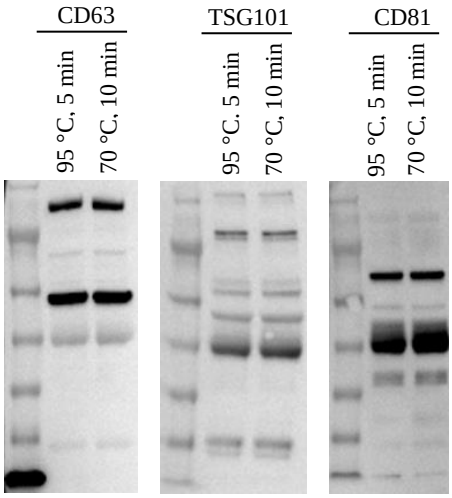

Figure S.3 – **Uncropped scan of Human Exosome Lysate Positive Protein Control prepared in different conditions of denaturation with anti-CD63, anti-TSG101 and anti-CD81.** From left to right: CD63, TSG101 and CD81 membranes exposed to LED light for 10 s, 25 s and 25 s, respectively. Polyclonal rabbit anti-CD63 (#EXOAB-CD63A-1), anti-TSG101 (#EXOAB-TSG101-1) and anti-CD81 (#EXOAB-CD81A-1) (SBI) primary antibodies were used at 1:1,000 dilution. Goat anti-rabbit HRP secondary antibody (SBI, # EXOAB-KIT-1) was used at 1: 5,000 dilution. CD63 membrane was incubated with Cytiva Amersham ECL Select Western Blotting Detection Reagent (GE Healthcare, 45-000-999), and the others with GE Healthcare Amersham™ ECL Prime Western Blotting Detection Reagent (GE Healthcare, # 12316992). Detection was performed in iBright FL1500 Imaging System (Invitrogen, #A44241), using Chemi Blots protocol.

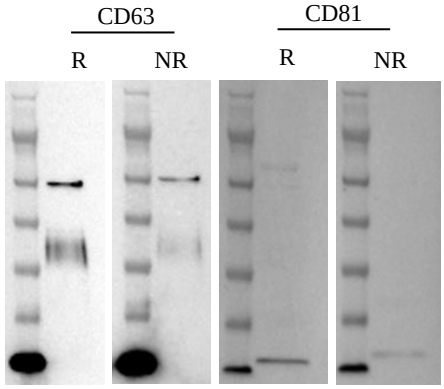

Figure S.4 – **Uncropped scan of ES-2 EVs prepared in reducing and non-reducing conditions with anti-CD63 and anti-CD81.** From left to right: CD63 (reducing conditions), CD63 (non-reducing conditions), CD81 (reducing conditions) and CD81 (non-reducing conditions) membranes exposed to LED light for 58 s (CD63) and 27 s (CD81). R – reducing conditions. NR – non-reducing conditions. Polyclonal rabbit anti-CD63 (#EXOAB-CD63A-1) and anti-CD81 (#EXOAB-CD81A-1) (SBI) primary antibodies were used at 1:1,000 dilution. Goat anti-rabbit HRP secondary antibody (SBI, # EXOAB-KIT-1) was used at 1: 20,000 dilution. CD63 membrane was incubated with Cytiva Amersham ECL Select Western Blotting Detection Reagent (GE Healthcare, 45-000-999), and CD81 membrane with GE Healthcare Amersham™ ECL Prime Western Blotting Detection Reagent (GE Healthcare, # 12316992). Detection was performed in iBright FL1500 Imaging System (Invitrogen, #A44241), using Chemi Blots protocol.

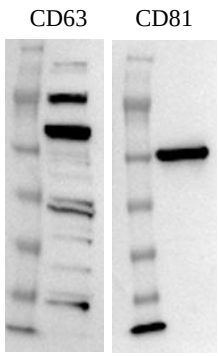

Figure S.5 – **Uncropped scan of MDA cells with anti-CD63 and anti-CD81.** From left to right: CD63 and CD81 membranes exposed to LED light for 7 s and 49 s, respectively. Polyclonal rabbit anti-CD63 (#EXOAB-CD63A-1) and anti-CD81 (#EXOAB-CD81A-1) (SBI) primary antibodies were used at 1:1,000 dilution. Goat anti-rabbit HRP secondary antibody (SBI, # EXOAB-KIT-1) was used at 1: 20,000 dilution. CD63 membrane was incubated with Cytiva Amersham ECL Select Western Blotting Detection Reagent (GE Healthcare, 45-000-999), and CD81 membrane with GE Healthcare Amersham™ ECL Prime Western Blotting Detection Reagent (GE Healthcare, # 12316992). Detection was performed in iBright FL1500 Imaging System (Invitrogen, #A44241), using Chemi Blots protocol.

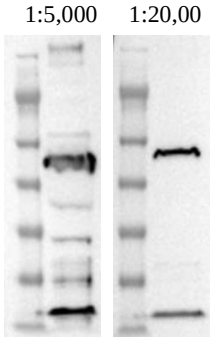

Figure S.6 – **Uncropped scan of ES-2 EVs prepared in different secondary antibody dilutions with anti-TSG101.** From left to right: TSG101 (1:5,000 dilution) and TSG101 (1:20,000 dilution) membranes exposed to LED light for 13 s. Each lane was loaded with 14.69 µg of protein. Polyclonal rabbit anti-TSG101 (SBI, #EXOAB-TSG101-1) primary antibody was used at 1:1,000 dilution. Goat anti-rabbit HRP secondary antibody (SBI, # EXOAB-KIT-1) was used at 1:5,000 and 1: 20,000 dilution. Membrane was incubated with GE Healthcare Amersham™ ECL Prime Western Blotting Detection Reagent (GE Healthcare, # 12316992). Detection was performed in iBright FL1500 Imaging System (Invitrogen, #A44241), using Chemi Blots protocol.

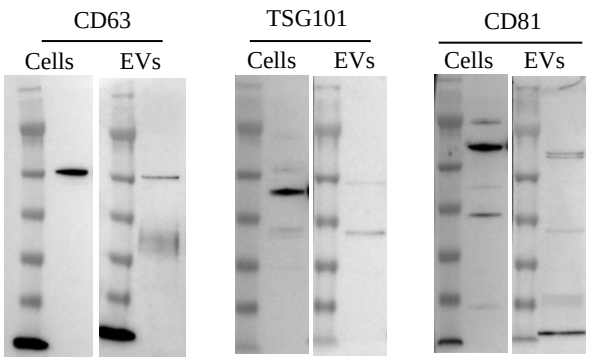

Figure S.7 – **Uncropped scan of ES-2 cells and EVs with anti-CD63, anti-TSG101 and anti-CD81.** From left to right: CD63 (ES-2 cells), CD63 (EVs from ES-2 cells), TSG101 (ES-2 cells), TSG101 (EVs from ES-2 cells), CD81 (ES-2 cells) and CD81 (EVs from ES-2 cells) membranes exposed to LED light for 1 min (CD63), 2 min (TSG101) and 49 s (CD81). Polyclonal rabbit anti-CD63 (#EXOAB-CD63A-1), anti-TSG101 (#EXOAB-TSG101-1) and anti-CD81 (#EXOAB-CD81A-1) (SBI) primary antibodies were used at 1:1,000 dilution. Goat anti-rabbit HRP secondary antibody (SBI, # EXOAB-KIT-1) was used at 1: 20,000 dilution. All membranes were incubated with Cytiva Amersham ECL Select Western Blotting Detection Reagent (GE Healthcare, 45-000-999). Detection was performed in iBright FL1500 Imaging System (Invitrogen, #A44241), using Chemi Blots protocol.

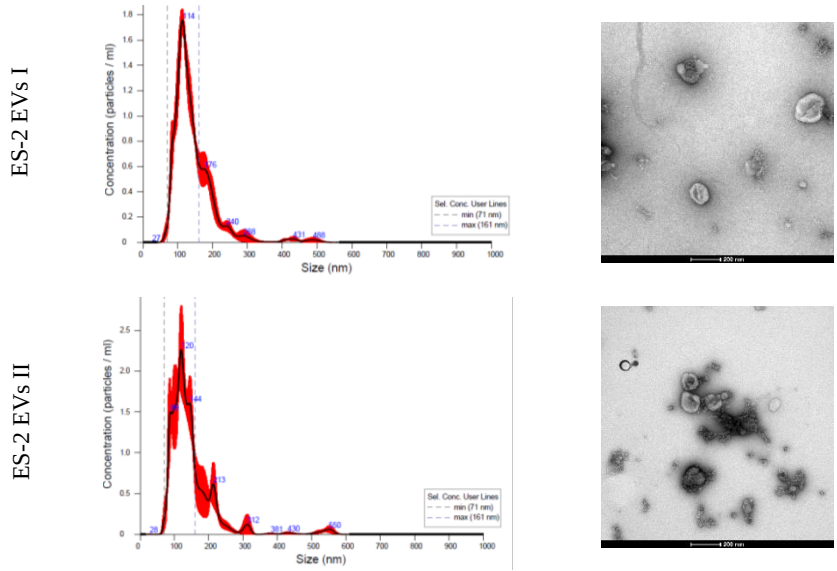

Figure S.8 – **NTA and TEM analysis of ES-2 EVs**. Top panel – Particle size distribution by NTA (left) and morphology by TEM (right) of ES-2 EVs isolated from cell culture replicate I at 9.6×10^{10} particles/mL. Bottom panel – Particle size distribution by NTA (left) and morphology by TEM (right) of ES-2 EVs isolated from cell culture replicate II at 4.5×10^{11}.

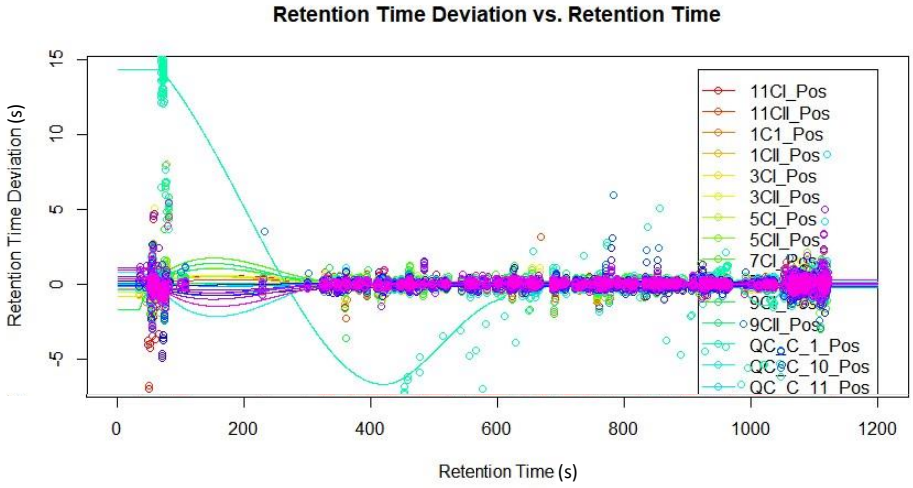

Figure S.9 – **Retention time deviation vs. retention time of extracted metabolites from ES-2 EVs using all condition QCs.** Data obtained by LC-MS using C18 column and positive ionization mode was processed with XCMS package.

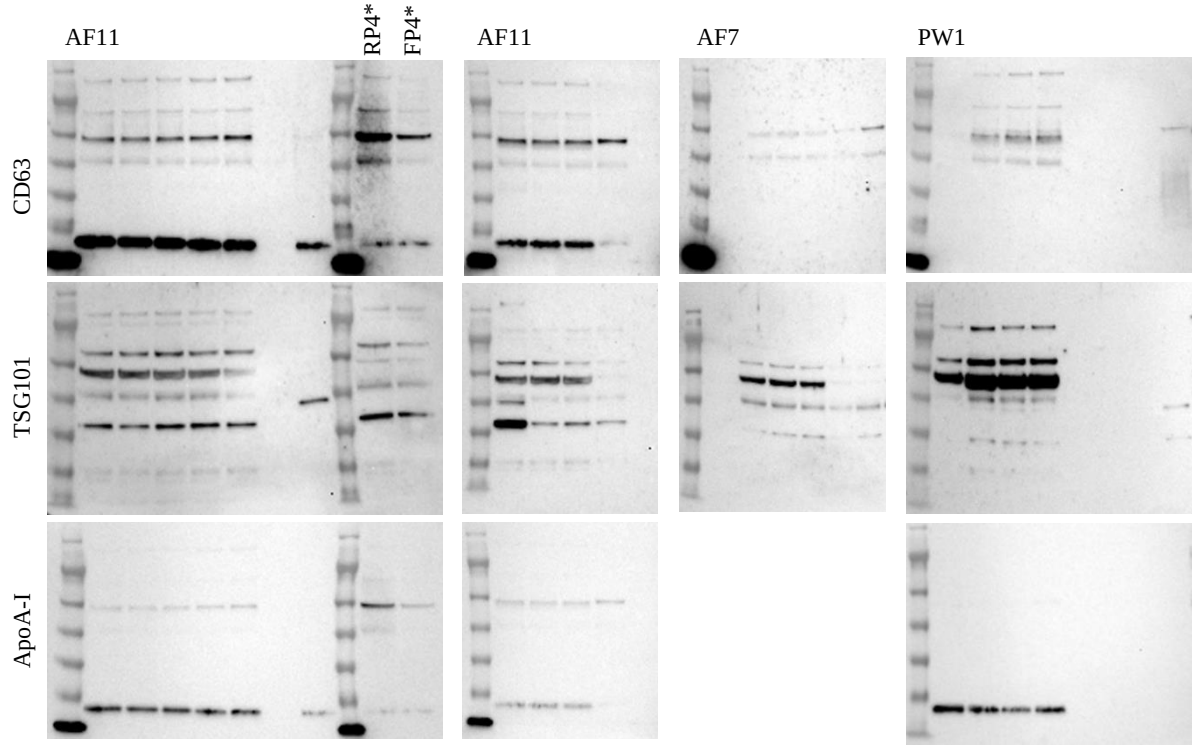

* TCA precipitation

Figure S.10 – **Uncropped scan of CD63, TSG101 and ApoA-I in isolation fractions of ascitic fluids and peritoneal washes for step-by-step characterization.** From left to right: CD63 membranes were exposed to LED light for 1 min 19 s (AF11 EV-fractions), 1 min (AF11 discarded), 20 min (AF7) and 3 min 20 s (PW1); TSG101 for 6 min 40 s (AF11 EV-fractions), 6 min 37 s (AF11 discarded), 11 min 21 s (AF7) and 11 min 30 s (PW1); and ApoA-I for 14 s (AF11 Isolated), 14 s (AF11 discarded) and 3 min 19 s (PW1). In a black box (AF11) are marked RP4 and FP4 fractions, respectively, prepared using TCA for protein precipitation. Polyclonal rabbit anti-CD63 (#EXOAB-CD63A-1), anti-TSG101 (#EXOAB-TSG101-1) (SBI) and monoclonal rabbit anti-ApoA-I (Abcam, UK, #ab52945) primary antibodies were used at 1:1,000 dilution. In AF11 membranes, anti-CD63 and anti-ApoA-I antibodies were incubated simultaneously. Goat anti-rabbit HRP secondary antibody (SBI, # EXOAB-KIT-1) was used at 1: 20,000 dilution. All CD63 membranes were incubated with Cytiva Amersham ECL Select Western Blotting Detection Reagent (GE Healthcare, 45-000-999). The others were incubated with GE Healthcare Amersham™ ECL Prime Western Blotting Detection Reagent (GE Healthcare, # 12316992). Detection was performed in iBright FL1500 Imaging System (Invitrogen, #A44241), using Chemi Blots protocol.

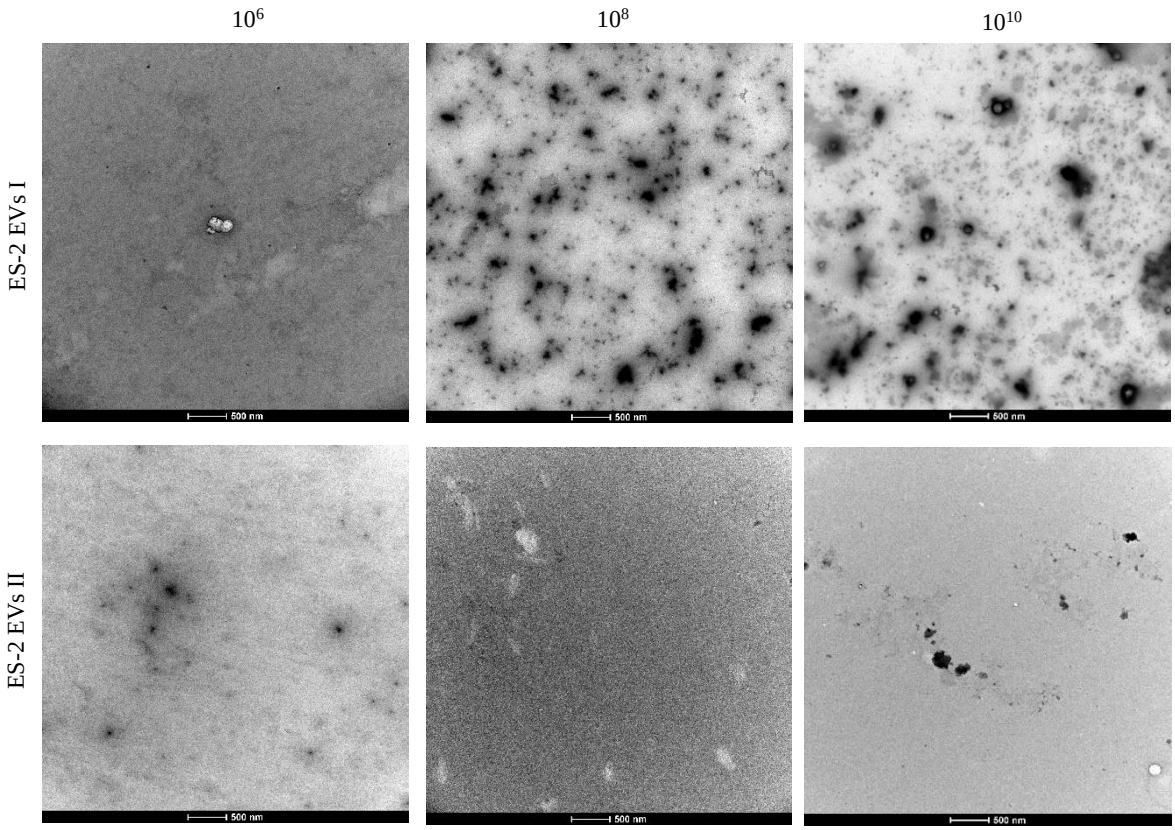

Figure S.11 – **Precipitate after metabolite extraction of ES-2 EVs.** Representative images of precipitate after metabolite extraction from EVs of ES-2 cell culture replicates I and II at concentration of 10^6 (left), 10^8 (middle), and 10^{10} (right) particles/mL.

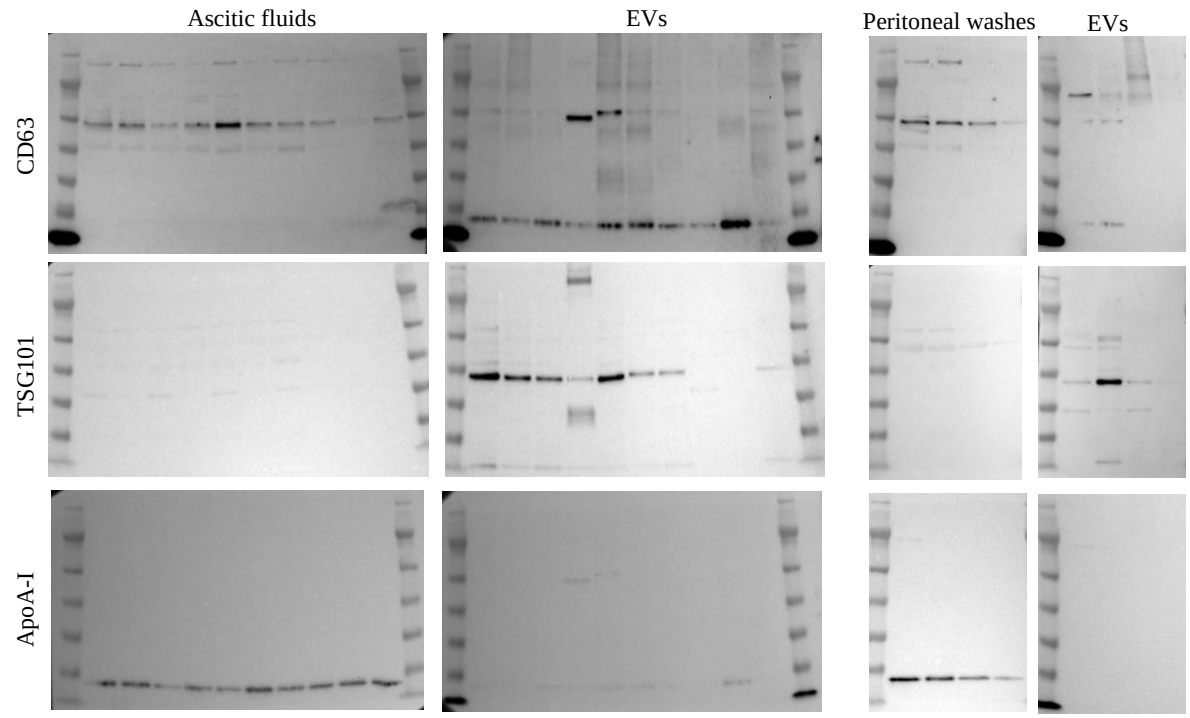

Figure S.12 – **Uncropped scan of CD63, TSG101 and ApoA-I in ascitic fluids or peritoneal washes and corresponding EVs**. From left to right: CD63 membranes were exposed to LED light for 1 min 40 s (ascitic fluids), 1 min 40 s (EVs from ascitic fluids), 9 min 26 s (peritoneal washes) and 9 min 26 s (EVs from peritoneal washes); TSG101 membranes for 7 s (ascitic fluids), 13 s (EVs from ascitic fluids), 40 s (peritoneal washes) and 40 s (EVs from peritoneal washes); and ApoA-I membranes for 7 s (ascitic fluids), 7 s (EVs from ascitic fluids), 34 s (peritoneal washes) and 34 s (EVs from peritoneal washes). Polyclonal rabbit anti-CD63 (#EXOAB-CD63A-1), anti-TSG101 (#EXOAB-TSG101-1) (SBI) and monoclonal rabbit anti-ApoA-I (Abcam, UK, #ab52945) primary antibodies were used at 1:1,000 dilution. In EV membranes, anti-CD63 and anti-ApoA-I antibodies were incubated simultaneously. Goat anti-rabbit HRP secondary antibody (SBI, # EXOAB-KIT-1) was used at 1: 20,000 dilution. All membranes were incubated with Cytiva Amersham ECL Select Western Blotting Detection Reagent (GE Healthcare, 45-000-999). Detection was performed in iBright FL1500 Imaging System (Invitrogen, #A44241), using Chemi Blots protocol.

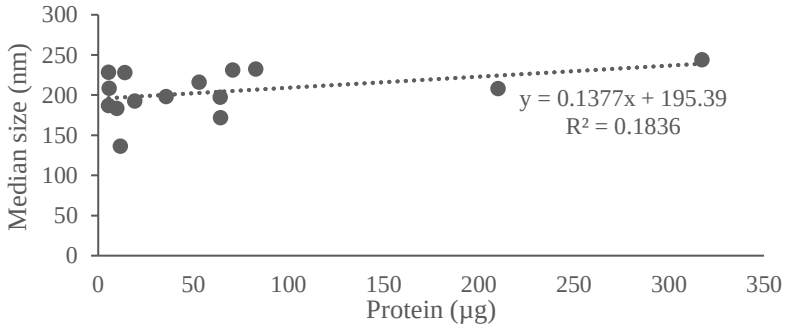

Figure S.13 – **Size median and total protein of EV fractions from ascitic fluids and peritoneal washes.**

B. **TABLES OF METABOLITES**

Table S.1 – **ES-2 EVs metabolite identifications using Compound Discoverer software for C18 column and positive mode of ionization**. Annot. Source – annotation source; Calc. MW – calculated molecular weight; RSD – relative standard deviation.

ID	Name
1	(2E)-2,5-Dichloro-4-oxo-2-hexenedioic acid
2	11-Aminoundecanoic acid
3	Phosphoric acid
4	Pivagabine
5	Mutagen X
6	Estra-1,3,5(10)-triene-3,6alpha,17beta-triol triacetate
7	PEG-4
8	Isopropyl catechol
9	2,2,6,6-Tetramethyl-4-piperidinol
10	3-Tropanol
11	PEG n5
12	Minoxidil
13	butoctamide
14	capuride
15	PEG n6
16	Betaine
17	Cyclopenta[cd]pyrene
18	benzarone
19	Triethanolamine
20	2-Hexenoylcarnitine
21	2064747
22	Urocanic acid
23	1,2,3,4,6,7,8-Heptachlorodibenzofuran

ID	Name
24	MFCD00216258
25	N-Acetyl-L-leucine
26	butoctamide
27	3-[(6-Oxodecanoyl)oxy]-4-(trimethylammonio)butanoate
28	1,2,3,4,6,7,8-Heptachlorooxanthrene
29	Adipic acid
30	Methylenediurea
31	D-(+)-Pyroglutamic Acid
32	Caprolactam
33	4230434
34	O-{Hydroxy[(2R)-2-[(11Z)-11-octadecenoyloxy]-3-(pentadecanoyloxy)propoxy]phosphoryl}-L-serine
35	N-docosanoylsphinganine
36	Succinylacetone
37	L-(+)-Leucine
38	Sumarotene
39	Leucine
40	TCA-ethadyl
41	Hydroxyamphetamine
42	4-Ethylphenol
43	4-Ethylphenol
44	Indane
45	asn-arg
46	Succinylacetone
47	Imagabalin

ID	Formula	Annot. Source: Predicted Compositions	Annot. Source: mzCloud Search	Annot. Source: ChemSpider Search	Annot. DeltaMass [ppm]	Calc. MW	RT [min]	Area (Max.)	# ChemSpider Results	# mzCloud Results	# Usable QC	RSD QC Areas [%]	RSD Corr. QC Areas [%]	MS2
1	C6H4Cl2O5	No results	No results	Full match	1.19	225.9439	0.878	6.11E+08	1	0	11	3	3	No MS2
2	C11H23NO2	No results	No results	Full match	-0.64	201.1728	1.765	4.44E+08	1	0	11	6	5	DDA for preferred ion
3	H3O4P	No results	No results	Full match	-0.79	97.97682	0.966	3.54E+08	1	0	11	7	7	DDA for preferred ion
4	C9H17NO3	No results	No results	Full match	-0.17	187.1208	6.875	3.1E+08	4	0	11	5	5	DDA for preferred ion
5	C5H3Cl3O3	No results	No results	Full match	2.87	215.9154	0.903	2.39E+08	1	0	11	2	2	DDA for preferred ion
6	C24H30O6	No results	No results	Full match	-0.61	414.204	11.438	2.22E+08	7	0	12	21	21	DDA for other ion
7	C8H18O5	No results	No results	Full match	-0.33	194.1154	5.397	1.58E+08	1	0	11	6	6	DDA for preferred ion
8	C9H12O2	No results	No results	Full match	-0.85	152.0836	6.873	1.47E+08	14	0	11	6	6	DDA for preferred ion
9	C9H19NO	No results	Full match	No results	-0.43	157.1466	1.645	1.11E+08	0	2	11	5	4	DDA for preferred ion
10	C8H15NO	No results	No results	Full match	0.11	141.1154	6.875	51656513	11	0	11	6	5	DDA for preferred ion
11	C10H22O6	No results	Full match	No results	-1.4	238.1413	5.766	50623079	0	1	11	6	6	DDA for preferred ion

ID	Formula	Annot. Source: Predicted Compositions	Annot. Source: mzCloud Search	Annot. Source: ChemSpider Search	Annot. DeltaMass [ppm]	Calc. MW	RT [min]	Area (Max.)	#ChemSpider Results	#mzCloud Results	#Usable QC	RSD QC Areas [%]	RSD Corr. QC Areas [%]	MS2
12	C9H15N5O	No results	No results	Full match	-2.94	209.1271	0.968	42219379	2	0	11	4	4	DDA for preferred ion
13	C16H29NO5	No results	No results	Full match	-0.47	315.2044	6.385	42179843	1	0	11	5	5	DDA for preferred ion
14	C9H18N2O2	No results	No results	Full match	0.26	186.1369	6.02	40075351	2	0	11	5	5	DDA for preferred ion
15	C12H26O7	No results	Full match	Full match	-0.81	282.1676	6.015	34830774	1	1	11	4	4	DDA for preferred ion
16	C5H11NO2	No results	Full match	Partial match	-1.25	117.0788	0.973	32830305	12	3	11	21	20	DDA for preferred ion
17	C18H10	No results	No results	Full match	2.34	226.0788	1.33	29888146	2	0	11	18	13	No MS2
18	C17H14O3	No results	No results	Full match	-0.01	266.0943	6.873	26188150	4	0	11	7	7	DDA for other ion
19	C6H15NO3	No results	No results	Full match	-0.07	149.1052	0.954	23412806	1	0	11	5	5	No MS2
20	C13H23NO4	No results	No results	Full match	-0.83	257.1625	5.787	23404330	1	0	11	5	5	DDA for preferred ion
21	C10Cl10	No results	No results	Full match	1.52	469.6892	0.935	19098712	1	0	11	13	13	No MS2
22	C6H6N2O2	No results	Full match	Partial match	0.15	138.043	1.336	18030165	8	6	11	8	8	DDA for preferred ion
23	C12HCl7O	No results	No results	Full match	2.52	405.7857	0.91	17729922	2	0	11	6	6	No MS2
24	C13H10S	No results	No results	Full match	0.5	198.0504	5.968	15701776	1	0	11	5	5	DDA for preferred ion
25	C8H15NO3	No results	No results	Full match	-0.14	173.1052	6.241	15566362	8	0	11	5	5	No MS2
26	C16H29NO5	No results	No results	Full match	-0.56	315.2044	6.098	13071752	1	0	11	24	23	DDA for preferred ion
27	C17H31NO5	No results	No results	Full match	-0.77	329.22	6.83	12830384	1	0	11	5	5	DDA for preferred ion
28	C12HCl7O2	No results	No results	Full match	2.08	421.7805	0.908	12823027	1	0	11	19	19	No MS2
29	C6H10O4	No results	No results	Full match	-0.38	146.0579	7.648	12475417	20	0	11	5	5	DDA for preferred ion
30	C3H8N4O2	No results	No results	Full match	-0.78	132.0646	1.078	10895251	1	0	11	11	9	No MS2
31	C5H7NO3	No results	Full match	Full match	0.16	129.0426	1.681	10464710	10	2	11	7	7	DDA for preferred ion
32	C6H11NO	No results	Full match	Full match	-0.43	113.084	5.988	10125600	4	1	11	13	13	DDA for preferred ion
33	C6H12N2O	No results	No results	Full match	-0.55	128.0949	0.962	9288225	2	0	11	7	7	DDA for preferred ion
34	C39H74NO10P	No results	No results	Full match	-1	747.5043	0.934	8333624	4	0	11	22	21	No MS2
35	C40H81NO3	No results	No results	Full match	1.84	623.6228	0.921	7546471	1	0	11	9	7	No MS2
36	C7H10O4	No results	No results	Full match	-0.3	158.0579	7.919	7480530	7	0	11	9	6	No MS2
37	C6H13NO2	No results	No results	Full match	0.88	131.0947	2.254	6606428	18	0	11	9	9	DDA for preferred ion
38	C24H30O2S	No results	No results	Full match	-0.66	382.1964	13.59	6018398	1	0	12	12	10	No MS2
39	C6H13NO2	No results	No results	Full match	0.88	131.0947	2.496	5992478	18	0	11	10	10	DDA for preferred ion
40	C6H4Cl6O4	No results	No results	Full match	0.09	349.8241	0.906	5763149	1	0	11	5	5	No MS2
41	C9H13NO	No results	No results	Full match	-0.38	151.0997	6.873	5030263	17	0	11	7	7	No MS2
42	C8H10O	No results	No results	Full match	0.7	122.0733	1.338	4920533	16	0	11	9	9	DDA for preferred ion
43	C8H10O	No results	No results	Full match	-1.09	122.073	1.339	4920533	16	0	11	9	9	DDA for preferred ion
44	C9H10	No results	No results	Full match	-0.41	118.0782	7.647	4746705	2	0	11	8	8	No MS2
45	C10H20N6O4	No results	No results	Full match	-0.03	288.1546	6.762	4274292	2	0	11	6	6	No MS2
46	C7H10O4	No results	No results	Full match	-0.31	158.0579	5.968	3644482	7	0	11	8	8	DDA for preferred ion
47	C9H19NO2	No results	No results	Full match	-0.36	173.1415	5.513	2830237	1	0	11	6	6	No MS2

Table S.2 – **ES-2 EVs metabolite identifications using Compound Discoverer software for C18 column and negative mode of ionization**. Annot. Source – annotation source; Calc. MW – calculated molecular weight; RSD – relative standard deviation.

ID	Name
1	Phosphoric acid
2	12,13-Epoxytrichothec-9-ene-3,4,8,15-tetrol
3	Pivagabine
4	12,13-Epoxytrichothec-9-ene-3,4,8,15-tetrol
5	DL-Lactic Acid
6	ETHYLENEBISDITHIOCARBAMIC ACID
7	N-Nonanoylglycine
8	Ceramide (d18:1/24:1(15Z))
9	1872050
10	(3alpha,5alpha,17beta)-17-Hydroxyandrostan-3-yl beta-D-glucopyranuronate
11	4-Oxoproline
12	(14R)-3beta,5,6beta,10,16-pentahydroxygrayanotoxan-14-yl acetate
13	N-Acetyl-DL-alloisoleucine
14	Capryloylglycine
15	1-(3,4-Dimethoxyphenyl)-3,5-decanediyl diacetate
16	Succinic acid
17	(2R)-3-{[(2-Aminoethoxy)(hydroxy)phosphoryl]oxy}-2-[(1Z,11Z)-1,11-octadecadien-1-yloxy]propyl (6Z,9Z,12Z,15Z)-6,9,12,15-octadecatetraenoate
18	Botrydial
19	Benzoic acid
20	Juliflorine
21	Tedatioxetine

ID	Formula	Annot. Source: Predicted Compositions	Annot. Source: mzCloud Search	Annot. Source: ChemSpider Search	Annot. DeltaMass [ppm]	Calc. MW	RT [min]	Area (Max.)	# ChemSpider Results	# mzCloud Results	# Usable QC	RSD QC Areas [%]	RSD Corr. QC Areas [%]	MS2
1	H3 O4 P	No results	No results	Full match	-1.66	97.97673	0.959	8.08E+08	1	0	11	7	6	DDA for preferred ion
2	C15 H22 O6	No results	No results	Full match	-1.29	298.1413	7.636	4.33E+08	4	0	12	6	6	DDA for preferred ion
3	C9 H17 N O3	No results	No results	Full match	-1.18	187.1206	6.86	2.13E+08	4	0	12	6	5	DDA for preferred ion
4	C15 H22 O6	No results	No results	Full match	-1.22	298.1413	7.764	79501315	4	0	12	8	7	DDA for preferred ion
5	C3 H6 O3	No results	No results	Full match	-1.22	90.03158	1.38	43718638	11	0	12	18	15	No MS2
6	C4 H8 N2 S4	No results	No results	Full match	-1.95	211.9566	0.786	35689758	1	0	11	16	13	No MS2
7	C11 H21 N O3	No results	No results	Full match	-0.55	215.152	8.075	28053927	2	0	12	5	5	DDA for preferred ion
8	C42 H81 N O3	No results	No results	Full match	2.4	647.6232	0.956	19623877	1	0	11	14	12	No MS2
9	C12 H23 N O3	No results	No results	Full match	-1.46	229.1675	8.651	17669269	1	0	12	4	3	DDA for preferred ion
10	C25 H40 O8	No results	No results	Full match	-1.48	468.2716	11.082	15224063	3	0	12	9	6	DDA for preferred ion

ID	Formula	Annot. Source: Predicted Compositions	Annot. Source: mzCloud Search	Annot. Source: ChemSpider Search	Annot. DeltaMass [ppm]	Calc. MW	RT [min]	Area (Max.)	# ChemSpider Results	# mzCloud Results	# Usable QC	RSD QC Areas [%]	RSD Corr. QC Areas [%]	MS2
11	C5 H7 N O3	No results	Full match	Full match	-0.71	129.0425	1.666	15024855	10	1	12	21	17	DDA for preferred ion
12	C22 H36 O7	No results	No results	Full match	-1.43	412.2455	9.832	12054002	1	0	12	8	7	DDA for preferred ion
13	C8 H15 N O3	No results	No results	Full match	-0.52	173.1051	6.231	11714413	8	0	11	6	5	DDA for preferred ion
14	C10 H19 N O3	No results	Full match	Full match	-0.64	201.1364	7.481	11282555	4	1	12	7	6	DDA for preferred ion
15	C22 H34 O6	No results	No results	Full match	-1.21	394.2351	11.027	10007600	2	0	12	23	21	DDA for preferred ion
16	C4 H6 O4	No results	No results	Full match	-1.03	118.0265	2.098	6771029	8	0	11	4	4	DDA for preferred ion
17	C41 H72 N O7 P	No results	No results	Full match	0.78	721.5052	0.926	6306022	6	0	11	15	15	No MS2
18	C17 H26 O5	No results	No results	Full match	-0.79	310.1778	11.214	5357492	3	0	12	13	12	No MS2
19	C7 H6 O2	No results	No results	Full match	-0.87	122.0367	6.546	4949323	6	0	11	21	17	No MS2
20	C40 H75 N3 O2	No results	No results	Full match	-1.58	629.5849	0.914	4360218	1	0	11	16	14	No MS2
21	C18 H21 N S	No results	No results	Full match	-0.94	283.1392	8.073	3701532	1	0	12	5	4	DDA for preferred ion

Table S.3 – **ES-2 EVs metabolite identifications using Compound Discoverer software for amide column and positive mode of ionization**. Annot. Source – annotation source; Calc. MW – calculated molecular weight; RSD – relative standard deviation.

ID	Name
1	Bis(4-ethylbenzylidene)sorbitol
2	Bis(4-ethylbenzylidene)sorbitol
3	12,13-Epoxytrichothec-9-ene-3,4,8,15-tetrol
4	Buclizine
5	12,13-Epoxytrichothec-9-ene-3,4,8,15-tetrol
6	Oleamide
7	11-Aminoundecanoic acid
8	Bis(2-ethylhexyl)adipate
9	2,4-Dimethylbenzaldehyde
10	α-L-Fucopyranose
11	2,4-Dimethylbenzaldehyde
12	PEG-4
13	α-L-Fucopyranose
14	Pivagabine
15	12,13-Epoxytrichothec-9-ene-3,4,8,15-tetrol
16	6,9-Dihydroxy-3,6,9-trimethyl-3,3a,4,5,6,8,9,9b-octahydroazuleno[4,5-b]furan-2,7-dione
17	PEG-4
18	Piperidione
19	Linoleamide
20	2-[(5E,8E)-5,8-Tetradecadien-1-yl]cyclobutanone
21	2,4-Dimethylbenzaldehyde
22	Hexadecanamide

ID	Name
23	(2S,3R)-3-Hydroxy-2-[(15Z)-15-tetracosenoylamino]octadecyl 5-acetamido-3,5-dideoxy-6-[(1R,2R)-1,2,3-trihydroxypropyl]-beta-L-threo-hex-2-ulopyranonosyl-(2->3)-[beta-D-galactopyranosyl-(1->3)-2-deoxy-2-(2-oxopropyl)-beta-D-galactopyranosyl-(1->4)]-beta-D-galactopyranosyl-(1->4)-beta-D-glucopyranoside
24	11-Aminoundecanoic acid
25	Phosphoric acid
26	Militarinone A
27	1-Hexadecanoylpyrrolidine
28	(2S,3R)-3-Hydroxy-2-(icosanoylamino)octadecyl 5-acetamido-6-[(1S,2R)-2-({5-acetamido-6-[(1S,2R)-2-({5-acetamido-3,5-dideoxy-6-[(1R,2R)-1,2,3-trihydroxypropyl]-beta-L-threo-hex-2-ulopyranonosyl}oxy)-1,3-dihydroxypropyl]-3,5-dideoxy-beta-L-threo-hex-2-ulopyranonosyl}oxy)-1,3-dihydroxypropyl]-3,5-dideoxy-beta-L-threo-hex-2-ulopyranonosyl-(2->3)-beta-D-galactopyranosyl-(1->4)-beta-D-glucopyranoside
29	butoctamide
30	Amide C18
31	Phenethylamine
32	6-Hydroxy-2-oxohexanoic acid
33	Phosphoribosyl pyrophosphate
34	2-(Diethylamino)ethanol
35	MFCD00002180
36	2-{2-[(2E)-3,6-Dimethyl-2-hepten-1-yl]-3,4-dihydroxyphenyl}-7-hydroxy-2,3-dihydro-4H-chromen-4-one
37	MDMA
38	Tributyl phosphate
39	3-Tropanol
40	5-Ethyl-4-hydroxy-3(2H)-furanone
41	KJ9800000
42	MFCD00058970
43	(+)-D-Isosorbide
44	N-Nonanoylglycine
45	N,N-Bis(2-hydroxyethyl)dodecanamide
46	2-Hexenoylcarnitine
47	2128
48	N-methylethanolamine phosphate
49	5,6-Dimethylbenzimidazole
50	1872050
51	Aceclidine
52	Elaeokanine C
53	Spiroxamine
54	1872050
55	Hexylresorcinol
56	N-Undecanoylglycine
57	AC 45594
58	Octylamine
59	Elaeokanine C
60	Elaeokanine C

ID	Name
61	Cyprodenate
62	Cinnamaldehyde
63	capuride
64	Pivagabine
65	Cyprodenate
66	3-Formyl-6,6,7b-trimethyl-2,4,4a,5,6,7,7a,7b-octahydro-1H-cyclobuta[e]inden-2-yl 3-chloro-6-hydroxy-4-methoxy-2-methylbenzoate
67	p-Xylene
68	Spinosyn D
69	1872050
70	11-Nitro-1-undecene
71	Capryloylglycine
72	2-(Diethylamino)ethanol
73	11-Nitro-1-undecene
74	N-Undecanoylglycine
75	2376
76	cyclandelate
77	11343172
78	Otonecine
79	apronalide
80	Triethanolamine
81	2,4-Diaminotoluene
82	Hydroquinone
83	2-morpholinoacetic acid
84	Skatole
85	Atagabalin
86	2638
87	Athamantin
88	3-Tropanol
89	Butyryl-L-homoserine lactone
90	Capryloylglycine
91	Furaneol
92	methyprylon
93	MFCD00674434
94	3,7,15-Trihydroxy-12,13-epoxytrichothec-9-en-8-one
95	Schradan
96	N-Undecanoylglycine
97	butoctamide
98	11-Aminoundecanoic acid
99	2S-Amino-tridecanoic acid

ID	Name
100	(+/-)-Tropinone
101	1-(3,4-Dimethoxyphenyl)-3,5-decanediyl diacetate
102	8,8a-Deoxyoleandolide

ID	Formula	Annot. Source: Predicted Compositions	Annot. Source: mzCloud Search	Annot. Source: ChemSpider Search	Annot. DeltaMass [ppm]	Calc. MW	RT [min]	Area (Max.)	#ChemSpider Results	#mzCloud Results	# Usable QC	RSD QC Areas [%]	RSD Corr. QC Areas [%]	MS2
1	C24 H30 O6	Full match	Full match	Partial match	0.29	414.2044	1.174	1.06E+10	7	1	12	7	7	DDA for preferred ion
2	C24 H30 O6	Full match	Full match	Partial match	2.41	414.2052	1.171	6E+09	7	1	12	5	4	DDA for preferred ion
3	C15 H22 O6	No results	No results	Full match	-0.83	298.1414	1.785	1.29E+09	4	0	12	5	5	DDA for preferred ion
4	C28 H33 Cl N2	No results	No results	Full match	1.49	432.2339	1.173	1.12E+09	1	0	12	5	4	No MS2
5	C15 H22 O6	No results	No results	Full match	-0.85	298.1414	1.707	9.5E+08	4	0	12	29	24	DDA for preferred ion
6	C18 H35 N O	No results	Full match	Partial match	-0.98	281.2716	1.126	7.92E+08	3	2	12	5	5	DDA for preferred ion
7	C11 H23 N O2	No results	No results	Full match	-0.24	201.1728	4.629	6.46E+08	1	0	12	21	18	DDA for preferred ion
8	C22 H42 O4	No results	Full match	Full match	-0.74	370.308	1.068	3.95E+08	3	1	12	3	2	DDA for preferred ion
9	C9 H10 O	No results	Full match	Partial match	-0.49	134.0731	1.784	3.43E+08	18	1	12	9	9	DDA for preferred ion
10	C6 H12 O5	No results	No results	Full match	-0.03	164.0685	1.785	2.78E+08	27	0	12	5	5	DDA for preferred ion
11	C9 H10 O	No results	Full match	Full match	-0.15	134.0731	1.714	2.58E+08	18	2	12	20	20	DDA for preferred ion
12	C8 H18 O5	No results	No results	Full match	0.18	194.1155	1.413	2.44E+08	1	0	12	21	16	DDA for other ion
13	C6 H12 O5	No results	No results	Full match	-0.16	164.0685	1.708	2.25E+08	27	0	12	20	18	DDA for preferred ion
14	C9 H17 N O3	No results	No results	Full match	-0.4	187.1208	1.832	2.07E+08	4	0	12	10	9	DDA for preferred ion
15	C15 H22 O6	No results	No results	Full match	-0.05	298.1416	1.17	2.06E+08	4	0	12	4	4	DDA for other ion
16	C15 H20 O5	No results	No results	Full match	-0.04	280.1311	1.171	2.01E+08	14	0	12	3	3	DDA for preferred ion
17	C8 H18 O5	No results	No results	Full match	0.08	194.1154	1.723	1.57E+08	1	0	12	13	8	DDA for other ion
18	C9 H15 N O2	No results	No results	Full match	-0.53	169.1102	1.82	1.53E+08	3	0	12	24	24	DDA for preferred ion
19	C18 H33 N O	No results	No results	Full match	-0.68	279.256	1.132	1.49E+08	1	0	12	18	14	DDA for preferred ion
20	C18 H30 O	No results	No results	Full match	-0.71	262.2295	1.183	1.45E+08	3	0	12	18	14	DDA for other ion
21	C9 H10 O	No results	Full match	Partial match	-0.67	134.0731	1.172	1.23E+08	18	1	12	10	10	DDA for preferred ion
22	C16 H33 N O	No results	Full match	Full match	-1.35	255.2559	1.133	95768203	1	1	12	4	4	DDA for preferred ion
23	C80 H144 N2 O31	No results	No results	Full match	-2.18	1628.972	6.549	92664022	1	0	12	20	20	No MS2
24	C11 H23 N O2	No results	No results	Full match	-0.24	201.1728	3.952	86026568	1	0	12	19	17	DDA for preferred ion
25	H3 O4 P	No results	No results	Full match	-0.65	97.97683	7.493	81366929	1	0	12	31	24	DDA for preferred ion
26	C26 H37 N O6	No results	No results	Full match	0.35	459.2623	1.178	80330441	2	0	12	21	20	DDA for preferred ion
27	C20 H39 N O	No results	No results	Full match	-0.98	309.3029	1.118	77015837	1	0	12	7	6	DDA for preferred ion
28	C83 H148 N4 O37	No results	No results	Full match	-1.93	1792.979	6.566	73013053	1	0	12	12	12	No MS2
29	C16 H29 N O5	No results	No results	Full match	-0.83	315.2043	1.385	72361750	1	0	12	18	17	DDA for preferred ion
30	C18 H37 N O	No results	No results	Full match	-1.82	283.287	1.122	68406927	1	0	12	4	4	No MS2
31	C8 H11 N	No results	No results	Full match	-0.89	121.089	1.606	67409121	10	0	12	10	10	No MS2

ID	Formula	Annot. Source: Predicted Compositions	Annot. Source: mzCloud Search	Annot. Source: ChemSpider Search	Annot. DeltaMass [ppm]	Calc. MW	RT [min]	Area (Max.)	#ChemSpider Results	#mzCloud Results	#Usable QC	RSD QC Areas [%]	RSD Corr. QC Areas [%]	MS2
32	C6H10O4	No results	No results	Full match	-0.3	146.0579	1.784	62704995	20	0	12	4	4	DDA for preferred ion
33	C5H13O14P3	No results	No results	Full match	-1.51	389.9512	6.529	58999299	3	0	12	27	23	No MS2
34	C6H15NO	No results	No results	Full match	-1.06	117.1152	4.652	55301368	1	0	12	10	10	No MS2
35	C20H20I2N2O5	No results	No results	Full match	0.09	621.9462	6.655	52440433	1	0	12	27	16	No MS2
36	C24H28O5	No results	No results	Full match	-0.06	396.1937	1.182	49131733	4	0	12	18	18	DDA for preferred ion
37	C11H15NO2	No results	No results	Full match	0.09	193.1103	6.03	48768080	13	0	12	7	5	No MS2
38	C12H27O4P	No results	No results	Full match	-1.28	266.1644	1.11	48473584	1	0	12	10	9	No MS2
39	C8H15NO	No results	No results	Full match	0.23	141.1154	1.833	46786705	11	0	12	7	6	DDA for preferred ion
40	C6H8O3	No results	No results	Full match	-0.56	128.0473	1.784	41216993	14	0	12	4	3	DDA for preferred ion
41	C18H39O7P	No results	No results	Full match	-0.48	398.2432	1.104	40028324	1	0	12	14	12	No MS2
42	C6H7O4P	No results	No results	Full match	-0.08	174.0082	1.077	37534172	1	0	12	4	3	No MS2
43	C6H10O4	No results	No results	Full match	-0.54	146.0578	1.709	37494930	20	0	12	13	10	DDA for preferred ion
44	C11H21NO3	No results	No results	Full match	-0.14	215.1521	1.676	34214394	2	0	12	7	6	DDA for preferred ion
45	C16H33NO3	No results	No results	Full match	-1.3	287.2457	1.619	33792548	1	0	12	23	18	No MS2
46	C13H23NO4	No results	No results	Full match	-1.26	257.1624	5.698	28750459	1	0	12	7	7	DDA for preferred ion
47	C9H12O2	No results	No results	Full match	-0.41	152.0837	1.134	28694819	14	0	12	7	6	No MS2
48	C3H10NO4P	No results	No results	Full match	0.35	155.0348	6.316	27447181	3	0	12	14	14	DDA for preferred ion
49	C9H10N2	No results	No results	Full match	-0.18	146.0844	1.606	26628067	6	0	12	19	18	DDA for preferred ion
50	C12H23NO3	No results	No results	Full match	-0.59	229.1677	1.215	25639787	1	0	12	16	14	DDA for other ion
51	C9H15NO2	No results	No results	Full match	-0.31	169.1102	1.22	25592605	3	0	12	7	6	No MS2
52	C12H21NO2	No results	No results	Full match	-0.5	211.1571	1.67	25124965	1	0	12	11	7	DDA for preferred ion
53	C18H35NO2	No results	No results	Full match	-0.9	297.2665	1.147	21075021	5	0	12	19	19	No MS2
54	C12H23NO3	No results	No results	Full match	-0.65	229.1676	1.132	20401641	1	0	12	7	7	No MS2
55	C12H18O2	No results	No results	Full match	-0.23	194.1306	1.133	17910108	21	0	12	9	9	No MS2
56	C13H25NO3	No results	No results	Full match	-0.77	243.1833	1.666	17348851	1	0	12	16	13	DDA for other ion
57	C13H20O2	No results	No results	Full match	-0.5	208.1462	1.116	16809493	15	0	12	9	7	No MS2
58	C8H19N	No results	No results	Full match	0.05	129.1518	1.246	16360021	2	0	12	21	13	No MS2
59	C12H21NO2	No results	No results	Full match	-0.48	211.1571	1.214	16126393	1	0	12	17	17	DDA for preferred ion
60	C12H21NO2	No results	No results	Full match	-0.29	211.1572	1.131	15134774	1	0	12	11	10	No MS2
61	C13H25NO2	No results	No results	Full match	-0.54	227.1884	1.126	14684973	1	0	12	10	8	No MS2
62	C9H8O	No results	No results	Full match	0.33	132.0576	1.17	13765235	6	0	12	13	12	No MS2
63	C9H18N2O2	No results	No results	Full match	-0.33	186.1368	1.848	13530574	2	0	12	14	13	No MS2
64	C9H17NO3	No results	No results	Full match	-0.2	187.1208	1.133	13140266	4	0	12	11	7	No MS2
65	C13H25NO2	No results	No results	Full match	-0.47	227.1884	1.207	12251558	1	0	12	17	15	No MS2
66	C24H29ClO5	No results	No results	Full match	-0.84	432.17	1.104	12128288	1	0	12	10	9	No MS2
67	C8H10	No results	No results	Full match	-0.64	106.0782	1.785	12034520	4	0	12	17	17	No MS2
68	C42H67NO10	No results	No results	Full match	-0.34	745.4763	1.09	11853945	1	0	12	10	9	No MS2
69	C12H23NO3	No results	No results	Full match	-0.66	229.1676	1.669	11815979	1	0	12	9	6	DDA for preferred ion
70	C11H21NO2	No results	No results	Full match	-0.06	199.1572	1.217	11532258	1	0	12	26	24	No MS2

ID	Formula	Annot. Source: Predicted Compositions	Annot. Source: mzCloud Search	Annot. Source: ChemSpider Search	Annot. DeltaMass [ppm]	Calc. MW	RT [min]	Area (Max.)	#ChemSpider Results	#mzCloud Results	#Usable QC	RSD QC Areas [%]	RSD Corr. QC Areas [%]	MS2
71	C10H19NO3	No results	No results	Full match	-0.12	201.1365	1.745	11435410	4	0	12	8	5	No MS2
72	C6H15NO	No results	No results	Full match	-1.11	117.1152	1.265	10961287	1	0	12	23	23	No MS2
73	C11H21NO2	No results	No results	Full match	-0.09	199.1572	1.127	9904720	1	0	12	9	7	No MS2
74	C13H25NO3	No results	No results	Full match	-0.93	243.1832	1.202	9707031	1	0	12	13	13	No MS2
75	C14H26O4	No results	No results	Full match	-1.04	258.1828	1.07	9197317	6	0	12	17	14	No MS2
76	C17H24O3	No results	No results	Full match	-1.05	276.1723	1.211	8889344	11	0	12	14	13	No MS2
77	C11H21NO3	No results	No results	Full match	-0.34	215.1521	1.126	8528952	2	0	12	8	7	No MS2
78	C9H15NO3	No results	No results	Full match	-0.15	185.1052	1.636	8444723	8	0	12	8	7	No MS2
79	C9H16N2O2	No results	No results	Full match	-0.15	184.1212	7.915	8328090	2	0	12	18	18	No MS2
80	C6H15NO3	No results	No results	Full match	0.06	149.1052	6.239	7984139	1	0	12	4	4	No MS2
81	C7H10N2	No results	No results	Full match	-0.73	122.0843	1.665	7836752	9	0	12	7	7	No MS2
82	C6H6O2	No results	No results	Full match	-0.52	110.0367	1.78	7654531	6	0	12	13	13	No MS2
83	C6H11NO3	No results	No results	Full match	-0.03	145.0739	1.664	7551791	13	0	12	10	9	No MS2
84	C9H9N	No results	No results	Full match	-0.24	131.0735	1.784	7481029	3	0	12	10	10	No MS2
85	C10H19NO2	No results	No results	Full match	0.07	185.1416	1.132	7100578	1	0	12	11	8	No MS2
86	C17H22O2	No results	No results	Full match	-1.58	258.1616	1.211	6127554	11	0	12	16	15	No MS2
87	C24H30O7	No results	No results	Full match	0.86	430.1995	1.22	5839551	4	0	12	8	7	No MS2
88	C8H15NO	No results	No results	Full match	0.23	141.1154	1.135	5826806	11	0	12	8	7	No MS2
89	C8H13NO3	No results	No results	Full match	-0.34	171.0895	1.671	5390948	3	0	12	11	11	No MS2
90	C10H19NO3	No results	No results	Full match	-0.16	201.1365	1.221	5262568	4	0	12	14	14	No MS2
91	C6H8O3	No results	No results	Full match	-0.73	128.0473	1.071	5098779	14	0	12	19	13	No MS2
92	C10H17NO2	No results	No results	Full match	0.02	183.1259	1.738	4914797	2	0	12	8	5	No MS2
93	C20H37NO2	No results	No results	Full match	-0.98	323.2821	1.14	4913985	1	0	12	8	7	No MS2
94	C15H20O6	No results	No results	Full match	-0.72	296.1258	1.212	4676229	8	0	12	12	11	No MS2
95	C8H24N4O3P2	No results	No results	Full match	2.29	286.133	1.077	4655050	1	0	12	11	10	No MS2
96	C13H25NO3	No results	No results	Full match	-0.94	243.1832	1.116	3820592	1	0	12	8	6	No MS2
97	C16H29NO5	No results	No results	Full match	-0.96	315.2043	1.71	3749506	1	0	12	14	10	DDA for preferredion
98	C11H23NO2	No results	No results	Full match	-0.02	201.1729	1.207	3478669	1	0	12	19	18	No MS2
99	C13H27NO2	No results	No results	Full match	-0.93	229.204	1.184	3001941	1	0	12	20	19	No MS2
100	C8H13NO	No results	No results	Full match	-0.26	139.0997	1.688	2711961	12	0	12	9	9	No MS2
101	C22H34O6	No results	No results	Full match	-1.42	394.235	1.214	2593411	2	0	12	9	8	No MS2
102	C20H36O6	No results	No results	Full match	-0.69	372.2509	1.661	2481868	1	0	12	25	21	No MS2

Table S.4 – **ES-2 EVs metabolite identifications using Compound Discoverer software for amide column and negative mode of ionization**. Annot. Source – annotation source; Calc. MW – calculated molecular weight; RSD – relative standard deviation.

ID	Name
1	Phosphoric acid

ID	Name
2	Carboxycyclophosphamide
3	Pyrophosphoric Acid
4	Phosphoric acid
5	Palmitic Acid
6	Stearic acid
7	laurilsulfate
8	Methylprednisolone Hemisuccinate
9	D-(-)-Mannitol
10	TU4153400
11	4-[(4E)-3-Hydroxy-4-decen-1-yl]-2-methoxyphenol
12	Oleic acid
13	2-Dodecylbenzenesulfonic acid
14	2-Dodecylbenzenesulfonic acid
15	laurilsulfate
16	4-Undecylbenzenesulfonic acid
17	4-Hydroxy-3-(hydroxymethyl)-6,6,7b-trimethyl-2,4,4a,5,6,7,7a,7b-octahydro-1H-cyclobuta[e]inden-2-yl 3-chloro-6-hydroxy-4-methoxy-2-methylbenzoate
18	Myristyl sulfate
19	8-Amino-7-oxononanoic acid
20	2-Hydroxy-3-(phosphonooxy)propyl (9Z,12Z,15Z)-9,12,15-octadecatrienoate
21	Enalkiren
22	Perfluorooctanoic Acid
23	2,6-di-tert-Butylphenol
24	1,3-Dihydroxy-2-propanyl (13Z)-13-docosenoate
25	Azelaic acid
26	1-nonanoic acid
27	5,4'-dihydroxy-3,3'-dimethoxy-6,7-methylenedioxyflavone
28	pentadecanoic acid
29	myristic acid
30	11-Methylhexadecanoic acid
31	Linoleic Acid
32	2-C-methylerythritol 4-phosphate
33	(+)-[6]-Gingerol
34	Palmitelaidic acid
35	Perfluorooctanoic Acid
36	Phthalic acid
37	Putaminoxin
38	a-yl decanoate
39	1-(3,4-Dimethoxyphenyl)-3,5-decanediyl diacetate
40	tolonidine
41	2-C-methylerythritol 4-phosphate

ID	Name
42	lauric acid
43	2376
44	Artemether
45	dilauroyl peroxide
46	(3alpha,5alpha,17beta)-17-Hydroxyandrostan-3-yl beta-D-glucopyranuronate
47	Arachidic acid
48	Decanoic acid
49	1872050
50	(3,6-Dioxo-1,4-cyclohexadien-1-yl)acetic acid
51	N-Nonanoylglycine
52	2080
53	Artemether
54	1780537
55	MFCD00083068
56	MFCD00133175
57	palinavir
58	Bisphenol S
59	(14R)-3beta,5,6beta,10,16-pentahydroxygrayanotoxan-14-yl acetate
60	(6S)-2,6-Anhydro-6-[(1S)-2-isopropyl-5-methylcyclohexyl]-L-gulonic acid
61	12-HSA
62	5-Pentyl-1,4-dioxan-2-one
63	3-oxopalmitic acid
64	(1S,4R,4'S,5'S,6'R,9S,10E,12E,14S,15S,16E,19R,21R)-4',9,15-Trihydroxy-6'-isopropyl-5',6,10,14,16-pentamethyl-3',4',5',6'-tetrahydro-3H,7H-spiro[2,20-dioxatricyclo[17.3.1.0~4,9~]tricosa-5,10,12,16-tetraene-21,2'-pyran]-3,7-dione
65	Pivagabine
66	Dimethyl (3-oxocyclohexyl)malonate
67	N-Undecanoylglycine
68	Juniperic acid
69	13S-hydroxyoctadecadienoic acid
70	2450
71	Valproic acid
72	DOA
73	butyrin
74	Artemotil
75	Capryloylglycine
76	Sebacic acid
77	p-Toluenesulfonic acid
78	Undecylic acid
79	2453103
80	guaietolin

ID	Name
81	8,8a-Deoxyoleandolide
82	Frangulin B
83	Dodecanedioic acid
84	Brassylic acid
85	8-Hydroxyoctanoic acid
86	3-Hydroxynonanoic acid
87	Diethyl phthalate

ID	Formula	Annot. Source: Predicted Compositions	Annot. Source: mzCloud Search	Annot. Source: ChemSpider Search	Annot. DeltaMass [ppm]	Calc. MW	RT [min]	Area (Max.)	#ChemSpider Results	#mzCloud Results	#Usable QC	RSD QC Areas [%]	RSD Corr. QC Areas [%]	MS2
1	H3O4P	No results	No results	Full match	-1.47	97.97675	7.484	3.69E+09	1	0	12	15	14	DDA for other ion
2	C7H15Cl2N2O4P	No results	No results	Full match	-0.85	292.0144	6.574	2.43E+09	3	0	12	17	16	DDA for preferred ion
3	H4O7P2	No results	No results	Full match	-1.52	177.943	7.484	1.21E+09	1	0	12	19	18	DDA for preferred ion
4	H3O4P	No results	No results	Full match	-1.43	97.97675	7.72	1.2E+09	1	0	12	14	14	DDA for other ion
5	C16H32O2	No results	No results	Full match	-1.06	256.24	1.125	9.26E+08	9	0	12	6	6	No MS2
6	C18H36O2	No results	Full match	Full match	-1.09	284.2712	1.115	7.54E+08	4	2	12	5	5	DDA for other ion
7	C12H26O4S	No results	No results	Full match	-1.26	266.1549	1.598	7.38E+08	1	0	12	14	13	No MS2
8	C26H34O8	Full match	No results	Full match	-1.14	474.2248	1.18	4.5E+08	4	0	12	2	2	DDA for preferred ion
9	C6H14O6	No results	Full match	Full match	-1.1	182.0788	5.927	3.75E+08	7	6	12	20	20	DDA for preferred ion
10	C25H32O8	No results	No results	Full match	-0.96	460.2093	1.18	3.55E+08	6	0	12	4	4	DDA for preferred ion
11	C17H26O3	No results	No results	Full match	-1.19	278.1879	1.155	3.31E+08	6	0	12	17	16	DDA for preferred ion
12	C18H34O2	No results	No results	Full match	-0.91	282.2556	1.119	2.52E+08	11	0	12	7	7	No MS2
13	C18H30O3S	No results	No results	Full match	-0.91	326.1913	1.593	1.92E+08	2	0	12	20	19	No MS2
14	C18H30O3S	No results	No results	Full match	-0.91	326.1913	0.962	1.81E+08	2	0	12	21	20	No MS2
15	C12H26O4S	No results	No results	Full match	-1.27	266.1548	0.942	1.75E+08	1	0	12	23	23	No MS2
16	C17H28O3S	No results	No results	Full match	-0.63	312.1757	0.969	1.54E+08	1	0	12	16	15	No MS2
17	C24H31ClO6	No results	No results	Full match	-1.1	450.1804	1.179	1.42E+08	1	0	12	6	5	DDA for preferred ion
18	C14H30O4S	No results	No results	Full match	-0.73	294.1863	1.593	1.05E+08	1	0	12	19	17	DDA for preferred ion
19	C9H17NO3	No results	No results	Full match	-0.87	187.1207	1.841	1E+08	4	0	12	9	8	DDA for preferred ion
20	C21H37O7P	No results	No results	Full match	-0.94	432.2273	1.217	9956350	4	0	12	8	8	DDA for preferred ion
21	C35H56N6O6	No results	No results	Full match	2.84	656.428	1.095	82736261	1	0	12	9	9	DDA for preferred ion
22	C8HF15O2	No results	No results	Full match	-0.97	413.9733	6.7	55008689	1	0	11	18	16	DDA for preferred ion
23	C14H22O	No results	Full match	Partial match	-0.8	206.1669	1.11	45689564	14	3	12	10	10	DDA for preferred ion
24	C25H48O4	No results	No results	Full match	-1.17	412.3548	1.104	45199748	2	0	12	30	24	No MS2
25	C9H16O4	No results	No results	Full match	-0.71	188.1047	1.758	44879248	11	0	12	6	6	No MS2
26	C9H18O2	No results	No results	Full match	-1.03	158.1305	1.184	40508399	25	0	12	8	8	No MS2
27	C18H14O8	No results	No results	Full match	-0.87	358.0686	4.046	40325510	2	0	12	15	15	No MS2
28	C15H30O2	No results	No results	Full match	-0.76	242.2244	1.13	32899816	14	0	12	8	7	No MS2
29	C14H28O2	No results	No results	Full match	-0.64	228.2088	1.136	32525129	14	0	12	11	11	No MS2

ID	Formula	Annot. Source: Predicted Compositions	Annot. Source: mzCloud Search	Annot. Source: ChemSpider Search	Annot. DeltaMass [ppm]	Calc. MW	RT [min]	Area (Max.)	#ChemSpider Results	#mzCloud Results	#Usable QC	RSD QC Areas [%]	RSD Corr. QC Areas [%]	MS2
30	C17H34O2	No results	No results	Full match	-0.9	270.2556	1.118	31583864	9	0	12	7	3	DDA for preferred ion
31	C18H32O2	No results	Full match	Full match	-0.91	280.24	1.123	30059542	15	1	12	5	5	DDA for preferred ion
32	C5H13O7P	No results	No results	Full match	0.4	216.04	6.129	29812405	1	0	12	10	10	No MS2
33	C17H26O4	No results	No results	Full match	-0.93	294.1828	1.206	28052826	8	0	12	6	6	DDA for preferred ion
34	C16H30O2	No results	No results	Full match	-0.65	254.2244	1.128	24112393	13	0	12	13	12	No MS2
35	C8HF15O2	No results	No results	Full match	-1	413.9733	6.53	22349783	1	0	12	22	22	No MS2
36	C8H6O4	No results	No results	Full match	-1.28	166.0264	5.58	19351544	7	0	12	9	9	No MS2
37	C12H20O3	No results	No results	Full match	-0.49	212.1411	1.129	18543616	8	0	12	13	13	DDA for preferred ion
38	C35H52O8	No results	No results	Full match	-0.8	600.3657	1.123	18091632	1	0	12	14	14	No MS2
39	C22H34O6	No results	No results	Full match	-0.87	394.2352	1.218	17120791	2	0	12	6	6	DDA for preferred ion
40	C10H12ClN3	No results	No results	Full match	0.17	209.072	4.379	15569582	1	0	12	5	5	DDA for preferred ion
41	C5H13O7P	No results	No results	Full match	0.31	216.04	6.475	14976861	1	0	12	16	16	No MS2
42	C12H24O2	No results	No results	Full match	-0.56	200.1775	1.15	14221797	12	0	12	22	22	No MS2
43	C14H26O4	No results	No results	Full match	-0.77	258.1829	1.171	13720769	6	0	12	9	8	No MS2
44	C16H26O5	No results	No results	Full match	-1.28	298.1776	1.182	13552689	1	0	12	12	12	DDA for preferred ion
45	C24H46O4	No results	No results	Full match	-1.83	398.3389	1.11	13508637	1	0	12	16	12	No MS2
46	C25H40O8	No results	No results	Full match	-1.02	468.2718	1.215	13395935	3	0	12	9	8	DDA for preferred ion
47	C20H40O2	No results	No results	Full match	-0.66	312.3026	1.107	12102931	9	0	12	6	6	No MS2
48	C10H20O2	No results	No results	Full match	-0.29	172.1463	1.17	11677032	35	0	12	22	21	No MS2
49	C12H23NO3	No results	No results	Full match	-1.2	229.1675	1.678	11675157	1	0	12	7	7	DDA for preferred ion
50	C8H6O4	No results	No results	Full match	-0.78	166.0265	1.152	11358398	7	0	12	19	15	DDA for preferred ion
51	C11H21NO3	No results	No results	Full match	-0.34	215.1521	1.683	11280634	2	0	12	6	5	DDA for preferred ion
52	C13H26O2	No results	No results	Full match	-0.54	214.1932	1.142	10552056	13	0	12	13	13	DDA for preferred ion
53	C16H26O5	No results	No results	Full match	-1.03	298.1777	1.66	9434554	1	0	12	9	7	DDA for preferred ion
54	C11H20O4	No results	No results	Full match	-0.95	216.136	1.676	8543263	2	0	12	7	7	No MS2
55	C27H52O4	No results	No results	Full match	-1.27	440.386	1.097	8207693	3	0	12	14	12	No MS2
56	C17H32O2	No results	No results	Full match	-0.88	268.24	1.127	7138621	7	0	12	13	11	No MS2
57	C41H52N6O5	No results	No results	Full match	-0.47	708.3996	1.12	6785588	1	0	12	19	19	No MS2
58	C12H10O4S	No results	No results	Full match	-1.02	250.0297	1.658	6181592	1	0	12	3	3	DDA for preferred ion
59	C22H36O7	No results	No results	Full match	-1.59	412.2455	1.228	5970630	1	0	12	10	10	No MS2
60	C16H28O6	No results	No results	Full match	-1.14	316.1882	1.667	5945206	1	0	12	7	7	No MS2
61	C18H36O3	No results	No results	Full match	-0.99	300.2662	1.163	5732651	14	0	12	18	18	No MS2
62	C9H16O3	No results	No results	Full match	-0.41	172.1099	1.226	5695774	10	0	12	10	10	DDA for other ion
63	C16H30O3	No results	No results	Full match	-0.85	270.2193	1.158	5669296	5	0	12	19	19	DDA for preferred ion
64	C33H48O8	No results	No results	Full match	-1.39	572.3341	1.181	5608735	1	0	12	8	8	No MS2
65	C9H17NO3	No results	No results	Full match	-0.93	187.1207	1.142	5593291	4	0	12	13	12	DDA for preferred ion
66	C11H16O5	No results	No results	Full match	-0.6	228.0996	1.67	5472720	1	0	12	9	7	DDA for preferred ion
67	C13H25NO3	No results	No results	Full match	-0.78	243.1833	1.673	5332599	1	0	12	4	4	No MS2
68	C16H32O3	No results	No results	Full match	-0.98	272.2349	1.193	4797766	12	0	12	8	7	No MS2

ID	Formula	Annot. Source: Predicted Compositions	Annot. Source: mzCloud Search	Annot. Source: ChemSpider Search	Annot. DeltaMass [ppm]	Calc. MW	RT [min]	Area (Max.)	#ChemSpider Results	#mzCloud Results	#Usable QC	RSD QC Areas [%]	RSD Corr. QC Areas [%]	MS2
69	C18H32O3	No results	No results	Full match	-1.83	296.2346	1.155	4688523	14	0	12	6	6	No MS2
70	C20H38O2	No results	No results	Full match	-0.88	310.2869	1.111	4611097	13	0	12	19	19	No MS2
71	C8H16O2	No results	No results	Full match	-0.83	144.1149	1.198	4435429	34	0	12	9	8	No MS2
72	C22H42O4	No results	No results	Full match	-1.59	370.3077	1.119	4240565	3	0	12	24	20	No MS2
73	C15H26O6	No results	No results	Full match	-0.65	302.1727	1.668	4236972	1	0	12	7	7	No MS2
74	C17H28O5	No results	No results	Full match	-0.89	312.1934	1.154	4076218	1	0	12	15	15	No MS2
75	C10H19NO3	No results	No results	Full match	-0.41	201.1364	1.757	4026927	4	0	12	5	5	DDA for preferred ion
76	C10H18O4	No results	No results	Full match	-0.29	202.1205	1.739	3931836	9	0	12	8	7	No MS2
77	C7H8O3S	No results	No results	Full match	-0.47	172.0193	1.208	3816784	1	0	12	14	13	No MS2
78	C11H22O2	No results	No results	Full match	-0.87	186.1618	1.158	3575482	25	0	12	20	19	No MS2
79	C13H18O3	No results	No results	Full match	-0.28	222.1255	1.221	3567738	14	0	12	9	7	No MS2
80	C11H16O4	No results	No results	Full match	-0.59	212.1047	1.666	3439330	2	0	12	10	10	No MS2
81	C20H36O6	No results	No results	Full match	-1.44	372.2507	1.657	3368236	1	0	12	12	12	No MS2
82	C20H18O9	No results	No results	Full match	-1.15	402.0946	1.686	3327868	5	0	12	26	24	DDA for preferred ion
83	C12H22O4	No results	No results	Full match	-1.11	230.1516	1.669	2775907	5	0	12	6	4	No MS2
84	C13H24O4	No results	No results	Full match	-1.06	244.1672	1.667	2752489	3	0	12	6	6	No MS2
85	C8H16O3	No results	No results	Full match	-0.75	160.1098	1.674	2692485	18	0	12	10	10	No MS2
86	C9H18O3	No results	No results	Full match	-0.88	174.1254	1.669	2384796	2	0	12	9	8	No MS2
87	C12H14O4	No results	No results	Full match	-0.79	222.089	1.667	2102291	23	0	12	9	8	No MS2

Table S.5 – **Input data for pathway enrichment analysis of ES-2 EVs metabolites using MetaboAnalyst software for C18 column and both modes of ionization.** Query – input compounds. HMDB – Human Metabolome Database; KEGG – Kyoto Encyclopedia of genes and genomes. SMILES – Simplified molecular input line entry system.

Query	Match	HMDB	PubChem	KEGG	SMILES
(2E)-2,5-Dichloro-4-oxo-2-hexenedioic acid	NA	NA	NA	NA	NA
11-Aminoundecanoic acid	(3beta,5alpha,9alpha,22E,24R)-3,5,9-Trihydroxy-23-methylergosta-7,22-dien-6-one	HMDB0032669	17083	NA	CC(C)C(C)C(\C)=C\C(C)C1CCC2C3=CC(=O)C4(O)CC(O)CCC4(C)C3(O)CCC12C
Phosphoric acid	Phosphoric acid	HMDB0002142	57424078	C00009	OP(=O)(O)O
Pivagabine	NA	NA	NA	NA	NA
Mutagen X	NA	NA	NA	NA	NA
Estra-1,3,5(10)-triene-3,6alpha,17beta-triol triacetate	NA	NA	NA	NA	NA
PEG-4	6-Oxopiperidine-2-carboxylic acid	HMDB0061705	3014237	NA	OC(=O)C1CCCC(O)=N1
Isopropyl catechol	NA	NA	NA	NA	NA
2,2,6,6-Tetramethyl-4-piperidinol	NA	NA	NA	NA	NA
3-Tropanol	Tropine	METPA0074	NA	C00729	NA

Query	Match	HMDB	PubChem	KEGG	SMILES
PEG n5	NA	NA	NA	NA	NA
Minoxidil	Minoxidil	HMDB0014494	NA	NA	NC1=CC(=NC(N)=[N+]1[O-])N1CCCCC1
butoctamide	NA	NA	NA	NA	NA
capuride	NA	NA	NA	NA	NA
PEG n6	NA	NA	NA	NA	NA
Betaine	Betaine	HMDB0000043	247	C00719	C[N+](C)(C)CC(=O)[O-]
Cyclopenta[cd]pyrene	NA	NA	NA	NA	NA
benzarone	NA	NA	NA	NA	NA
Triethanolamine	Triethanolamine	HMDB0032538	7618	C06771	C(CO)N(CCO)CCO
2-Hexenoylcarnitine	2-Hexenoylcarnitine	HMDB0013161	53481638	NA	CCC/C=C/C(=O)OC(CC(=O)[O-])C[N+](C)(C)C
2064747	NA	NA	NA	NA	NA
Urocanic acid	Urocanic acid	HMDB0000301	736715	C00785	C1=C(NC=N1)/C=C/C(=O)O
1,2,3,4,6,7,8-Heptachlorodibenzofuran	1,2,3,4,6,7,8-Heptachlorodibenzo-furan	NA	96024328	C18111	NA
MFCD00216258	NA	NA	NA	NA	NA
N-Acetyl-L-leucine	N-Acetylleucine	HMDB0011756	70912	C02710	CC(C)C[C@@H](C(=O)O)NC(=O)C
3-[(6-Oxodecanoyl)oxy]-4-(trimethylammonio)butanoate	NA	NA	NA	NA	NA
1,2,3,4,6,7,8-Heptachlorooxanthrene	NA	NA	NA	NA	NA
Adipic acid	Adipic acid	HMDB0000448	196	C06104	C(CCC(=O)O)CC(=O)O
Methylenediurea	NA	NA	NA	NA	NA
D-(+)-Pyroglutamic Acid	Pyroglutamic acid	HMDB0000267	7405	C01879	C1CC(=O)N[C@@H]1C(=O)O
Caprolactam	epsilon-Caprolactam	METPA0843	NA	C06593	NA
4230434	NA	NA	NA	NA	NA
O-{Hydroxy[(2R)-2-[(11Z)-11-octadecenoyloxy]-3-(pentadecanoyloxy)propoxy]phosphoryl}-L-serine	NA	NA	NA	NA	NA
N-docosanoylsphinganine	NA	NA	NA	NA	NA
Succinylacetone	Succinylacetone	HMDB0000635	5312	NA	CC(=O)CC(=O)CCC(=O)O
L-(+)-Leucine	L-Leucine	HMDB0000687	6106	C00123	CC(C)C[C@@H](C(=O)O)N
Sumarotene	NA	NA	NA	NA	NA
Leucine	L-Leucine	HMDB0000687	6106	C00123	CC(C)C[C@@H](C(=O)O)N

Query	Match	HMDB	PubChem	KEGG	SMILES
TCA-ethadyl	NA	NA	NA	NA	NA
Hydroxyamphetamine	NA	NA	NA	NA	NA
4-Ethylphenol	4-Ethylphenol	HMDB0029306	31242	C13637	CCC1=CC=C(C=C1)O
Indane	NA	NA	NA	NA	NA
asn-arg	Asparaginyl-Arginine	HMDB0028725	9835593	NA	NC(CC(N)=O)C(=O)NC(CCCNC(N)=N)C(O)=O
Imagabalin	NA	NA	NA	NA	NA
12,13-Epoxytrichothec-9-ene-3,4,8,15-tetrol	NA	NA	NA	NA	NA
DL-Lactic Acid	NA	NA	NA	NA	NA
ETHYLENEBISDITHIOCARBAMIC ACID	NA	NA	NA	NA	NA
N-Nonanoylglycine	N-Nonanoylglycine	HMDB0013279	10176752	NA	CCCCCCCCC(=O)NCC(=O)O
Ceramide (d18:1/24:1(15Z))	Cer(d18:1/24:1(15Z))	HMDB0004953	5283568	C00195	CCCCCCCCCCCCCC/C=C/[C@H]([C@H](CO)NC(=O)CCCCCCCCCCCCCC/C=C\CCCCCCCC)O
1872050	NA	NA	NA	NA	NA
(3alpha,5alpha,17beta)-17-Hydroxyandrostan-3-yl beta-D-glucopyranuronate	NA	NA	NA	NA	NA
4-Oxoproline	4-Oxoproline	METPA0228	NA	C01877	NA
(14R)-3beta,5,6beta,10,16-pentahydroxygrayanotoxan-14-yl acetate	NA	NA	NA	NA	NA
N-Acetyl-DL-alloisoleucine	NA	NA	NA	NA	NA
Capryloylglycine	Capryloylglycine	HMDB0000832	84290	NA	CCCCCCCC(=O)NCC(=O)O
1-(3,4-Dimethoxyphenyl)-3,5-decanediyl diacetate	NA	NA	NA	NA	NA
Succinic acid	Succinic acid	HMDB0000254	1110	C00042	C(CC(=O)O)C(=O)O
(2R)-3-{[(2-Aminoethoxy)(hydroxy)phosphoryl]oxy}-2-[(1Z,11Z)-1,11-octadecadien-1-yloxy]propyl (6Z,9Z,12Z,15Z)-6,9,12,15-octadecatetraenoate	NA	NA	NA	NA	NA
Botrydial	Botrydial	NA	185781	C09622	CC(=O)O1C(C)(C=O)2(O)1C(C)(C)C2(C)C=O
Benzoic acid	Benzoic acid	HMDB0001870	243	C00539	C1=CC=C(C=C1)C(=O)O
Juliflorine	NA	NA	NA	NA	NA
Tedatioxetine	NA	NA	NA	NA	NA

Table S.6 - **Pathway enrichment analysis of ES-2 EVs metabolites using MetaboAnalyst software for C18 column and both modes of ionization.** Expected – expected hits; hits – observed hits; raw p – raw p-value; Holm p – p-values adjusted by the Holm-Bonferroni method; FDR – false discovery rates enrichment ratio – hits to observed ratio**.**

	total	expected	hits	Raw p	Holm p	FDR	Enrichment ratio
Glutathione Metabolism	21	0.513	2	0.0905	1	1	3.898635
Ammonia Recycling	32	0.781	2	0.182	1	1	2.560819

	total	expected	hits	Raw p	Holm p	FDR	Enrichment ratio
Glycerol Phosphate Shuttle	11	0.269	1	0.239	1	1	3.717472
Ketone Body Metabolism	13	0.317	1	0.276	1	1	3.154574
Glutamate Metabolism	49	1.2	2	0.338	1	1	1.666667
Arginine and Proline Metabolism	53	1.29	2	0.375	1	1	1.550388
Butyrate Metabolism	19	0.464	1	0.377	1	1	2.155172
Mitochondrial Electron Transport Chain	19	0.464	1	0.377	1	1	2.155172
Vitamin B6 Metabolism	20	0.488	1	0.393	1	1	2.04918
Lactose Synthesis	20	0.488	1	0.393	1	1	2.04918
Betaine Metabolism	21	0.513	1	0.408	1	1	1.949318
Warburg Effect	58	1.42	2	0.419	1	1	1.408451
Carnitine Synthesis	22	0.537	1	0.423	1	1	1.862197
Valine, Leucine and Isoleucine Degradation	60	1.46	2	0.437	1	1	1.369863
Glycolysis	25	0.61	1	0.465	1	1	1.639344
Cysteine Metabolism	26	0.635	1	0.478	1	1	1.574803
Oxidation of Branched Chain Fatty Acids	26	0.635	1	0.478	1	1	1.574803
Phytanic Acid Peroxisomal Oxidation	26	0.635	1	0.478	1	1	1.574803
Inositol Phosphate Metabolism	26	0.635	1	0.478	1	1	1.574803
Selenoamino Acid Metabolism	28	0.684	1	0.504	1	1	1.461988
Urea Cycle	29	0.708	1	0.517	1	1	1.412429
Citric Acid Cycle	32	0.781	1	0.552	1	1	1.28041
Fructose and Mannose Degradation	32	0.781	1	0.552	1	1	1.28041
Inositol Metabolism	33	0.806	1	0.563	1	1	1.240695
Gluconeogenesis	35	0.854	1	0.585	1	1	1.17096
Nicotinate and Nicotinamide Metabolism	37	0.903	1	0.606	1	1	1.10742
Propanoate Metabolism	42	1.03	1	0.653	1	1	0.970874
Methionine Metabolism	43	1.05	1	0.662	1	1	0.952381
Histidine Metabolism	43	1.05	1	0.662	1	1	0.952381
Pyruvate Metabolism	48	1.17	1	0.703	1	1	0.854701
Glycine and Serine Metabolism	59	1.44	1	0.777	1	1	0.694444
Pyrimidine Metabolism	59	1.44	1	0.777	1	1	0.694444
Purine Metabolism	74	1.81	1	0.85	1	1	0.552486

Table S.7 – **Input data for pathway enrichment analysis of ES-2 EVs metabolites using MetaboAnalyst software for amide column and both modes of ionization.** Query – input compounds. HMDB – Human Metabolome Database; KEGG – Kyoto Encyclopedia of genes and genomes. SMILES – Simplified molecular input line entry system.

Query	Match	HMDB	Pub-Chem	KEGG	SMILES
12,13-Epoxytrichothec-9-ene-3,4,8,15-tetrol	NA	NA	NA	NA	NA

Query	Match	HMDB	Pub-Chem	KEGG	SMILES
Buclizine	Buclizine	HMDB0014498	6729	C07777	CC(C)(C)C1=CC=C(C=C1)CN2CCN(CC2)C(C3=CC=CC=C3)C4=CC=C(C=C4)Cl
Oleamide	Oleamide	HMDB0002117	5283387	C19670	CCCCCCCCC/C=C\CCCCCCCC(=O)N
11-Aminoundecanoic acid	(3beta,5alpha,9alpha,22E,24R)-3,5,9-Trihydroxy-23-methylergosta-7,22-dien-6-one	HMDB0032669	17083	NA	CC(C)C(C)C(\C)=C\C(C)C1CCC2C3=CC(=O)C4(O)CC(O)CCC4(C)C3(O)CCC12C
Bis(2-ethylhexyl)adipate	NA	NA	NA	NA	NA
2,4-Dimethylbenzaldehyde	2,4-Dimethylbenzaldehyde	HMDB0032142	61814	NA	CC1=CC(=C(C=C1)C=O)C
Î±-L-Fucopyranose	NA	NA	NA	NA	NA
PEG-4	6-Oxopiperidine-2-carboxylic acid	HMDB0061705	3014237	NA	OC(=O)C1CCCC(O)=N1
Linoleamide	Linoleamide	HMDB0062656	6435901	NA	[H]\C(CCCCC)=C(/[H])C\C([H])=C(\[H])CCCCCCCC(O)=N
2-[(5E,8E)-5,8-Tetradecadien-1-yl]cyclobutanone	NA	NA	NA	NA	NA
1-Hexadecanoylpyrrolidine	N-Hexadecanoylpyrrolidine	HMDB0032740	247220	NA	CCCCCCCCCCCCCCCCC(=O)N1CCCC1
Amide C18	Octadecanamide	HMDB0034146	31292	C13846	CCCCCCCCCCCCCCCCCC(=O)N
Phosphoribosyl pyrophosphate	Phosphoribosyl pyrophosphate	HMDB0000280	7339	C00119	C([C@@H]1[C@H]([C@H]([C@H](O1)OP(=O)(O)OP(=O)(O)O)O)O)OP(=O)(O)O
2-(Diethylamino)ethanol	2-Diethylaminoethanol	HMDB0033971	7497	NA	CCN(CC)CCO
2-{2-[(2E)-3,6-Dimethyl-2-hepten-1-yl]-3,4-dihydroxyphenyl}-7-hydroxy-2,3-dihydro-4H-chromen-4-one	NA	NA	NA	NA	NA
MDMA	NA	NA	NA	NA	NA
5-Ethyl-4-hydroxy-3(2H)-furanone	2-Ethyl-3,4-dihydroxyfuran	HMDB0031847	20333861	NA	CCC1=C(O)C(=O)CO1
N-Nonanoylglycine	N-Nonanoylglycine	HMDB0013279	10176752	NA	CCCCCCCCC(=O)NCC(=O)O
N,N-Bis(2-hydroxyethyl)dodecanamide	NA	NA	NA	NA	NA
2-Hexenoylcarnitine	2-Hexenoylcarnitine	HMDB0013161	53481638	NA	CCC/C=C/C(=O)OC(CC(=O)[O-])C[N+](C)(C)C
5,6-Dimethylbenzimidazole	Dimethylbenzimidazole	HMDB0003701	675	C03114	CC1=CC2=C(C=C1C)N=CN2
Hexylresorcinol	Hexylresorcinol	HMDB0032567	3610	NA	CCCCCCC1=C(C=C(C=C1)O)O
N-Undecanoylglycine	N-Undecanoylglycine	HMDB0013286	454092	NA	CCCCCCCCCCC(=O)NCC(=O)O
Elaeokanine C	NA	NA	NA	NA	NA

Query	Match	HMDB	Pub-Chem	KEGG	SMILES
Cinnamaldehyde	Cinnamaldehyde	HMDB0003441	637511	C00903	C1=CC=C(C=C1)/C=C/C=O
Pivagabine	NA	NA	NA	NA	NA
p-Xylene	p-Xylene	HMDB0059924	7809	C06756	CC1=CC=C(C)C=C1
11-Nitro-1-undecene	NA	NA	NA	NA	NA
Capryloylglycine	Capryloylglycine	HMDB0000832	84290	NA	CCCCCCCC(=O)NCC(=O)O
cyclandelate	Cyclandelate	HMDB0015586	2893	NA	CC1CC(CC(C1)(C)C)OC(=O)C(C2=CC=CC=C2)O
Triethanolamine	Triethanolamine	HMDB0032538	7618	C06771	C(CO)N(CCO)CCO
2,4-Diaminotoluene	NA	NA	NA	NA	NA
Hydroquinone	Hydroquinone	HMDB0002434	785	C00530	C1=CC(=CC=C1O)O
Skatole	3-Methylindole	HMDB0000466	6736	C08313	CC1=CNC2=CC=CC=C12
Furaneol	NA	NA	NA	NA	NA
methyprylon	Methyprylon	HMDB0015239	4162	NA	CCC1(C(=O)C(CNC1=O)C)CC
butoctamide	NA	NA	NA	NA	NA
2S-Amino-tridecanoic acid	Tridecanoic acid	HMDB0000910	656741	C17076	CCCCCCCCCCCCC(=O)O
Carboxycyclophosphamide	Morphine-3-glucuronide	HMDB0041936	5484731	C16643	[H][C@@]12CC3=C4C(O[C@H]5[C@@H](O)C=C[C@@H]1[C@@]45CCN2C)=C(O[C@@H]1O[C@@H]([C@@H](O)[C@H](O)[C@H]1O)C(O)=O)C=C3
Pyrophosphoric Acid	Pyrophosphate	HMDB0000250	644102	C00013	[O-]P(=O)([O-])OP(=O)([O-])[O-]
Palmitic Acid	Palmitic acid	HMDB0000220	985	C00249	CCCCCCCCCCCCCCCC(=O)O
Stearic acid	Stearic acid	HMDB0000827	5281	C01530	CCCCCCCCCCCCCCCCCC(=O)O
D-(-)-Mannitol	Mannitol	HMDB0000765	6251	C00392	C([C@H]([C@H]([C@@H]([C@@H](CO)O)O)O)O)O
4-[(4E)-3-Hydroxy-4-decen-1-yl]-2-methoxyphenol	NA	NA	NA	NA	NA
2-Dodecylbenzenesulfonic acid	2-Dodecylbenzenesulfonic acid	HMDB0031031	25457	NA	CCCCCCCCCCCCC1=CC=CC=C1S(=O)(=O)O
4-Undecylbenzenesulfonic acid	N-Undecylbenzenesulfonic acid	HMDB0032549	38222	NA	CCCCCCCCCCCC1=CC=C(C=C1)S(=O)(=O)O
8-Amino-7-oxononanoic acid	8-Amino-7-oxononanoate	METPA0126	NA	C01092	NA

Query	Match	HMDB	Pub-Chem	KEGG	SMILES
Perfluorooctanoic Acid	NA	NA	NA	NA	NA
2,6-di-tert-Butylphenol	NA	NA	NA	NA	NA
Azelaic acid	Azelaic acid	HMDB0000784	2266	C08261	C(CCCC(=O)O)CCCC(=O)O
1-nonanoic acid	Pelargonic acid	HMDB0000847	8158	C01601	CCCCCCCCC(=O)O
5,4'-dihydroxy-3,3'-dimethoxy-6,7-methylenedioxyflavone	5,4'-Dihydroxy-3,3'-dimethoxy-6:7-methylenedi-oxyflavone	HMDB0029272	44259873	NA	COC1=C(C=CC(=C1)C2=C(C(=O)C3=C(C4=C(C=C3O2)OCO4)O)OC)O
pentadecanoic acid	Pentadecanoic acid	HMDB0000826	13849	C16537	CCCCCCCCCCCCCCC(=O)O
myristic acid	Myristic acid	HMDB0000806	11005	C06424	CCCCCCCCCCCCCC(=O)O
11-Methylhexadecanoic acid	(+/-)-11-Methylhexadecanoic acid	HMDB40598	5312293	NA	CCCCCC(C)CCCCCCCCCC(=O)O
Linoleic Acid	Linoleic acid	HMDB0000673	5280450	C01595	CCCCC/C=C\C/C=C\CCCCCCCC(=O)O
(+)-[6]-Gingerol	NA	NA	NA	NA	NA
Palmitelaidic acid	Palmitelaidic acid	HMDB0012328	5282745	NA	CCCCCC/C=C/CCCCCCCC(=O)O
Phthalic acid	Phthalic acid	HMDB0002107	1017	C01606	C1=CC=C(C(=C1)C(=O)O)C(=O)O
2-C-methylerythritol 4-phosphate	NA	NA	NA	NA	NA
lauric acid	Dodecanoic acid	HMDB0000638	3893	C02679	CCCCCCCCCCCC(=O)O
Artemether	Artemether	HMDB0015643	68911	NA	C[C@@H]1CC[C@H]2[C@H]([C@H](O[C@H]3[C@@]24[C@H]1CC[C@](O3)(OO4)C)OC)C
Arachidic acid	Arachidic acid	HMDB0002212	10467	C06425	CCCCCCCCCCCCCCCCCCCC(=O)O
Decanoic acid	Capric acid	HMDB0000511	2969	C01571	CCCCCCCCCC(=O)O
Bisphenol S	Bisphenol S	HMDB0240712	6626	C14216	OC1=CC=C(C=C1)S(=O)(=O)C1=CC=C(O)C=C1
5-Pentyl-1,4-dioxan-2-one	NA	NA	NA	NA	NA
Juniperic acid	16-Hydroxy hexadecanoic acid	HMDB0006294	7058075	C18218	C(CCCCCCCC(=O)[O-])CCCCCCCO
13S-hydroxyoctadecadienoic acid	13S-hydroxyoctadecadienoic acid	HMDB0004667	6443013	C14762	CCCCC[C@@H](/C=C/C=C\CCCCCCCC(=O)O)O
Valproic acid	Valproic acid	HMDB0001877	3121	C07185	CCCC(CCC)C(=O)O
DOA	NA	NA	NA	NA	NA

Query	Match	HMDB	Pub-Chem	KEGG	SMILES
butyrin	Glycerol tributanoate	HMDB0031094	6050	C13870	CCCC(=O)OCC(COC(=O)CCC)OC(=O)CCC
Sebacic acid	Sebacic acid	HMDB0000792	5192	C08277	C(CCCCC(=O)O)CCCC(=O)O
p-Toluenesulfonic acid	p-Toluenesulfonic acid	HMDB0059933	6101	C06677	CC1=CC=C(C=C1)S(O)(=O)=O
Dodecanedioic acid	Dodecanedioic acid	HMDB0000623	12736	C02678	C(CCCCCC(=O)O)CCCCC(=O)O
Brassylic acid	1,11-Undecanedicarboxylic acid	HMDB0002327	10458	NA	C(CCCCCC(=O)O)CCCCCC(=O)O
8-Hydroxyoctanoic acid	NA	NA	NA	NA	NA
3-Hydroxynonanoic acid	(Â±)-3-Hydroxynonanoic acid	HMDB0031513	36599	NA	CCCCCCC(CC(=O)O)O
Diethyl phthalate	NA	NA	NA	NA	NA

Table S.8 – **Pathway enrichment analysis of ES-2 EVs metabolites using MetaboAnalyst software for amide column and both modes of ionization.** Expected – expected hits; hits – observed hits; raw p – raw p-value; Holm p – p-values adjusted by the Holm-Bonferroni method; FDR – false discovery rates enrichment ratio – hits to observed ratio**.**

	total	expected	hits	Raw p	Holm p	FDR	Enrichment ratio
Riboflavin Metabolism	20	1.09	3	0.0912	1	1	1.834862
Fatty Acid Biosynthesis	35	1.91	4	0.119	1	1	1.04712
Beta Oxidation of Very Long Chain Fatty Acids	17	0.93	2	0.237	1	1	1.075269
Biotin Metabolism	8	0.438	1	0.363	1	1	2.283105
Phenylacetate Metabolism	9	0.492	1	0.398	1	1	2.03252
Glycerolipid Metabolism	25	1.37	2	0.402	1	1	0.729927
Mitochondrial Beta-Oxidation of Medium Chain Saturated Fatty Acids	27	1.48	2	0.441	1	1	0.675676
Mitochondrial Beta-Oxidation of Long Chain Saturated Fatty Acids	28	1.53	2	0.46	1	1	0.653595
Glycerol Phosphate Shuttle	11	0.602	1	0.463	1	1	1.66113
Cardiolipin Biosynthesis	11	0.602	1	0.463	1	1	1.66113
Phosphatidylethanolamine Biosynthesis	12	0.656	1	0.493	1	1	1.52439
Phosphatidylcholine Biosynthesis	14	0.766	1	0.547	1	1	1.305483
Nicotinate and Nicotinamide Metabolism	37	2.02	2	0.613	1	1	0.49505
Alanine Metabolism	17	0.93	1	0.619	1	1	1.075269
Spermidine and Spermine Biosynthesis	18	0.984	1	0.64	1	1	2.03252
Alpha Linolenic Acid and Linoleic Acid Metabolism	19	1.04	1	0.66	1	1	0.961538
Butyrate Metabolism	19	1.04	1	0.66	1	1	0.961538
Ethanol Degradation	19	1.04	1	0.66	1	1	0.961538
Nucleotide Sugars Metabolism	20	1.09	1	0.679	1	1	0.917431

	total	expected	hits	Raw p	Holm p	FDR	Enrichment ratio
Ubiquinone Biosynthesis	20	1.09	1	0.679	1	1	1.834862
Lactose Synthesis	20	1.09	1	0.679	1	1	0.917431
Fatty acid Metabolism	43	2.35	2	0.696	1	1	0.425532
Pantothenate and CoA Biosynthesis	21	1.15	1	0.697	1	1	0.869565
Betaine Metabolism	21	1.15	1	0.697	1	1	0.869565
Sulfate/Sulfite Metabolism	22	1.2	1	0.714	1	1	1.666667
Steroid Biosynthesis	48	2.62	2	0.753	1	1	0.381679
Glutamate Metabolism	49	2.68	2	0.764	1	1	0.373134
Cysteine Metabolism	26	1.42	1	0.773	1	1	0.704225
Oxidation of Branched Chain Fatty Acids	26	1.42	1	0.773	1	1	0.704225
Phytanic Acid Peroxisomal Oxidation	26	1.42	1	0.773	1	1	0
Plasmalogen Synthesis	26	1.42	1	0.773	1	1	0
Mitochondrial Beta-Oxidation of Short Chain Saturated Fatty Acids	27	1.48	1	0.785	1	1	0
Phenylalanine and Tyrosine Metabolism	28	1.53	1	0.797	1	1	0
Selenoamino Acid Metabolism	28	1.53	1	0.797	1	1	0
Pentose Phosphate Pathway	29	1.59	1	0.809	1	1	0
Urea Cycle	29	1.59	1	0.809	1	1	0
Starch and Sucrose Metabolism	31	1.7	1	0.83	1	1	0
Ammonia Recycling	32	1.75	1	0.839	1	1	0
Fructose and Mannose Degradation	32	1.75	1	0.839	1	1	0
Pyrimidine Metabolism	59	3.23	2	0.848	1	1	0
Inositol Metabolism	33	1.8	1	0.848	1	1	0
Amino Sugar Metabolism	33	1.8	1	0.848	1	1	0
Fatty Acid Elongation In Mitochondria	35	1.91	1	0.865	1	1	0
Aspartate Metabolism	35	1.91	1	0.865	1	1	0
Bile Acid Biosynthesis	65	3.55	2	0.885	1	1	0
Galactose Metabolism	38	2.08	1	0.887	1	1	0
Propanoate Metabolism	42	2.3	1	0.91	1	1	0
Methionine Metabolism	43	2.35	1	0.915	1	1	0
Histidine Metabolism	43	2.35	1	0.915	1	1	0
Purine Metabolism	74	4.05	2	0.925	1	1	0
Pyruvate Metabolism	48	2.62	1	0.937	1	1	0
Arginine and Proline Metabolism	53	2.9	1	0.953	1	1	0
Glycine and Serine Metabolism	59	3.23	1	0.967	1	1	0
Tryptophan Metabolism	60	3.28	1	0.969	1	1	0

Table S.9 – **ES-2 EVs I lipid identifications using Compound Discoverer software**. Annot. Source – annotation source; Calc. MW – calculated molecular weight; RSD – relative standard deviation.

ID	Name	Formula	Annot. Source: Predicted Compositions	Annot. Source: mzCloud Search	Annot. Source: ChemSpider Search	Annot. DeltaMass [ppm]	Calc. MW	RT [min]	Area (Max.)
1	11-Aminoundecanoic acid	C11 H23 N O2	No results	No results	Full match	0.4	201.17296	1.154	1.69E+09
2	2-(11,17-Dihydroxy-10,13,16-trimethyl-3-oxo-4,5,6,7,8,9,10,11,12,13,14,15,16,17-tetradecahydro-3H-cyclopenta[a]phenanthren-17-yl)-2-oxoethyl acetate	C24 H34 O6	No results	Invalid mass	No results	-7.12	418.23256	1.658	7.00E+08
3	methyl 2-(1,3,5-trihydroxy-4a-methyl-8-oxo-decahydronaphthalen-2-yl)prop-2-enoate	C15 H22 O6	No match	Invalid mass	No results	73728.85	320.12328	1.342	5.51E+08
4	Irgafos 168	C42 H63 O3 P	No results	Full match	No results	-1.26	646.45067	33.098	3.88E+08
5	N-{(1R,9S)-11-[(1-Methyl-1H-indol-3-yl)methyl]-6-oxo-7,11-diazatricyclo[7.3.1.02,7]trideca-2,4-dien-5-yl}benzamide	C28 H28 N4 O2	No results	Invalid mass	No results	-39835.76	434.20665	1.663	3.34E+08
6	5-({[(2R,4S,5R)-5-(6-Cyclopentyl-2-methyl-4-pyrimidinyl)-1-azabicyclo[2.2.2]oct-2-yl]methyl}amino)-5-oxopentanoic acid	C23 H34 N4 O3	No results	Invalid mass	No match	-43480.45	396.25075	1.656	3.03E+08
7	5-hydroxy-2-(4-hydroxyphenyl)-8,8-dimethyl-4H,8H-pyrano[3,2-g]chromen-4-one	C20 H16 O5	No results	Invalid mass	No results	-7.97	336.09709	1.332	1.90E+08
8	Bis(4-ethylbenzylidene)sorbitol	C24 H30 O6	No results	Full match	Partial match	-1.17	414.20375	1.629	1.19E+08
9	NP-007953	C15 H24 O5	No results	Invalid mass	No results	59918.48	301.18895	1.153	9.12E+07
10	Tris(hydroxymethyl)aminomethane	C4 H11 N O3	No results	No results	Full match	-0.13	121.07388	1.139	2.63E+07

ID	# ChemSpider Results	# mzCloud Results	mzCloud Best Match	mzCloud Best Match Confidence	MS2	Area: QC_HSS_blk	Area: QC_HSS_blk	Area: HSS_pos_QC_20ul	Area: HSS_neg_QC_20ul.
1	1	0			DDA for preferred ion			1.69E+09	
2	0	2	81.1	9.1	DDA for preferred ion			7.00E+08	
3	0	12	100	10	DDA for preferred ion			5.51E+08	
4	0	3	96.8	9.8	DDA for preferred ion			3.88E+08	
5	0	8	99.2	10	DDA for preferred ion			3.34E+08	
6	2	2	93.5	9.7	DDA for preferred ion				3.03E+08
7	0	10	98.2	9.9	DDA for preferred ion			1.90E+08	
8	5	6	99.7	10	DDA for preferred ion			1.19E+08	
9	0	1	31.9	38	DDA for preferred ion			9.12E+07	
10	1	0			No MS2			2.63E+07	

Table S.10 – **ES-2 EVs II lipid identifications using Compound Discoverer software in positive mode**. Annot. Source – annotation source; Calc. MW – calculated molecular weight; RSD – relative standard deviation; CCM – cell culture media. EB – Extraction blank.

ID	Name
1	(9R)-6-Hydroxy-6-oxido-12-oxo-5,7,11-trioxa-2-aza-6lambda~5~-phosphaheptacosan-9-yl (9Z)-9-octadecenoate
2	Triglyceride POO,sn
3	DL-Dipalmitoylphosphatidylcholine
4	Triolein
5	(9R)-6-Hydroxy-6-oxido-12-oxo-5,7,11-trioxa-2-aza-6lambda~5~-phosphaheptacosan-9-yl palmitate
6	TG(16:1(9Z)/16:1(9Z)/18:0)[iso3]
7	TG(16:1(9Z)/18:1(9Z)/18:1(9Z))[iso3]
8	(9R)-6-Hydroxy-6-oxido-12-oxo-5,7,11-trioxa-2-aza-6lambda~5~-phosphaheptacosan-9-yl (9Z)-9-octadecenoate
9	Palmitoyl sphingomyelin
10	Dioleoylphosphatidylethanolamine
11	DL-Arginine
12	TG(16:0/16:1(9Z)/16:1(9Z))[iso3]
13	DL-Glutamine
14	Pyridoxine
15	Penicillin G
16	1-Palmitoyl-2-linoleoyl PE
17	L-Histidine
18	6-Hydroxy-6-oxido-12-oxo-5,7,11-trioxa-2-aza-6lambda~5~-phosphanonacosan-9-yl stearate
19	1-palmitoyl-2-oleoyl-sn-glycero-3-phosphoethanolamine
20	Betaine
21	1-stearoyl-2-oleoyl-sn-glycero-3-phosphoethanolamine zwitterion
22	Thiamine
23	Creatine
24	Octadecanamine
25	5,5-dimethyl-2-{[(2-phenylacetyl)amino]methyl}-1,3-thiazolane-4-carboxylic acid
26	1,2-dioleoyl-sn-glycero-3-phospho-N,N-dimethylethanolamine
27	L-Pyroglutamic acid
28	Dioleoylphosphatidylethanolamine
29	N1-phenethylbenzene-1-carbothioamide
30	24-Amino-21-hydroxy-21-oxido-15-oxo-16,20,22-trioxa-21lambda~5~-phosphatetracosan-18-yl palmitate
31	1-stearoyl-2-arachidonoyl-sn-glycero-3-phosphoethanolamine
32	1-stearoyl-2-oleoyl-sn-glycero-3-phosphoserine
33	1-stearoyl-2-arachidonoyl-sn-glycero-3-phosphoethanolamine
34	DL-Lysine
35	(2R)-1-{[(2-Aminoethyl)(hydroxy)phosphoryl]oxy}-3-(palmitoyloxy)-2-propanyl (9Z)-9-octadecenoate
36	Nicotinamide
37	1-oleoyl-2-linoleyl-sn-glycero-3-phosphoethanolamine

ID	Name
38	MFCD00042876
39	Ceramide (d18:1/16:0)
40	1-hexadecanoyl-2-(4Z,7Z,10Z,13Z,16Z,19Z-docosahexaenoyl)-sn-glycero-3-phosphoethanolamine
41	1-hexadecanoyl-2-(5Z,8Z,11Z,14Z-icosatetraenoyl)-sn-glycero-3-phosphoethanolamine
42	N-[(2S,3R,4E)-1-(beta-D-erythro-Hexopyranosyloxy)-3-hydroxy-4-octadecen-2-yl]hexadecanamide
43	1-palmitoyl-2-oleoyl-sn-glycero-3-phospho-l-serine
44	1-octadecanoyl-2-(4Z,7Z,10Z,13Z,16Z,19Z-docosahexaenoyl)-sn-glycero-3-phosphoethanolamine
45	Dioleoylphosphatidylethanolamine
46	1-stearoyl-2-oleoyl-sn-glycero-3-phosphoethanolamine zwitterion
47	1-oleoyl-2-linoleyl-sn-glycero-3-phosphoethanolamine
48	1-palmitoyl-2-oleoyl-sn-glycero-3-phosphoethanolamine
49	1-hexadecanoyl-2-(5Z,8Z,11Z,14Z-icosatetraenoyl)-sn-glycero-3-phosphoethanolamine
50	L(-)-Pipecolinic acid
51	MFCD00042876
52	Indole-3-acetic acid
53	TG(18:2(9Z,12Z)/18:2(9Z,12Z)/20:1(11Z))[iso3]
54	(24R)-30-Amino-27-hydroxy-27-oxido-21-oxo-22,26,28-trioxa-27lambda~5~-phosphatriacontan-24-yl (4Z,7Z,10Z,13Z,16Z,19Z)-4,7,10,13,16,19-docosahexaenoate
55	1730602
56	Choline
57	Cetrimonium
58	Bis(2-ethylhexyl) phthalate
59	2-[(11Z)-11-Icosenoyloxy]-3-[(9Z,12Z,15Z)-9,12,15-octadecatrienoyloxy]propyl (11Z,14Z)-11,14-icosadienoate
60	(2R)-3-{[(2-Aminoethoxy)(hydroxy)phosphoryl]oxy}-2-[(9Z)-9-hexadecenoyloxy]propyl (9Z)-9-hexadecenoate
61	Nicotinamide
62	(24R)-30-Amino-27-hydroxy-27-oxido-21-oxo-22,26,28-trioxa-27lambda~5~-phosphatriacontan-24-yl (4Z,7Z,10Z,13Z,16Z,19Z)-4,7,10,13,16,19-docosahexaenoate
63	(1'S,2'S)-3',11'-dihydroxy-1',2',5'-trimethyl-8'-oxaspiro[oxirane-2,12'-tricyclo[7.2.1.0Â?,â• ·]dodecan]-5'-en-4'-one
64	2-Amino-4-methylpyrimidine
65	N3,N4-Dimethyl-L-arginine
66	1-Oleoyl-2-hydroxy-sn-glycero-3-PE
67	4-Methyl-5-thiazoleethanol
68	4-Methyl-5-thiazoleethanol

ID	Formula	Annot. Source: mzCloud Search	Annot. Source: ChemSpider Search	Annot. DeltaMass [ppm]	Calc. MW	RT [min]	Area (Max.)	# ChemSpider Results	# mzCloud Results	mzCloud Best Match	mzCloud Best Match Confidence	# Usable QC	RSD QC Areas [%]	RSD Corr. QC Areas [%]	MS2
1	C40 H78 N O8 P	No results	Full match	-0.21	731.54635	9.495	3.06E+10	3	0			13	15	15	DDA for preferred ion
2	C55 H102 O6	No results	Full match	-1.13	858.76667	32.815	1.14E+10	12	0			13	14	14	DDA for other ion

ID	Formula	Annot. Source: mzCloud Search	Annot. Source: ChemSpider Search	Annot. DeltaMass [ppm]	Calc. MW	RT [min]	Area (Max.)	# ChemSpider Results	# mzCloud Results	mzCloud Best Match	mzCloud Best Match Confidence	# Usable QC	RSD QC Areas [%]	RSD Corr. QC Areas [%]	MS2
3	C40 H80 N O8 P	Full match	Partial match	-0.39	733.56187	11.261	8.90E+09	10	1	92.7	9.6	13	11	11	DDA for preferred ion
4	C57 H104 O6	No results	Full match	-0.77	884.78261	32.795	8.81E+09	24	0			13	10	10	DDA for other ion
5	C38 H76 N O8 P	No results	Full match	-0.49	705.53051	9.28	8.77E+09	8	0			13	11	11	DDA for preferred ion
6	C53 H98 O6	No results	Full match	-0.86	830.73563	32.195	8.06E+09	6	0			13	16	17	DDA for other ion
7	C55 H100 O6	No results	Full match	-0.65	856.75143	32.189	6.28E+09	13	0			13	15	15	DDA for other ion
8	C40 H78 N O8 P	No results	Full match	-0.14	731.5464	9.806	5.15E+09	3	0			13	13	13	DDA for preferred ion
9	C39 H79 N2 O6 P	Full match	No results	-0.51	702.56722	9.228	4.10E+09	0	2	86.1	9.3	13	10	10	DDA for preferred ion
10	C41 H78 N O8 P	No results	Full match	-0.73	743.54596	12.277	2.98E+09	9	0			13	27	24	DDA for preferred ion
11	C6 H14 N4 O2	Full match	No results	-0.76	174.11154	1.223	2.81E+09	0	6	98.7	94.7	13	12	11	DDA for preferred ion
12	C51 H94 O6	No results	Full match	-0.12	802.70494	31.51	2.52E+09	1	0			13	20	20	DDA for other ion
13	C5 H10 N2 O3	Full match	No results	-0.27	146.0691	1.199	2.25E+09	0	6	95	73.9	13	22	22	DDA for preferred ion
14	C8 H11 N O3	Full match	No results	-0.94	169.07373	1.145	2.07E+09	0	2	99.3	98	13	26	20	DDA for preferred ion
15	C16 H18 N2 O4 S	Full match	No results	-1.05	334.09838	1.216	1.97E+09	0	1	99.5	10	13	5	5	DDA for preferred ion
16	C39 H74 N O8 P	No results	Full match	-0.72	715.51469	10.177	1.62E+09	1	0			13	11	11	DDA for preferred ion
17	C6 H9 N3 O2	Full match	No results	-0.12	155.06946	1.243	1.42E+09	0	2	99.9	98.9	13	16	16	DDA for preferred ion
18	C42 H84 N O8 P	No results	Full match	-0.93	761.59275	13.743	1.26E+09	9	0			13	8	8	DDA for preferred ion
19	C39 H76 N O8 P	No results	Full match	-0.69	717.53036	12.192	1.17E+09	7	0			13	18	18	DDA for preferred ion
20	C5 H11 N O2	Full match	Partial match	-1.01	117.07886	1.149	1.06E+09	3	5	87.5	9.4	13	12	11	DDA for preferred ion
21	C41 H80 N O8 P	No results	Full match	-0.8	745.56156	10.421	8.62E+08	11	0			13	17	17	DDA for preferred ion
22	C12 H16 N4 O S	Full match	No results	-1.09	264.10419	1.065	8.26E+08	0	1	100	10	13	14	14	DDA for preferred ion
23	C4 H9 N3 O2	Full match	No results	-0.4	131.06942	1.144	8.15E+08	0	2	50.8	41.1	13	14	12	DDA for preferred ion
24	C18 H39 N	Full match	No results	-1.02	269.30798	2.199	8.12E+08	0	4	97.1	9.9	13	11	9	DDA for preferred ion
25	C15 H20 N2 O3 S	Full match	No results	-0.99	308.11916	1.22	7.75E+08	0	3	94.3	83.9	13	15	15	DDA for preferred ion
26	C43 H82 N O8 P	No results	Full match	-0.9	771.57711	10.536	7.69E+08	11	0			13	15	14	DDA for preferred ion
27	C5 H7 N O3	Full match	No results	-0.35	129.04255	1.196	6.94E+08	0	6	96.9	9.8	13	22	22	DDA for preferred ion
28	C41 H78 N O8 P	No results	Full match	-0.62	743.54604	12.397	6.71E+08	9	0			13	24	24	DDA for preferred ion
29	C15 H15 N S	Full match	No results	-0.81	241.09232	1.19	6.61E+08	0	1	86	9.3	13	13	12	DDA for preferred ion
30	C36 H72 N O8 P	No results	Full match	-0.61	677.49914	7.292	6.45E+08	6	0			13	12	12	DDA for preferred ion
31	C43 H78 N O8 P	No results	Full match	-0.59	767.54605	12.376	5.78E+08	11	0			13	12	11	DDA for preferred ion
32	C42 H80 N O10 P	No results	Full match	-0.69	789.55144	14.408	5.72E+08	4	0			13	14	12	DDA for preferred ion
33	C43 H78 N O8 P	No results	Full match	-0.49	767.54613	11.853	5.43E+08	11	0			13	11	10	DDA for preferred ion
34	C6 H14 N2 O2	Full match	No results	-0.38	146.10547	1.226	5.40E+08	0	8	85.7	9.3	13	14	14	DDA for preferred ion
35	C39 H76 N O7 P	No results	Full match	-0.88	701.53533	13.536	5.39E+08	1	0			13	10	9	DDA for preferred ion
36	C6 H6 N2 O	Full match	No results	-0.9	122.0479	1.18	5.01E+08	0	1	99.7	98.9	13	11	11	DDA for preferred ion
37	C41 H76 N O8 P	No results	Full match	-0.55	741.53044	10.631	4.46E+08	2	0			13	11	11	DDA for preferred ion
38	C39 H78 N O8 P	No results	Full match	-0.58	719.54609	10.212	4.06E+08	9	0			13	12	12	DDA for preferred ion
39	C34 H67 N O3	No results	Full match	-0.13	537.51202	12.235	3.72E+08	1	0			13	14	13	DDA for preferred ion

ID	Formula	Annot. Source: mzCloud Search	Annot. Source: ChemSpider Search	Annot. DeltaMass [ppm]	Calc. MW	RT [min]	Area (Max.)	# ChemSpider Results	# mzCloud Results	mzCloud Best Match	mzCloud Best Match Confidence	# Usable QC	RSD QC Areas [%]	RSD Corr. QC Areas [%]	MS2
40	C43 H74 N O8 P	No results	Full match	-1.03	763.51442	9.689	3.67E+08	1	0			13	13	13	DDA for preferred ion
41	C41 H74 N O8 P	No results	Full match	-0.86	739.51457	10.165	3.51E+08	6	0			13	11	11	DDA for preferred ion
42	C40 H77 N O8	No results	Full match	-0.67	699.56445	10.088	3.40E+08	1	0			13	12	12	DDA for preferred ion
43	C40 H76 N O10 P	No results	Full match	-0.25	761.52049	11.752	3.12E+08	4	0			13	15	15	DDA for preferred ion
44	C45 H78 N O8 P	No results	Full match	-0.75	791.54591	11.748	2.81E+08	1	0			13	12	12	DDA for preferred ion
45	C41 H78 N O8 P	No results	Full match	-1.09	743.54569	8.752	2.78E+08	9	0			13	15	14	DDA for preferred ion
46	C41 H80 N O8 P	No results	Full match	-0.75	745.56159	14.948	2.65E+08	11	0			13	11	11	DDA for preferred ion
47	C41 H76 N O8 P	No results	Full match	-0.87	741.53021	11.723	2.59E+08	2	0			13	11	11	DDA for preferred ion
48	C39 H76 N O8 P	No results	Full match	-0.62	717.53041	8.57	2.56E+08	7	0			13	11	11	DDA for preferred ion
49	C41 H74 N O8 P	No results	Full match	-0.86	739.51457	9.836	2.52E+08	6	0			13	11	11	DDA for preferred ion
50	C6 H11 N O2	Full match	No results	-0.21	129.07895	1.209	2.46E+08	0	12	84.2	9.2	13	7	7	DDA for preferred ion
51	C39 H78 N O8 P	No results	Full match	-0.69	719.54601	9.871	2.09E+08	9	0			13	4	4	DDA for preferred ion
52	C10 H9 N O2	Full match	No results	-0.48	175.06324	1.217	2.07E+08	0	2	46	7.3	13	9	9	DDA for preferred ion
53	C59 H104 O6	No results	Full match	-1.92	908.78154	33.404	2.00E+08	33	0			13	9	9	DDA for preferred ion
54	C48 H84 N O8 P	No results	Full match	-0.82	833.59277	11.087	1.94E+08	1	0			13	18	16	DDA for preferred ion
55	C37 H74 N O8 P	No results	Full match	-0.74	691.5147	11.965	1.91E+08	6	0			13	9	8	DDA for preferred ion
56	C5 H13 N O	Full match	No results	-0.4	103.09967	1.079	1.89E+08	0	1	99.4	10	13	20	20	DDA for preferred ion
57	C19 H41 N	Full match	No results	-0.75	283.32369	2.151	1.79E+08	0	1	93.3	9.7	13	10	9	DDA for preferred ion
58	C24 H38 O4	Full match	Partial match	-1.05	390.2766	4.208	1.55E+08	53	27	95.2	74.3	13	11	11	DDA for preferred ion
59	C61 H106 O6	No results	Full match	-1.64	934.79741	33.348	1.40E+08	38	0			13	14	13	DDA for preferred ion
60	C37 H70 N O8 P	No results	Full match	-0.4	687.48363	8.358	1.38E+08	2	0			13	11	11	DDA for preferred ion
61	C6 H6 N2 O	Full match	No results	-0.96	122.0479	1.066	1.35E+08	0	1	95.4	84.1	13	21	21	DDA for preferred ion
62	C48 H84 N O8 P	No results	Full match	-1.27	833.59239	9.824	1.32E+08	1	0			13	14	14	DDA for preferred ion
63	C15 H20 O5	Full match	No results	-0.92	280.13082	1.365	1.24E+08	0	1	30.9	40.9	13	8	7	DDA for preferred ion
64	C5 H7 N3	Full match	No results	-0.61	109.06393	1.237	1.22E+08	0	1	58.9	42.4	13	16	15	DDA for preferred ion
65	C8 H18 N4 O2	Full match	No results	-0.17	202.14294	1.122	1.08E+08	0	1	38.9	58.8	13	19	17	DDA for preferred ion
66	C23 H46 N O7 P	No results	Full match	-0.11	479.30113	2.024	1.07E+08	2	0			13	10	10	DDA for preferred ion
67	C6 H9 N O S	Full match	No results	-0.09	143.04047	1.081	8.95E+07	0	1	99.3	97.6	13	11	11	DDA for preferred ion
68	C6 H9 N O S	Full match	No results	0.09	143.0405	1.062	7.80E+07	0	1	99.3	97.6	13	5	4	DDA for preferred ion

ID	Norm. Area: BLK04	Norm. Area: C18_pos_QC_MS	Norm. Area: C18_pos_QC_MS_01	Norm. Area: C18_pos_QC_MS_02	Norm. Area: C18_pos_QC_MS_03	Norm. Area: C18_pos_QC_MS_04	Norm. Area: C18_pos_QC_MS_05	Norm. Area: C18_pos_QC_MS_06	Norm. Area: C18_pos_QC_MS_07	Norm. Area: C18_pos_QC_MS_08	Norm. Area: C18_pos_QC_MS_09	Norm. Area: C18_pos_QC_MS_10	Norm. Area: C18_pos_Hep_CCM2	Norm. Area: C18_pos_Hep_Cells1	Norm. Area: C18_pos_Hep_CCM1	Norm. Area: C18_pos_QC_MS_11	Norm. Area: C18_pos_EVs_II	Norm. Area: C18_pos_Hep_EB	Norm. Area: C18_pos_Hep_Cells2	Norm. Area: C18_pos_QC_MS
1	1.3E+06	7.0E+09	1.0E+10	1.0E+10	1.0E+10	6.8E+09	1.1E+10	1.1E+10	1.0E+10	1.1E+10	9.5E+09	1.0E+10	3.6E+08	3.0E+10	4.0E+08	9.8E+09	1.1E+09	1.8E+08	2.7E+10	8.3E+09

ID	Norm.Area:BLK04	Norm.Area: C18_pos_QC_MS	Norm.Area: C18_pos_QC_MS_01	Norm.Area: C18_pos_QC_MS_02	Norm.Area: C18_pos_QC_MS_03	Norm.Area: C18_pos_QC_MS_04	Norm.Area: C18_pos_QC_MS_05	Norm.Area: C18_pos_QC_MS_06	Norm.Area: C18_pos_QC_MS_07	Norm.Area: C18_pos_QC_MS_08	Norm.Area: C18_pos_QC_MS_09	Norm.Area: C18_pos_QC_MS_10	Norm.Area: C18_pos_Hep_CCM2	Norm.Area: C18_pos_Hep_Cells1	Norm.Area: C18_pos_Hep_CCM1	Norm.Area: C18_pos_QC_MS_11	Norm.Area: C18_pos_EVs_II	Norm.Area: C18_pos_Hep_FB	Norm.Area: C18_pos_Hep_Cells2	Norm.Area: C18_pos_QC_MS
2	8.8E+06	2.4E+09	2.9E+09	2.8E+09	2.9E+09	2.5E+09	2.9E+09	3.0E+09	1.6E+09	2.4E+09	2.7E+09	2.9E+09	2.4E+08	1.1E+10	2.7E+08	2.7E+09	2.6E+07	4.0E+07	6.9E+09	2.7E+09
3	1.3E+06	2.1E+09	3.0E+09	3.0E+09	3.2E+09	3.0E+09	3.3E+09	3.3E+09	3.1E+09	3.1E+09	3.0E+09	3.0E+09	1.4E+08	8.7E+09	1.4E+08	2.9E+09	3.3E+09	1.7E+08	6.6E+09	2.6E+09
4	4.5E+07	1.8E+09	2.6E+09	2.5E+09	2.7E+09	2.7E+09	2.8E+09	2.8E+09	2.7E+09	2.7E+09	2.8E+09	2.4E+09	1.8E+08	8.6E+09	2.2E+08	2.5E+09	3.5E+07	8.0E+07	7.2E+09	2.3E+09
5	1.4E+06	1.8E+09	2.6E+09	2.7E+09	2.6E+09	2.8E+09	2.8E+09	3.0E+09	2.7E+09	2.6E+09	2.6E+09	2.6E+09	8.7E+07	8.6E+09	9.4E+07	2.5E+09	2.1E+09	6.7E+07	6.5E+09	2.3E+09
6	1.1E+07	9.7E+08	2.0E+09	2.0E+09	2.0E+09	2.1E+09	2.0E+09	2.2E+09	1.8E+09	2.0E+09	1.8E+09	2.0E+09	1.5E+08	7.7E+09	1.6E+08	1.7E+09	7.9E+06	4.3E+06	5.1E+09	1.7E+09
7	1.2E+07	1.2E+09	2.0E+09	1.9E+09	1.9E+09	2.1E+09	2.4E+09	2.0E+09	2.1E+09	1.8E+09	1.8E+09	2.2E+09	1.0E+08	6.0E+09	1.1E+08	2.0E+09	1.4E+07	4.7E+06	5.7E+09	1.6E+09
8	6.8E+05	1.1E+09	1.7E+09	1.4E+09	1.6E+09	1.8E+09	1.7E+09	1.7E+09	1.7E+09	1.9E+09	1.6E+09	1.5E+09	3.4E+07	5.0E+09	6.6E+07	1.5E+09	2.3E+08	2.0E+07	3.9E+09	1.4E+09
9	1.2E+06	9.9E+08	1.4E+09	1.4E+09	1.5E+09	1.5E+09	1.6E+09	1.6E+09	1.4E+09	1.4E+09	1.4E+09	1.4E+09	2.0E+08	4.0E+09	2.2E+08	1.3E+09	1.8E+09	2.2E+08	3.1E+09	1.3E+09
10	1.3E+06	3.8E+08	6.6E+08	5.4E+08	7.7E+08	6.4E+08	7.0E+08	6.3E+08	5.9E+08	6.0E+08	1.0E+09	6.2E+08	1.0E+07	2.6E+09	8.1E+06	5.3E+08	8.7E+06	1.4E+07	1.5E+09	5.7E+08
11	7.2E+05	9.9E+08	1.1E+09	1.1E+09	1.1E+09	1.2E+09	1.2E+09	1.3E+09	1.2E+09	1.4E+09	1.1E+09	1.1E+09	2.7E+09	2.0E+07	1.9E+09	9.4E+08	1.2E+08	3.2E+06	2.6E+07	1.1E+09
12	6.3E+06	2.4E+08	5.7E+08	6.3E+08	5.9E+08	6.3E+08	7.5E+08	6.6E+08	6.0E+08	6.2E+08	5.8E+08	5.6E+08	3.1E+07	2.4E+09	4.4E+07	5.1E+08	1.8E+06	3.7E+06	1.5E+09	5.1E+08
13	1.4E+06	1.5E+09	1.2E+09	1.2E+09	1.2E+09	1.9E+09	2.3E+09	1.2E+09	1.5E+09	1.5E+09	1.2E+09	1.4E+09	1.6E+09	2.2E+08	1.4E+09	1.6E+09	2.9E+06	5.3E+06	2.3E+08	1.3E+09
14	1.2E+06	1.2E+09	1.1E+09	1.3E+09	1.3E+09	1.3E+09	1.1E+09	1.2E+09	1.6E+09	1.5E+09	1.9E+09	9.2E+08	1.0E+09	1.2E+07	5.9E+08	1.2E+09	7.6E+06	3.3E+06	1.0E+07	1.2E+09
15	1.5E+06	7.7E+08	8.3E+08	8.3E+08	9.1E+08	8.5E+08	9.3E+08	8.7E+08	8.9E+08	8.7E+08	8.4E+08	8.3E+08	8.1E+08	3.2E+06	1.9E+09	8.1E+08	7.0E+06	1.4E+06	2.6E+06	8.4E+08
16	9.0E+05	3.9E+08	5.2E+08	5.5E+08	6.1E+08	5.6E+08	5.4E+08	5.8E+08	5.5E+08	6.0E+08	6.0E+08	5.4E+08	4.8E+06	1.4E+09	5.7E+06	5.0E+08	2.2E+08	4.5E+06	1.6E+09	4.8E+08
17	1.0E+06	3.2E+08	5.1E+08	5.5E+08	5.9E+08	4.0E+08	5.1E+08	5.8E+08	4.6E+08	4.4E+08	4.5E+08	4.2E+08	1.8E+08	3.4E+06	1.3E+09	5.3E+08	3.1E+06	1.1E+06	6.4E+06	4.5E+08
18	8.0E+05	2.9E+08	3.8E+08	3.8E+08	4.1E+08	3.7E+08	3.9E+08	4.0E+08	3.7E+08	3.7E+08	3.6E+08	3.8E+08	3.0E+07	5.0E+08	3.4E+07	3.6E+08	1.3E+09	3.7E+07	3.8E+08	3.5E+08
19	8.5E+05	1.8E+08	2.9E+08	2.6E+08	2.8E+08	2.6E+08	3.0E+08	4.0E+08	3.0E+08	2.7E+08	2.9E+08	2.8E+08	1.4E+06	1.2E+09	1.7E+06	2.6E+08	2.0E+08	6.9E+06	6.8E+08	2.4E+08
20	8.5E+06	5.4E+08	6.0E+08	5.2E+08	6.8E+08	5.1E+08	5.4E+08	5.2E+08	4.8E+08	5.4E+08	4.9E+08	6.4E+08	5.6E+08	3.9E+07	1.0E+09	4.8E+08	1.1E+07	1.3E+06	4.2E+07	6.1E+08
21	8.6E+05	2.1E+08	2.8E+08	2.3E+08	3.0E+08	1.9E+08	2.8E+08	3.5E+08	2.9E+08	2.4E+08	2.3E+08	2.9E+08	3.3E+07	8.2E+08	3.7E+07	2.4E+08	1.4E+08	1.6E+07	7.4E+08	2.5E+08
22	2.6E+05	5.3E+08	4.1E+08	4.9E+08	5.3E+08	5.5E+08	4.8E+08	5.3E+08	4.4E+08	5.4E+08	4.9E+08	6.9E+08	8.4E+08	4.5E+07	7.2E+08	5.0E+08	5.3E+06	1.4E+06	3.2E+07	4.3E+08
23	8.0E+05	4.6E+08	5.1E+08	4.3E+08	4.3E+08	5.5E+08	4.3E+08	4.2E+08	4.7E+08	4.7E+08	5.4E+08	3.8E+08	2.7E+08	7.3E+08	2.7E+08	3.8E+08	1.8E+07	2.4E+06	7.1E+08	5.2E+08
24	1.8E+06	1.5E+08	1.8E+08	1.9E+08	2.1E+08	1.8E+08	2.0E+08	2.1E+08	1.8E+08	2.2E+08	1.9E+08	1.8E+08	5.2E+05	1.2E+06	2.0E+06	1.8E+08	9.2E+08	4.1E+05	4.4E+05	1.8E+08
25	5.3E+05	2.7E+08	2.8E+08	2.7E+08	2.8E+08	2.6E+08	3.0E+08	2.8E+08	2.8E+08	2.8E+08	2.8E+08	1.4E+08	7.8E+08	7.5E+05	7.8E+08	2.8E+08	3.3E+07	5.3E+05	6.6E+05	3.1E+08
26	9.2E+05	1.3E+08	2.1E+08	2.0E+08	1.9E+08	2.3E+08	2.3E+08	2.4E+08	2.2E+08	2.2E+08	1.9E+08	1.9E+08	2.7E+06	8.0E+08	3.3E+06	1.9E+08	2.0E+07	1.1E+07	6.5E+08	1.8E+08
27	6.4E+05	5.3E+08	4.8E+08	1.5E+08	5.2E+08	5.5E+08	5.8E+08	5.3E+08	4.9E+08	4.7E+08	5.0E+08	4.7E+08	4.0E+08	9.0E+07	6.8E+08	4.8E+08	8.3E+05	1.6E+06	9.2E+07	4.2E+08
28	5.9E+05	1.7E+08	2.0E+08	2.4E+08	1.7E+08	2.0E+08	1.3E+08	2.6E+08	2.7E+08	1.6E+08	1.5E+08	1.2E+08	5.7E+06	7.2E+08	4.3E+06	2.0E+08	3.3E+08	1.3E+07	4.1E+08	2.2E+08
29	4.9E+05	4.4E+08	4.2E+08	4.4E+08	4.9E+08	4.3E+08	3.6E+08	5.1E+08	4.4E+08	4.4E+08	3.1E+08	4.1E+08	3.4E+08	1.9E+07	6.1E+08	4.4E+08	5.6E+06	3.9E+06	2.1E+07	4.6E+08
30	7.8E+05	1.5E+08	2.4E+08	2.3E+08	2.5E+08	2.4E+08	2.5E+08	2.6E+08	2.2E+08	2.3E+08	2.2E+08	2.1E+08	7.2E+06	6.4E+08	7.9E+06	2.2E+08	2.6E+08	5.1E+06	5.8E+08	2.2E+08
31	7.4E+05	1.0E+08	1.4E+08	1.4E+08	1.5E+08	1.4E+08	1.6E+08	1.6E+08	1.4E+08	1.5E+08	1.4E+08	1.5E+08	6.0E+05	5.6E+08	1.2E+06	1.3E+08	3.2E+07	5.9E+06	4.3E+08	1.3E+08
32	1.0E+06	1.1E+08	1.9E+08	1.8E+08	1.7E+08	1.7E+08	1.8E+08	1.7E+08	1.6E+08	1.6E+08	1.6E+08	1.4E+08	1.2E+06	1.7E+08	1.5E+06	1.6E+08	6.3E+08	1.5E+07	1.6E+08	1.6E+08
33	1.2E+06	9.2E+07	1.3E+08	1.3E+08	1.4E+08	1.3E+08	1.4E+08	1.4E+08	1.3E+08	1.3E+08	1.3E+08	1.4E+08	1.7E+06	5.3E+08	1.8E+06	1.2E+08	8.3E+05	1.7E+06	3.8E+08	1.1E+08
34	1.6E+06	1.6E+08	2.1E+08	2.2E+08	2.5E+08	2.5E+08	2.4E+08	2.2E+08	2.3E+08	2.8E+08	2.6E+08	2.1E+08	5.3E+08	2.8E+06	4.1E+08	2.2E+08	1.7E+06	1.6E+06	2.4E+06	1.9E+08
35	5.8E+05	8.1E+07	1.2E+08	1.1E+08	1.1E+08	9.8E+07	1.1E+08	1.2E+08	1.1E+08	1.1E+08	1.1E+08	1.1E+08	4.4E+05	1.0E+06	4.1E+05	1.1E+08	5.6E+08	1.5E+06	4.3E+05	9.3E+07
36	6.7E+05	4.1E+08	4.8E+08	4.8E+08	4.7E+08	4.6E+08	5.0E+08	3.0E+08	4.4E+08	4.4E+08	4.5E+08	4.6E+08	3.7E+08	8.9E+07	8.8E+07	4.6E+08	9.7E+06	4.7E+06	9.8E+07	4.6E+08
37	1.2E+06	1.1E+08	1.4E+08	1.5E+08	1.6E+08	1.6E+08	1.5E+08	1.5E+08	1.6E+08	1.4E+08	1.4E+08	1.5E+08	1.7E+06	4.4E+08	1.4E+06	1.3E+08	7.2E+06	7.9E+05	2.9E+08	1.4E+08

ID	Norm.Area BLK04	Norm.Area C18_pos_QC_MS	Norm.Area C18_pos_QC_MS_01	Norm.Area C18_pos_QC_MS_02	Norm.Area C18_pos_QC_MS_03	Norm.Area C18_pos_QC_MS_04	Norm.Area C18_pos_QC_MS_05	Norm.Area C18_pos_QC_MS_06	Norm.Area C18_pos_QC_MS_07	Norm.Area C18_pos_QC_MS_08	Norm.Area C18_pos_QC_MS_09	Norm.Area C18_pos_QC_MS_10	Norm.Area C18_pos_Hep_CCM2	Norm.Area C18_pos_Hep_Cells1	Norm.Area C18_pos_Hep_CCM1	Norm.Area C18_pos_QC_MS_11	Norm.Area C18_pos_EVs_II	Norm.Area C18_pos_Hep_FB	Norm.Area C18_pos_Hep_Cells2	Norm.Area C18_pos_QC_MS
38	6.9E+05	7.0E+07	1.0E+08	9.9E+07	1.2E+08	1.1E+08	1.2E+08	1.2E+08	1.1E+08	1.1E+08	1.1E+08	9.2E+07	5.7E+06	4.0E+08	6.7E+06	9.8E+07	7.6E+07	6.3E+06	2.8E+08	9.7E+07
39	1.6E+06	6.2E+07	9.2E+07	9.2E+07	1.0E+08	1.0E+08	1.1E+08	1.1E+08	9.8E+07	1.0E+08	1.0E+08	1.0E+08	1.6E+06	3.5E+08	9.7E+05	9.2E+07	5.1E+07	2.4E+06	2.8E+08	8.1E+07
40	8.0E+05	6.2E+07	1.1E+08	9.6E+07	9.9E+07	1.0E+08	1.1E+08	1.1E+08	1.0E+08	1.0E+08	9.8E+07	9.9E+07	5.6E+05	3.6E+08	8.1E+05	9.5E+07	7.2E+06	9.8E+05	2.8E+08	8.6E+07
41	9.6E+05	5.8E+07	8.7E+07	8.9E+07	9.0E+07	9.0E+07	9.6E+07	9.7E+07	8.9E+07	8.8E+07	8.8E+07	9.0E+07	6.5E+05	3.4E+08	6.1E+05	8.0E+07	4.4E+06	6.0E+05	3.2E+08	7.8E+07
42	1.3E+06	4.2E+07	6.6E+07	6.4E+07	6.6E+07	6.5E+07	6.7E+07	7.2E+07	6.0E+07	6.5E+07	6.3E+07	6.4E+07	8.6E+05	2.7E+07	7.8E+05	5.7E+07	3.2E+08	8.7E+05	1.8E+07	5.9E+07
43	1.4E+06	6.6E+07	9.9E+07	1.2E+08	1.0E+08	1.1E+08	1.3E+08	1.2E+08	1.1E+08	1.0E+08	1.1E+08	1.2E+08	9.5E+05	3.0E+08	1.6E+06	9.7E+07	9.7E+07	4.5E+06	2.1E+08	8.9E+07
44	7.4E+05	4.4E+07	6.8E+07	6.5E+07	6.8E+07	6.5E+07	7.3E+07	7.1E+07	7.3E+07	6.5E+07	6.6E+07	6.9E+07	7.5E+05	2.7E+08	1.1E+06	6.4E+07	1.8E+07	4.6E+05	1.7E+08	5.7E+07
45	9.3E+05	5.2E+07	7.0E+07	7.5E+07	7.9E+07	7.8E+07	8.5E+07	9.7E+07	8.1E+07	8.1E+07	8.1E+07	8.4E+07	1.8E+06	2.7E+08	2.7E+06	6.9E+07	2.4E+06	5.3E+05	2.0E+08	6.5E+07
46	9.4E+05	1.2E+08	1.5E+08	1.3E+08	1.6E+08	1.7E+08	1.5E+08	1.5E+08	1.3E+08	1.3E+08	1.3E+08	1.3E+08	2.2E+06	2.7E+08	2.1E+06	1.5E+08	2.7E+08	8.5E+06	2.4E+08	1.4E+08
47	8.2E+05	4.1E+07	6.0E+07	5.9E+07	6.0E+07	6.0E+07	6.6E+07	6.6E+07	6.0E+07	6.2E+07	6.1E+07	6.2E+07	5.6E+05	2.5E+08	5.0E+05	5.7E+07	7.2E+05	6.3E+05	2.0E+08	5.2E+07
48	8.2E+05	6.2E+07	8.9E+07	8.2E+07	8.6E+07	8.6E+07	1.0E+08	9.0E+07	9.4E+07	9.3E+07	8.8E+07	8.5E+07	3.0E+06	2.3E+08	3.8E+06	8.1E+07	1.6E+07	1.2E+06	2.5E+08	7.6E+07
49	6.0E+05	7.6E+07	9.1E+07	9.9E+07	1.0E+08	1.2E+08	1.1E+08	1.1E+08	8.8E+07	8.5E+07	9.8E+07	9.9E+07	4.5E+05	2.5E+08	4.3E+05	9.8E+07	5.5E+05	5.3E+05	1.8E+08	9.3E+07
50	3.7E+06	8.4E+07	9.9E+07	8.7E+07	1.0E+08	9.9E+07	9.7E+07	1.0E+08	9.0E+07	9.8E+07	1.0E+08	9.1E+07	2.4E+08	2.9E+06	1.5E+08	9.0E+07	2.3E+06	2.4E+06	2.0E+06	9.5E+07
51	7.6E+05	7.5E+07	7.0E+07	7.4E+07	7.6E+07	7.3E+07	7.8E+07	8.1E+07	7.5E+07	8.0E+07	7.4E+07	7.7E+07	5.7E+05	2.1E+08	5.4E+05	7.3E+07	1.0E+08	5.6E+05	1.6E+08	7.3E+07
52	5.7E+05	8.0E+07	9.1E+07	9.2E+07	9.5E+07	9.2E+07	1.1E+08	9.8E+07	1.0E+08	9.3E+07	9.2E+07	8.1E+07	1.2E+08	1.0E+06	2.0E+08	8.7E+07	6.2E+05	7.8E+05	6.6E+05	9.4E+07
53	1.5E+06	3.8E+07	4.8E+07	4.7E+07	4.2E+07	4.6E+07	4.8E+07	4.9E+07	4.8E+07	4.7E+07	4.9E+07	5.4E+07	1.3E+06	2.0E+08	3.2E+06	4.1E+07	1.2E+06	1.2E+06	1.0E+08	4.2E+07
54	7.8E+05	8.1E+07	1.0E+08	1.0E+08	1.1E+08	1.1E+08	1.2E+08	1.2E+08	1.1E+08	1.1E+08	1.0E+08	1.5E+08	1.0E+08	1.8E+08	1.2E+08	9.2E+07	4.4E+07	1.7E+07	1.4E+08	9.3E+07
55	5.6E+05	3.3E+07	4.4E+07	4.2E+07	4.3E+07	4.2E+07	4.6E+07	4.3E+07	4.1E+07	3.8E+07	4.4E+07	4.2E+07	4.4E+05	2.8E+07	4.3E+05	4.0E+07	2.0E+08	4.1E+05	2.0E+07	3.9E+07
56	3.2E+05	1.1E+08	9.6E+07	1.5E+08	9.8E+07	7.2E+07	1.4E+08	1.1E+08	9.0E+07	1.3E+08	1.3E+08	8.4E+07	1.8E+08	1.5E+08	1.8E+08	1.2E+08	4.1E+06	5.7E+05	1.5E+08	1.1E+08
57	6.9E+05	2.4E+07	3.3E+07	3.4E+07	3.5E+07	3.1E+07	3.2E+07	3.4E+07	3.1E+07	3.0E+07	3.3E+07	3.3E+07	1.8E+06	8.1E+05	1.6E+06	3.0E+07	1.9E+08	1.6E+06	9.2E+05	3.0E+07
58	5.8E+05	2.9E+07	3.9E+07	4.2E+07	4.0E+07	3.7E+07	4.4E+07	4.4E+07	4.1E+07	3.7E+07	4.0E+07	4.1E+07	1.2E+07	1.5E+08	1.2E+07	3.8E+07	1.4E+07	2.3E+06	9.6E+07	3.5E+07
59	1.8E+06	3.1E+07	3.8E+07	3.9E+07	3.9E+07	4.4E+07	3.6E+07	3.7E+07	4.6E+07	4.8E+07	3.3E+07	4.3E+07	3.8E+06	1.3E+08	1.6E+06	3.7E+07	1.2E+06	1.2E+06	1.0E+08	3.5E+07
60	8.4E+05	2.8E+07	4.0E+07	4.0E+07	4.1E+07	4.4E+07	4.4E+07	4.6E+07	4.2E+07	4.1E+07	4.2E+07	4.2E+07	5.8E+05	1.3E+08	5.4E+05	3.9E+07	1.1E+07	5.3E+05	1.1E+08	3.5E+07
61	6.3E+05	1.1E+07	9.2E+06	1.2E+07	1.1E+07	7.5E+06	9.5E+06	1.3E+07	1.4E+07	6.8E+06	1.1E+07	1.4E+07	1.3E+06	1.2E+08	1.2E+06	1.1E+07	7.9E+05	7.8E+05	1.3E+08	9.3E+06
62	7.4E+05	3.0E+07	5.5E+07	5.5E+07	5.8E+07	5.3E+07	5.7E+07	5.5E+07	5.6E+07	5.3E+07	5.6E+07	5.5E+07	1.2E+07	1.3E+08	1.2E+07	5.0E+07	2.2E+07	5.3E+05	1.2E+08	4.6E+07
63	4.0E+05	2.5E+07	3.1E+07	3.1E+07	3.3E+07	3.3E+07	3.2E+07	3.0E+07	3.0E+07	2.9E+07	3.1E+07	3.0E+07	3.8E+05	5.0E+06	1.5E+06	3.0E+07	1.3E+08	5.8E+06	4.1E+06	3.0E+07
64	6.5E+05	3.6E+07	5.9E+07	5.8E+07	5.5E+07	5.9E+07	5.8E+07	7.1E+07	5.4E+07	6.6E+07	5.3E+07	4.6E+07	1.2E+08	8.2E+05	1.0E+08	5.3E+07	1.0E+06	5.6E+05	6.9E+05	5.4E+07
65	5.8E+05	3.6E+07	4.2E+07	4.0E+07	3.6E+07	4.1E+07	3.3E+07	4.5E+07	2.7E+07	4.2E+07	4.3E+07	5.5E+07	1.0E+08	2.6E+06	7.6E+07	3.9E+07	8.6E+05	8.5E+05	4.0E+06	3.4E+07
66	5.2E+05	2.2E+07	3.0E+07	2.9E+07	3.2E+07	3.1E+07	3.4E+07	3.3E+07	2.8E+07	3.1E+07	3.0E+07	3.0E+07	3.5E+05	1.0E+08	3.1E+05	2.8E+07	3.8E+06	4.7E+05	8.1E+07	2.8E+07
67	2.8E+05	5.4E+07	5.8E+07	5.9E+07	6.2E+07	5.8E+07	4.3E+07	4.3E+07	6.0E+07	6.3E+07	5.8E+07	5.9E+07	9.1E+07	7.6E+06	3.7E+07	5.7E+07	9.2E+05	6.2E+05	4.7E+06	5.5E+07
68	2.6E+05	5.3E+07	5.8E+07	5.9E+07	6.2E+07	5.8E+07	5.9E+07	6.1E+07	6.0E+07	6.3E+07	5.8E+07	5.9E+07	8.0E+07	7.6E+06	7.5E+07	5.8E+07	9.4E+05	6.4E+05	4.7E+06	5.6E+07

Table S.11 – **ES-2 EVs II lipid identifications using Compound Discoverer software in negative mode**. Annot. Source – annotation source; Calc. MW – calculated molecular weight; RSD – relative standard deviation; CCM – cell culture media. EB – Extraction blank.

ID	Name	Formula	Annot. Source: mzCloud Search	Annot. Source: ChemSpider Search	Annot. DeltaMass [ppm]	Calc. MW	RT [min]	Area (Max.)	# ChemSpider Results	# mzCloud Results	mzCloud Best Match	mzCloud Best Match Confidence	# Usable QC	RSD QC Areas [%]	RSD Corr. QC Areas [%]	MS2
1	4-Oxoproline	C5 H7 N O3	Full match	No results	-1.14	129.0425	1.18	3.29E+09	0	1	99.7	10	12	18	18	DDA for preferred ion
2	Pantothenic acid	C9 H17 N O5	Full match	No results	-1.36	219.1104	1.19	2.39E+09	0	2	98.5	97.7	12	15	15	DDA for preferred ion
3	O-{Hydroxy[2-(nonadecanoyloxy)-3-(stearoyloxy)propoxy]phosphoryl}-L-serine	C43 H84 N O10 P	No results	Full match	-0.28	805.5831	11.473	1.05E+09	1	0			12	6	5	DDA for preferred ion
4	5,5-dimethyl-2-{[(2-phenylacetyl)amino]methyl}-1,3-thiazolane-4-carboxylic acid	C15 H20 N2 O3 S	Full match	No results	-1.05	308.1191	1.201	8.14E+08	0	2	93.4	80.5	12	5	5	DDA for preferred ion
5	Dioleoylphosphatidylethanolamine	C41 H78 N O8 P	No results	Full match	-0.53	743.5461	12.34	6.96E+08	9	0			12	9	9	DDA for preferred ion
6	1-Palmitoyl-2-linoleoyl PE	C39 H74 N O8 P	No results	Full match	-0.41	715.5149	10.223	6.17E+08	1	0			12	12	12	DDA for preferred ion
7	D-(-)-Glutamine	C5 H10 N2 O3	Full match	No results	-0.92	146.069	1.179	4.09E+08	0	1	95.3	100	12	4	4	DDA for preferred ion
8	Pyridoxine	C8 H11 N O3	Full match	No results	-0.89	169.0737	1.204	3.51E+08	0	2	98	93.3	12	8	8	DDA for preferred ion
9	1-stearoyl-2-oleoyl-sn-glycero-3-phosphoserine	C42 H80 N O10 P	No results	Full match	-0.35	789.5517	14.192	3.33E+08	4	0			12	7	6	DDA for preferred ion
10	5-Oxohexanoic acid	C6 H10 O3	No results	Full match	-0.68	130.0629	1.182	2.83E+08	4	0			12	19	19	DDA for preferred ion
11	(2R)-1-{[(2-Aminoethyl)(hydroxy)phosphoryl]oxy}-3-(palmitoyloxy)-2-propanyl (9Z)-9-octadecenoate	C39 H76 N O7 P	No results	Full match	-0.49	701.5356	13.581	2.46E+08	1	0			12	4	2	DDA for preferred ion
12	1-palmitoyl-2-oleoyl-sn-glycero-3-phosphoethanolamine	C39 H76 N O8 P	No results	Full match	-0.32	717.5306	12.243	2.16E+08	7	0			12	7	5	DDA for preferred ion
13	Pyridoxine	C8 H11 N O3	Full match	No results	-0.91	169.0737	1.119	1.98E+08	0	2	98	93.3	12	11	11	DDA for preferred ion
14	4-Acetamidobenzoic acid	C9 H9 N O3	Full match	No results	-0.95	179.0581	1.198	1.85E+08	0	3	90.6	52.7	12	8	8	DDA for preferred ion
15	L-Histidine	C6 H9 N3 O2	Full match	No results	-0.85	155.0693	1.249	1.58E+08	0	2	99.3	100	12	10	9	DDA for preferred ion
16	D-(+)-Malic acid	C4 H6 O5	Full match	No results	-0.96	134.0214	1.207	1.12E+08	0	3	98.9	73.2	12	23	22	DDA for preferred ion
17	L-Threonic acid	C4 H8 O5	Full match	Full match	-0.85	136.0371	1.196	9.60E+07	2	1	97.4	99	12	14	13	DDA for preferred ion
18	Paracetamol	C8 H9 N O2	Full match	No results	-1.05	151.0632	1.203	8.27E+07	0	1	36.8	6.8	12	10	10	DDA for preferred ion

ID	Norm. Area: C18_neg_EVs_II	Norm. Area: C18_neg_Hep_EB	Norm. Area: C18_neg_Hep_Cells1	Norm. Area: C18_neg_Hep_Cells2	Norm. Area: C18_neg_Hep_CCM1	Norm. Area: C18_neg_Hep_CCM1	Norm. Area: C18_neg_QC_MS_01	Norm. Area: C18_neg_QC_MS_02	Norm. Area: C18_neg_QC_MS_03	Norm. Area: C18_neg_QC_MS_04	Norm. Area: C18_neg_QC_MS_05	Norm. Area: C18_neg_QC_MS_06	Norm. Area: C18_neg_QC_MS_07	Norm. Area: C18_neg_QC_MS_08.	Norm. Area: C18_neg_QC_MS_09	Norm. Area: C18_neg_QC_MS_10.	Norm. Area: C18_neg_QC_MS_11.	Norm. Area: C18_neg_QC_MS_12
1	5.7E+06	7.7E+06	2.0E+08	1.8E+08	2.5E+09	2.4E+09	2.3E+09	2.3E+09	1.6E+09	2.2E+09	2.3E+09	2.3E+09	2.4E+09	3.3E+09	2.2E+09	2.1E+09	2.7E+09	1.8E+09
2	2.4E+06	1.2E+06	4.0E+07	3.6E+07	1.8E+09	2.3E+09	6.5E+08	3.2E+08	6.5E+08	6.3E+08	6.3E+08	5.8E+08	6.2E+08	5.9E+08	6.1E+08	5.9E+08	5.6E+08	5.6E+08
3	2.7E+08	2.1E+07	1.1E+09	1.0E+09	4.6E+07	4.3E+07	4.8E+08	5.5E+08	5.2E+08	4.7E+08	4.8E+08	5.3E+08	5.1E+08	5.3E+08	5.3E+08	5.3E+08	5.3E+08	4.8E+08
4	2.9E+07	3.4E+06	3.3E+06	3.3E+06	8.5E+08	7.7E+08	3.9E+08	3.8E+08	4.2E+08	3.8E+08	3.6E+08	3.5E+08	3.8E+08	3.8E+08	4.0E+08	3.8E+08	3.9E+08	3.9E+08
5	1.3E+08	6.4E+06	7.1E+08	5.3E+08	4.3E+06	4.1E+06	2.2E+08	2.0E+08	2.1E+08	1.9E+08	2.2E+08	2.0E+08	2.0E+08	2.1E+08	2.1E+08	1.7E+08	2.4E+08	2.0E+08
6	9.0E+07	2.0E+06	6.3E+08	3.5E+08	2.6E+06	1.8E+06	2.0E+08	2.5E+08	2.1E+08	1.8E+08	1.9E+08	1.8E+08	2.0E+08	2.4E+08	1.8E+08	2.0E+08	2.2E+08	2.1E+08
7	3.4E+06	1.4E+06	4.3E+07	4.0E+07	3.9E+08	4.1E+08	2.5E+08	2.8E+08	2.9E+08	2.9E+08	2.7E+08	2.5E+08	2.7E+08	2.8E+08	2.8E+08	2.8E+08	2.7E+08	2.7E+08
8	2.8E+06	3.0E+06	2.4E+06	2.4E+06	3.1E+08	3.5E+08	1.3E+08	1.2E+08	1.1E+08	1.1E+08	1.3E+08	1.0E+08	1.2E+08	1.2E+08	1.3E+08	1.3E+08	1.2E+08	1.2E+08

ID	Norm. Area: C18_neg_EVs_II	Norm. Area: C18_neg_Hep_EB	Norm. Area: C18_neg_Hep_Cells1	Norm. Area: C18_neg_Hep_Cells2	Norm. Area: C18_neg_Hep_CCM1	Norm. Area: C18_neg_Hep_CCM1	Norm. Area: C18_neg_QC_MS_01	Norm. Area: C18_neg_QC_MS_02	Norm. Area: C18_neg_QC_MS_03	Norm. Area: C18_neg_QC_MS_04	Norm. Area: C18_neg_QC_MS_05	Norm. Area: C18_neg_QC_MS_06	Norm. Area: C18_neg_QC_MS_07	Norm. Area: C18_neg_QC_MS_08.	Norm. Area: C18_neg_QC_MS_09	Norm. Area: C18_neg_QC_MS_10.	Norm. Area: C18_neg_QC_MS_11.	Norm. Area: C18_neg_QC_MS_12
9	3.5E+08	9.0E+06	8.6E+07	6.6E+07	3.4E+05	2.7E+05	8.8E+07	9.0E+07	9.0E+07	8.5E+07	8.7E+07	8.2E+07	7.4E+07	8.7E+07	7.9E+07	8.9E+07	8.8E+07	9.0E+07
10	2.0E+06	1.3E+06	7.9E+05	9.1E+05	2.8E+08	2.9E+08	9.4E+07	9.8E+07	1.0E+08	6.3E+07	9.8E+07	7.4E+07	9.0E+07	5.0E+07	8.9E+07	8.6E+07	8.3E+07	1.0E+08
11	2.6E+08	1.0E+06	4.0E+05	2.0E+05	1.9E+05	1.9E+05	4.0E+07	3.9E+07	3.9E+07	3.8E+07	3.8E+07	3.9E+07	3.6E+07	3.8E+07	3.9E+07	3.9E+07	3.9E+07	3.9E+07
12	1.3E+08	3.1E+06	2.3E+08	1.8E+08	1.4E+06	9.9E+05	1.4E+08	1.3E+08	1.3E+08	1.3E+08	1.4E+08	1.4E+08	1.2E+08	1.4E+08	1.2E+08	1.3E+08	1.3E+08	1.3E+08
13	5.9E+05	6.4E+05	1.7E+05	1.6E+05	5.0E+07	2.0E+08	4.9E+07	4.1E+07	5.1E+07	5.5E+07	5.0E+07	4.6E+07	4.3E+07	4.7E+07	3.6E+07	5.2E+07	4.6E+07	5.1E+07
14	1.4E+06	1.1E+06	8.1E+05	8.9E+05	1.8E+08	1.0E+08	9.3E+07	9.0E+07	6.9E+07	9.9E+07	8.9E+07	9.1E+07	9.5E+07	9.4E+07	8.9E+07	9.0E+07	9.2E+07	8.5E+07
15	1.7E+06	7.7E+05	2.6E+06	2.7E+06	1.7E+08	1.4E+08	1.1E+08	1.2E+08	1.1E+08	1.2E+08	1.4E+08	9.8E+07	1.3E+08	1.2E+08	1.2E+08	1.2E+08	1.1E+08	1.2E+08
16	2.9E+06	2.0E+06	3.8E+07	4.0E+07	1.0E+08	7.7E+07	9.5E+07	8.2E+07	7.5E+07	5.4E+07	1.0E+08	5.1E+07	7.7E+07	1.0E+08	6.7E+07	1.1E+08	7.5E+07	7.8E+07
17	5.6E+06	1.5E+06	9.3E+05	1.1E+06	1.0E+08	9.7E+07	5.6E+07	7.9E+07	8.6E+07	8.7E+07	7.4E+07	7.0E+07	8.4E+07	6.5E+07	8.3E+07	6.4E+07	6.9E+07	7.9E+07
18	9.2E+05	1.0E+06	7.7E+05	7.9E+05	8.1E+07	5.7E+07	3.6E+07	3.7E+07	2.6E+07	3.5E+07	3.4E+07	2.9E+07	3.3E+07	3.2E+07	3.4E+07	3.2E+07	3.3E+07	3.5E+07

Table S.12 – **Input data for pathway enrichment analysis of ES-2 EVs II lipids using MetaboAnalyst software for amide column and both modes of ionization.** Query – input compounds. HMDB – Human Metabolome Database; KEGG – Kyoto Encyclopedia of genes and genomes. SMILES – Simplified molecular input line entry system.

Query	Match	HMDB	Pub-Chem	KEGG	SMILES
(9R)-6-Hydroxy-6-oxido-12-oxo-5,7,11-trioxa-2-aza-6lambda~5~-phosphaheptacosan-9-yl (9Z)-9-octadecenoate	NA	NA	NA	NA	NA
Triglyceride POO,sn	NA	NA	NA	NA	NA
DL-Dipalmitoylphosphatidylcholine	NA	NA	NA	NA	NA
Triolein	NA	NA	NA	NA	NA
(9R)-6-Hydroxy-6-oxido-12-oxo-5,7,11-trioxa-2-aza-6lambda~5~-phosphaheptacosan-9-yl palmitate	NA	NA	NA	NA	NA
TG(16:1(9Z)/16:1(9Z)/18:0)[iso3	NA	NA	NA	NA	NA
TG(16:1(9Z)/18:1(9Z)/18:1(9Z))[iso3	NA	NA	NA	NA	NA
Palmitoyl sphingomyelin	NA	NA	NA	NA	NA
Dioleoylphosphatidylethanolamine	NA	NA	NA	NA	NA
DL-Arginine	L-Arginine	HMDB0000517	6322	C00062	C(C[C@@H](C(=O)O)N)CN=C(N)N
TG(16:0/16:1(9Z)/16:1(9Z))[iso3	NA	NA	NA	NA	NA
DL-Glutamine	L-Glutamine	HMDB0000641	5961	C00064	C(CC(=O)N)[C@@H](C(=O)O)N
Pyridoxine	Pyridoxine	HMDB0000239	1054	C00314	CC1=NC=C(C(=C1O)CO)CO

Query	Match	HMDB	Pub-Chem	KEGG	SMILES
Penicillin G	Penicillin G	HMDB0015186	5904	C05551	CC1([C@@H](N2[C@H](S1)[C@@H](C2=O)NC(=O)CC3=CC=CC=C3)C(=O)O)C
1-Palmitoyl-2-linoleoyl PE	NA	NA	NA	NA	NA
L-Histidine	L-Histidine	HMDB0000177	6274	C00135	C1=C(NC=N1)C[C@@H](C(=O)O)N
6-Hydroxy-6-oxido-12-oxo-5,7,11-trioxa-2-aza-6lambda~5~-phosphanonacosan-9-yl stearate	NA	NA	NA	NA	NA
1-palmitoyl-2-oleoyl-sn-glycero-3-phosphoethanolamine	PE(16:0/18:1(9Z))	HMDB0008927	5283496	C00350	CCCCCCCCCCCCCCCC(=O)OC[C@H](COP(=O)(O)OCCN)OC(=O)CCCCCCC/C=C\CCCCCCCC
Betaine	Betaine	HMDB0000043	247	C00719	C[N+](C)(C)CC(=O)[O-]
1-stearoyl-2-oleoyl-sn-glycero-3-phosphoethanolamine zwitterion	NA	NA	NA	NA	NA
Thiamine	Thiamine	HMDB0000235	1130	C00378	CC1=C(SC=[N+]1CC2=CN=C(N=C2N)C)CCO
Creatine	Creatine	HMDB0000064	586	C00300	CN(CC(=O)O)C(=N)N
Octadecanamine	Octadecylamine	HMDB0029586	15793	NA	CCCCCCCCCCCCCCCCCCN
5,5-dimethyl-2-{[(2-phenylacetyl)amino]methyl}-1,3-thiazolane-4-carboxylic acid	NA	NA	NA	NA	NA
1,2-dioleoyl-sn-glycero-3-phospho-N,N-dimethylethanolamine	NA	NA	NA	NA	NA
N1-phenethylbenzene-1-carbothioamide	NA	NA	NA	NA	NA
24-Amino-21-hydroxy-21-oxido-15-oxo-16,20,22-trioxa-21lambda~5~-phosphatetracosan-18-yl palmitate	NA	NA	NA	NA	NA
1-stearoyl-2-arachidonoyl-sn-glycero-3-phosphoethanolamine	PE(18:0/20:4(5Z,8Z,11Z,14Z))	HMDB0009003	5289133	C00350	CCCCCCCCCCCCCCCCCCC(=O)OC[C@H](COP(=O)(O)OCCN)OC(=O)CCC/C=C\C/C=C\C/C=C\C/C=C\CCCCC
1-stearoyl-2-oleoyl-sn-glycero-3-phosphoserine	PS(18:0/18:1(9Z))	HMDB0010163	5972071 7	C02737	CCCCCCCCCCCCCCCCCCC(=O)OC[C@H](COP(=O)(O)OC[C@@H](C(=O)[O-])[NH3+])OC(=O)CCCCCCC/C=C\CCCCCCCC
DL-Lysine	L-Lysine	HMDB0000182	5962	C00047	C(CCN)C[C@@H](C(=O)O)N
(2R)-1-{[(2-Aminoethyl)(hydroxy)phosphoryl]oxy}-3-(palmitoyloxy)-2-propanyl (9Z)-9-octadecenoate	NA	NA	NA	NA	NA
Nicotinamide	Niacinamide	HMDB0001406	936	C00153	C1=CC(=CN=C1)C(=O)N
1-oleoyl-2-linoleyl-sn-glycero-3-phosphoethanolamine	NA	NA	NA	NA	NA
MFCD00042876	NA	NA	NA	NA	NA
Ceramide (d18:1/16:0)	Ceramide (d18:1/16:0)	HMDB0004949	5283564	C00195	CCCCCCCCCCCCCCCCC(=O)N[C@@H](CO)[C@@H](/C=C/CCCCCCCCCCCCC)O
1-hexadecanoyl-2-(4Z,7Z,10Z,13Z,16Z,19Z-docosahexaenoyl)-sn-glycero-3-phosphoethanolamine	PE(16:0/22:6(4Z,7Z,10Z,13Z,16Z,19Z))	HMDB0008946	9546799	C00350	CCCCCCCCCCCCCCCC(=O)OC[C@H](COP(=O)(O)OCCN)OC(=O)CC/C=C\C/C=C\C/C=C\C/C=C\C/C=C\C/C=C\CC
1-hexadecanoyl-2-(5Z,8Z,11Z,14Z-icosatetraenoyl)-sn-glycero-3-phosphoethanolamine	NA	NA	NA	NA	NA
N-[(2S,3R,4E)-1-(beta-D-erythro-Hexopyranosyloxy)-3-hydroxy-4-octadecen-2-yl]hexadecanamide	NA	NA	NA	NA	NA
1-palmitoyl-2-oleoyl-sn-glycero-3-phospho-l-serine	NA	NA	NA	NA	NA

Query	Match	HMDB	Pub-Chem	KEGG	SMILES
1-octadecanoyl-2-(4Z,7Z,10Z,13Z,16Z,19Z-docosahexaenoyl)-sn-glycero-3-phosphoethanolamine	PE(18:0/22:6(4Z,7Z,10Z,13Z,16Z,19Z))	HMDB0009012	9546798	C00350	CCCCCCCCCCCCCCCCCC(=O)OC[C@H](COP(=O)(O)OCCN)OC(=O)CC/C=C\C/C=C\C/C=C\C/C=C\C/C=C\C/C=C\CC
L(-)-Pipecolinic acid	L-Pipecolic acid	HMDB0000716	439227	C00408	C1CCN[C@@H](C1)C(=O)O
TG(18:2(9Z,12Z)/18:2(9Z,12Z)/20:1(11Z))[iso3	NA	NA	NA	NA	NA
(24R)-30-Amino-27-hydroxy-27-oxido-21-oxo-22,26,28-trioxa-27lambda~5~-phosphatriacontan-24-yl (4Z,7Z,10Z,13Z,16Z,19Z)-4,7,10,13,16,19-docosahexaenoate	NA	NA	NA	NA	NA
1730602	NA	NA	NA	NA	NA
Choline	Choline	HMDB0000097	305	C00114	C[N+](C)(C)CCO
Cetrimonium	NA	NA	NA	NA	NA
Bis(2-ethylhexyl) phthalate	NA	NA	NA	NA	NA
2-[(11Z)-11-Icosenoyloxy]-3-[(9Z,12Z,15Z)-9,12,15-octadecatrienoyloxy]propyl (11Z,14Z)-11,14-icosadienoate	NA	NA	NA	NA	NA
(2R)-3-{[(2-Aminoethoxy)(hydroxy)phosphoryl]oxy}-2-[(9Z)-9-hexadecenoyloxy]propyl (9Z)-9-hexadecenoate	NA	NA	NA	NA	NA
(1'S,2'S)-3',11'-dihydroxy-1',2',5'-trimethyl-8'-oxaspiro[oxirane-2,12'-tricyclo[7.2.1.0Ã,?,Ã¢Â• Â·]dodecan]-5'-en-4'-one	NA	NA	NA	NA	NA
2-Amino-4-methylpyrimidine	NA	NA	NA	NA	NA
1-Oleoyl-2-hydroxy-sn-glycero-3-PE	NA	NA	NA	NA	NA
4-Oxoproline	4-Oxoproline	METPA0228	NA	C01877	NA
Pantothenic acid	Pantothenic acid	HMDB0000210	6613	C00864	CC(C)(CO)C(C(=O)NCCC(=O)O)O
O-{Hydroxy[2-(nonadecanoyloxy)-3-(stearoyloxy)propoxy]phosphoryl}-L-serine	NA	NA	NA	NA	NA
D-(-)-Glutamine	L-Glutamine	HMDB0000641	5961	C00064	C(CC(=O)N)[C@@H](C(=O)O)N
5-Oxohexanoic acid	NA	NA	NA	NA	NA
4-Acetamidobenzoic acid	NA	NA	NA	NA	NA
D-(+)-Malic acid	D-Malic acid	HMDB0031518	92824	C00497	C([C@H](C(=O)O)O)C(=O)O
L-Threonic acid	NA	NA	NA	NA	NA

Table S.13 – **Pathway enrichment analysis of ES-2 EVs metabolites using MetaboAnalyst software for amide column and both modes of ionization.** Expected – expected hits; hits – observed hits; raw p – raw p-value; Holm p – p-values adjusted by the Holm-Bonferroni method; FDR – false discovery rates enrichment ratio – hits to observed ratio

	total	expected	hits	Raw p	Holm p	FDR	Enrichment ratio
Betaine Metabolism	21	0.451	2	0.0723	1	1	4.43459
Methylhistidine Metabolism	4	0.0859	1	0.0833	1	1	11.64144

	total	expected	hits	Raw p	Holm p	FDR	Enrichment ratio
Urea Cycle	29	0.623	2	0.126	1	1	3.210273
Glycine and Serine Metabolism	59	1.27	3	0.128	1	1	2.362205
Lysine Degradation	30	0.645	2	0.133	1	1	3.100775
Ammonia Recycling	32	0.688	2	0.148	1	1	2.906977
Biotin Metabolism	8	0.172	1	0.16	1	1	5.813953
Beta-Alanine Metabolism	34	0.73	2	0.164	1	1	2.739726
Aspartate Metabolism	35	0.752	2	0.171	1	1	2.659574
Thiamine Metabolism	9	0.193	1	0.178	1	1	5.181347
Phenylacetate Metabolism	9	0.193	1	0.178	1	1	5.181347
Nicotinate and Nicotinamide Metabolism	37	0.795	2	0.187	1	1	2.515723
Phosphatidylethanolamine Biosynthesis	12	0.258	1	0.231	1	1	3.875969
Methionine Metabolism	43	0.924	2	0.235	1	1	2.164502
Phosphatidylcholine Biosynthesis	14	0.301	1	0.264	1	1	3.322259
Arginine and Proline Metabolism	53	1.14	2	0.317	1	1	1.754386
Vitamin B6 Metabolism	20	0.43	1	0.355	1	1	2.325581
Pantothenate and CoA Biosynthesis	21	0.451	1	0.369	1	1	2.217295
Carnitine Synthesis	22	0.473	1	0.383	1	1	2.114165
Phospholipid Biosynthesis	29	0.623	1	0.472	1	1	1.605136
Amino Sugar Metabolism	33	0.709	1	0.517	1	1	1.410437
Histidine Metabolism	43	0.924	1	0.615	1	1	1.082251
Glutamate Metabolism	49	1.05	1	0.664	1	1	0.952381
Warburg Effect	58	1.25	1	0.727	1	1	0.8
Pyrimidine Metabolism	59	1.27	1	0.733	1	1	0.787402
Purine Metabolism	74	1.59	1	0.811	1	1	0.628931

2022

LEANDRA JOSÉ SILVA RODRIGUES

CHARACTERIZATION OF EXTRACELLULAR VESICLES FROM ASCITIC FLUID IN OVARIAN CANCER PATIENTS

NOVA SCHOOL OF SCIENCE & TECHNOLOGY